FZR-419

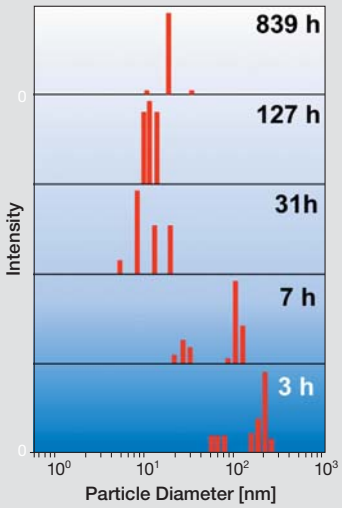

Wissenschaftlich-Technische Berichte
FZR-419 2005 · ISSN 1437-322X

Annual Report 2004

Institute of Radiochemistry

Forschungszentrum
Rossendorf

Wissenschaftlich-Technische Berichte
FZR-419
2005

Annual Report 2004

Institute of Radiochemistry

Editor: **Prof. Dr. G. Bernhard**

Editorial staff: **Dr. H. Foerstendorf**
Dr. J. Mibus
Dr. A. Richter
Dr. K.-U. Ulrich

Forschungszentrum
Rossendorf

Contact:

Forschungszentrum Rossendorf
Institute of Radiochemistry

Postal Address	*Address for visitors*
P.O. Box 51 01 19	Bautzner Landstraße (SW) 128
D-01314 Dresden	D-01328 Dresden
Germany	Germany

Phone: ++49 (0) 351 260 3210
Fax: ++49 (0) 351 260 3553
http://www.fz-rossendorf.de/FWR
e-mail: contact.radiochemistry@fz-rossendorf.de

Cover pictures:

Determination of particle size of environmentally relevant colloids

Top: Optical components of Laser-Induced Breakdown Detection (LIBD).

Left below: Particle size distribution of freshly formed FeOOH colloids measured by Photon Correlation Spectroscopy (PCS).

Right below: Mouth of the mine drainage gallery „Rothschönberger Stolln“ near Meißen.

Preface

The Institute of Radiochemistry (IRC), one of the six Institutes of the Forschungszentrum Rossendorf (FZR) performs basic and applied research in the fields of radiochemistry and radioecology. Motivation and background of our research are environmental processes relevant for the installation of nuclear waste repositories, for remediation of uranium mining and milling sites, and for radioactive contaminations caused by nuclear accidents and fallout. Because of their high radiotoxicity and long half-life the actinides are of special interest. The research is focused on a better understanding of the chemical behavior of actinides in the environment on a molecular level.
We will increase our efforts to study both the speciation of actinides on bio-molecular interfaces and their transport in bio-systems.
Current topics of our research work are:

- Aquatic chemistry of actinides
- Actinides in bio-systems
- Interaction of actinides with solid phases
- Reactive transport of actinides

About 60 scientists, technicians and PhD students are employed at the Institute of Radiochemistry.
We accomplished many new scientific results in the past year, which are presented in this Annual Report. Among them only few can be highlighted in this preface. Further progress was achieved in understanding the formation and characterization of uranium containing colloids. The newly installed method of laser-induced breakdown detection was very helpful for the identification of uranium colloids under anoxic conditions. We were very successful in the determination of formation pathways and structure of various actinide complexes. These results contribute to a better understanding of actinide speciation in geo- and bio-systems, especially with respect to the chemical processes on the interfaces. The results achieved in the characterization of the properties, modification, and interaction of the S-layers of *Bacillus sphaericus* with uranium and some other heavy metals strengthen our hope to use this material to separate heavy metals from very low contaminated waters or to produce well-structured metal templates in future. Studies about the interaction of actinides with different bacterial strains improved our understanding about the different binding in biological systems. Our investigations about interaction, sorption, and diffusion of actinides in clay in presence of fulvic and humic acids are included in national projects and in international collaborations. Furthermore we can report that our new radiochemical experimental station on the Free Electron IR-Laser of the Rossendorf accelerator ELBE is now in operation. After first tests we will start our research work in 2005.

In 2004 the research work of the Institute of Radiochemistry was evaluated by the "Scientific Advisory Board of the FZR". We can proudly report that we have got a very good testimonial by this Board concerning our scientific work. We will follow the given helpful hints to further improve our work.

I would like to thank the visitors, German and international ones, for their interest in our research and for their participation in the Institute's seminars. I would also like to thank our scientific collaborators and the visiting scientists for coming to Rossendorf/Dresden in 2004 to share their knowledge and experience with us. We continue to strongly encourage the collaborations and visits by scientists in the future. Special thanks are due to the Executive Board of the Forschungszentrum Rossendorf, the Ministry of Science and Arts of the State Saxony, the Federal Ministry of Education and Research, the Federal Ministry of Economics and Labour, the Deutsche Forschungsgemeinschaft, the European Commission, and other organizations for their support.

Prof. Dr. G. Bernhard

Content

Scientific contributions

Part 1: Aquatic chemistry of actinides

Part 2: Actinides in bio-systems

Part 3: Interaction of actinides with solid phases

Part 1:

Aquatic chemistry of actinides

The structure of uranium aquo chloro complexes. Part 1: U(VI) species

C. Hennig, J. Tutschku, A. Rossberg, A.C. Scheinost, G. Bernhard

ABSTRACT. The coordination of U(VI) in concentrated aqueous chloride solution has been studied by U L_{III}-edge EXAFS. Between 3 and 9 M Cl^- we observed the species $UO_2(H_2O)_4Cl^+$, $UO_2(H_2O)_3Cl_2^0$ and $UO_2(H_2O)_2Cl_3^-$.

Comprehensive reviews of thermodynamic data have been reported on U(VI) complexes. A weighted linear regression, using experimental values from different references, yields stability constants of $log\ \beta_1^0 = 0.17 \pm 0.02$ and $log\ \beta_2^0 = -1.1 \pm 0.02$ for the reaction $UO_2^{2+} + nCl^- \rightleftharpoons UO_2Cl_n^{2-n}$ [1]. Formation constants $log\ \beta_n^0$ for species with $n > 2$ have not been published so far. UV-Vis spectroscopy shows significant spectral features which allowed to discriminate the species UO_2^{2+}, UO_2Cl^+ and $UO_2Cl_2^0$ quantitatively [2]. Allen *et al.* [3] observed the species $UO_2(H_2O)_5^{2+}$, $UO_2(H_2O)_xCl^+$, $UO_2(H_2O)_xCl_2$, and $UO_2(H_2O)_xCl_3^-$ recently by EXAFS spectroscopy.

EXAFS measurements at 0, 3, 6 and 9 M Cl^-were carried out on the Rossendorf Beamline. Two stock solutions of 0.1 M U were prepared by dissolving UO_3 either in 0.3 M $HClO_4$ for the chloride-free sample or in 0.3 M HCl for the chloride-containing samples. Four 0.01 M U(VI) aqueous solutions with chloride concentration of 0, 3, 6 and 9 M were prepared. LiCl was dissolved in 2.5 mL U stock solution and 2.5 mL of 1 M HCl obtaining 25 mL of 0.01 M U solutions.

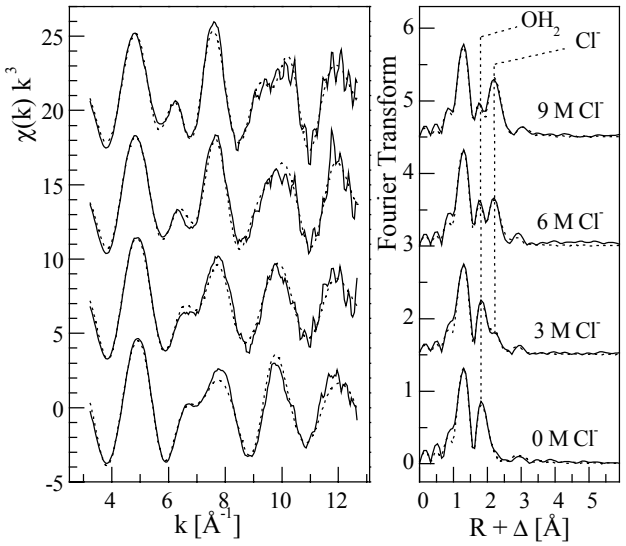

Fig. 1: U L_{III}-edge k^3 weighted EXAFS data (left) and corresponding Fourier transforms (right, $3.2 \le k \le 12.7$ Å^{-1}) of UO_2^{2+} at four different Cl^- concentrations. Curve fits are shown as dotted lines.

The FT of all samples shows two peaks which arise from two axial oxygen atoms (O_{ax}) at 1.76±0.02 Å (Fig. 1). The UO_2^{2+} aquo ion in the absence of Cl^- has 5 equatorial oxygen atoms (O_{eq}) at 2.41 ± 0.02 Å. The FTs of the Cl^- solutions show an additional peak at a distance of 2.73 ± 0.02 Å indicative of Cl^- in the first coordination sphere. The intensity of this Cl peak increases with increasing Cl^- concentration. Correspondingly, N_{Cl} increased from 1.0 to 2.7 in subsequent EXAFS fits. With increasing Cl^- concentration the dominant FT peak shifts to higher R values indicating a systematic replacement of H_2O by Cl^- in the first coordination sphere. Although possible solution species comprising $UO_2(H_2O)_5^{2+}$ and $UO_2(H_2O)_{5-n}Cl_n^{2-n}$ are averaged to a common radial distribution, the structural parameters extracted by EXAFS suggest the species $UO_2(H_2O)_4Cl^+$, $UO_2(H_2O)_3Cl_2^0$ and $UO_2(H_2O)_2Cl_3^-$ according to Fig. 2.

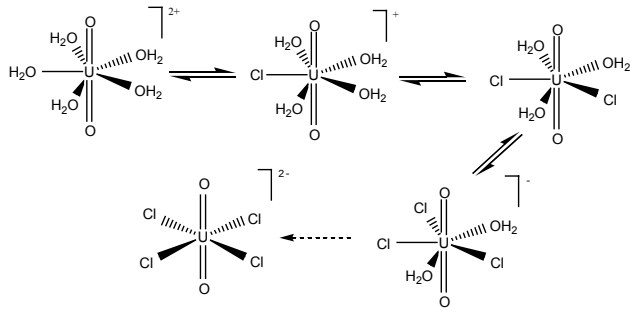

Fig. 2: U(VI) aquo chloro species.

We assume, that in all aquo chloro species the equatorial coordination number remains 5, because in a fourfold coordination as in $UO_2Cl_4^{2-}$ the U-Cl bond length would be reduced to 2.671 Å [4]. With increasing Cl^- concentration the coordination number of Cl increases stepwise. The ligands are coordinated in an inner-sphere fashion. A possible additional outer-sphere coordination could not be verified since EXAFS measurement is not sensitive for the backscattering signals at $R + \Delta > 3$ Å under the used experimental conditions and the outer sphere coordination would most likely be too disordered to be detectable.

REFERENCES

[1] Grenthe, I. *et al.* (1992) *Chemical Thermodynamics of Uranium*, Elsevier Sci. Publ., Amsterdam.
[2] Paviet-Hartmann, P. *et al.* (1999) *Mat. Res. Soc. Symp. Proc.* **556**, 977.
[3] Allen, P.G. *et al.* (1997) *Inorg. Chem.* **36**, 4676-4683.
[4] Watkin, D.J. *et al.* (1991) *Acta Cryst. C* **47**, 2517-2519.

The structure of uranium aquo chloro complexes. Part 2: U(IV) species

C. Hennig, J. Tutschku, A. Rossberg, A.C. Scheinost, G. Bernhard

ABSTRACT. A spectro-electrochemical cell was used for the EXAFS investigation of U(IV) in concentrated aqueous chloride solutions. The complexes $U(H_2O)_8Cl^{3+}$, $U(H_2O)_{6\text{-}7}Cl_2^{2+}$ and $U(H_2O)_5Cl_3^{+}$ were identified between 3 and 9 M Cl^-.

In contrast to U(VI), little is known on chloride complexation by U(IV). The formation constant according to the reaction $U^{4+} + nCl^- \rightleftharpoons UCl_n^{4-n}$ extrapolated to an ionic strength $I = 0$ yields $log\ \beta_1^0 = 1.72 \pm 0.13$ [1]. Only one experimental value is reported for n = 2 with a $log\ \beta_2 = 0.06$ ($I = 2$ M) [2].

To preserve the tetravalent oxidation state during the EXAFS measurements, we used an electrochemical cell. The design of this spectro-electrochemical cell comprising two safety compartments and a special electrode arrangement has been described previously [3]. The use of this cell enabled us to study the transition from U(VI) to U(IV) in one system. The electrochemical reduction of U(VI) to U(IV) involves an electron transfer and a chemical reaction transforming the trans-dioxo cation. The reaction at the cathode is:

$$UO_2^{2+} + 2e^- + 2H^+ \rightarrow U^{4+} + 2H_2O. \quad (1)$$

At the anode silver is dissolved and precipitates as silver chloride:

$$2Ag + 2Cl^- \rightarrow 2AgCl\downarrow + 2e^-. \quad (2)$$

The dissolved Ag^+ ions are in equilibrium with solid AgCl and the equilibrium potential of the electrode is then determined by the solubility constant of the precipitate.

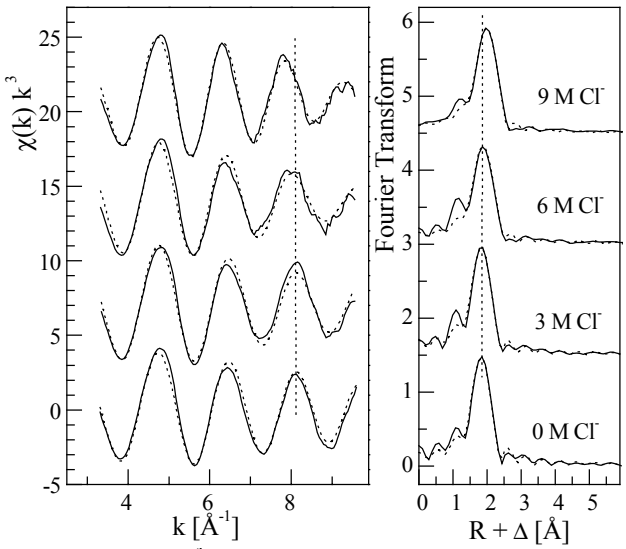

Fig. 1: U L_{III}-edge k^3 weighted EXAFS data (left) and corresponding Fourier transforms (right, $3.2 \le k \le 9.6$ Å^{-1}) of U(IV) at different Cl^- concentrations. Curve fits are shown as dotted lines.

At the experimental conditions chosen, the electrochemical potential was always far away from the decomposition potential of water, which is important since the formation of H_2 had to be prevented for radiochemical safety reasons. In order to avoid a high polarization of the cell, no diaphragm was used. The reduction of 0.01 moles of U(VI) to U(IV) at the cathode is accompanied by a decrease in the chloride concentration due to the precipitation of 0.02 moles of AgCl. However, this decrease of $[Cl^-]$ is small and therefore negligible at background $[Cl^-]$ of 3, 6 and 9 M. In order to enforce the anode reaction in the nominally 0 M Cl^- solution, 0.02 moles of LiCl were added.

In non-complexing perchloric acid the aquo ion has 8.7 spherically arranged oxygen atoms at a distance of 2.41 Å (Fig. 1, sample 0 M Cl^-). With increasing Cl^- concentration the dominant FT peak shifts to higher R values indicating a systematic replacement of H_2O by Cl^- in a distance of 2.71 Å. During the fits, the σ^2 value of the U-O shell was fixed to 0.0070 Å^{-2}, obtained from the U(IV) aquo ion, and that of the U-Cl shell was fixed to 0.0050 Å^{-2} following the value obtained for U(VI). The coordination number N_{Cl} increased from 0.3 to 2.1 and the coordination number N_O decreased from 8.5 to 6.1. The aquo chloro species derived from EXAFS measurements are identified as $U(H_2O)_8Cl^{3+}$, $U(H_2O)_{6\text{-}7}Cl_2^{2+}$ and $U(H_2O)_5Cl_3^{+}$ (Fig. 2). The extraction of principal components by factor analysis showed that the coordination number N_{O+Cl} decreases from 9 in $U(H_2O)_8Cl^{3+}$ to 8 in $U(H_2O)_5Cl_3^{+}$ [4].

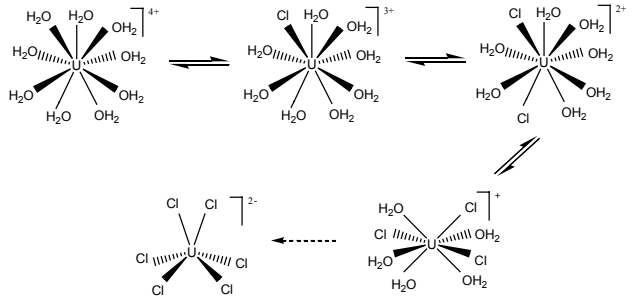

Fig. 2: U(IV) aquo chloro species.

The structure of U(IV) chloride complexes was not investigated up to now. Allen et al. found clear evidence for inner-sphere formation of Np(IV) aquo chloride complexes. Due to the chemical similarity of U(IV) and Np(IV) an equivalent coordination was assumed for U(IV). A comparison of the Cl^- concentrations necessary to reach a coordination number of $N_{Cl} < 1$, which is higher for U(IV) than for Np(IV), confirms that $log\ \beta_1$ follows the trend U(IV) > Np(IV). The similar bond lengths for U-O and U-Cl for the U(VI) and U(IV) aquo chloro species suggest that, despite the difference in formal oxidation state, the effective ionic radii of U(VI) and U(IV) are similar, as has been pointed out in the literature [5].

REFERENCES

[1] Grenthe, I. *et al.* (1992) *Chemical Thermodynamics of Uranium*, Elsevier Sci. Publ., Amsterdam.
[2] Day, R.A. *et al.* (1955) *J. Am. Chem. Soc.* **77**, 3180-3182.
[3] Tutschku, J. *et al.* (2003) *Report FZR–400*, p. 13.
[4] Hennig, C. *et al.* (2005) *Inorg. Chem.*, submitted.
[5] Denning, R.G. (1992) *Struct. Bonding*, **79**.

UV-vis measurements of uranium(VI) and uranium(IV) in concentrated solutions of carbonate in alkaline medium prepared with the electrochemical cell

J. Tutschku, G. Geipel, G. Bernhard

ABSTRACT. U(VI) was reduced to U(IV) in a saturated carbonate solution. It was possible to enhance the solubility of U(IV) by complex formation of uranium with carbonate. We were able to detect the transformation from U(VI) to U(IV) in solution by UV-vis spectroscopy.

INTRODUCTION. Up to now, studies of uranium(IV) in alkaline media were not performed due to the low solubility of U(IV). The electrochemical reduction on a Pt working electrode was not successful, because uranium(IV) was deposited on the Pt-electrode probably as oxihydrate. Only with a mercury electrode we are able to reduce uranium(VI) to uranium(IV).
Uranium(VI) forms strong carbonate complexes in solution. Therefore, in relation to uranium(VI) perchlorate, the UV-vis spectrum is shifted (Fig. 1).
From the literature it is known that uranium(IV) forms a strong complex with carbonate [1].

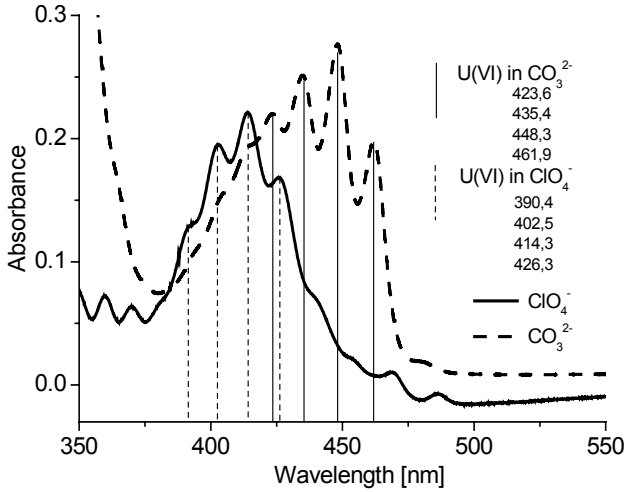

Fig. 1: Comparison of UV-vis spectra of uranium(VI) perchloride and carbonate solutions.

EXPERIMENTS. We utilized mercury (Hg) as cathode in the electrochemical cell [2]. The anode material was Ag. The potential referred to Ag/AgCl.
Due to the hydrogen overvoltage on Hg we are able to reduce uranium in alkaline solution excluding the formation of hydrogen gas.
In order to keep U(IV) dissolved in the solution, we added sodium carbonate until saturation. A small amount of chloride was added in order to enforce the AgCl precipitation at the anode.
The composition of the solution was adjusted to
0.01 M UO_2CO_3
0.05 M NaCl
sat. Na_2CO_3

RESULTS. The first UV/vis-measurements were taken at – 700 mV (Fig. 2) but no change was observed in the spectrum.
The U(VI)/U(IV) reduction potential was determined to be – 1350 mV (Fig. 3). The UV/Vis spectrum taken after reduction at – 1350 mV (Fig. 2) shows clear the presence of U(IV). However, the large background in the spectrum indicates also the precipitation of uranium(IV) in the solution.

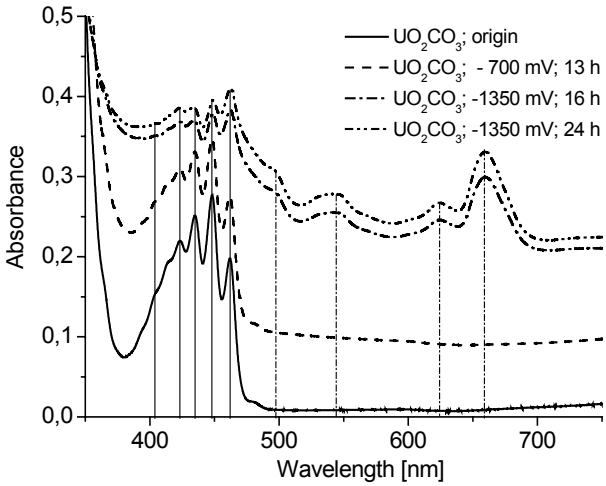

Fig. 2: UV-vis spectra recorded after reduction of UO_2CO_3 in high concentrated carbonate solution.

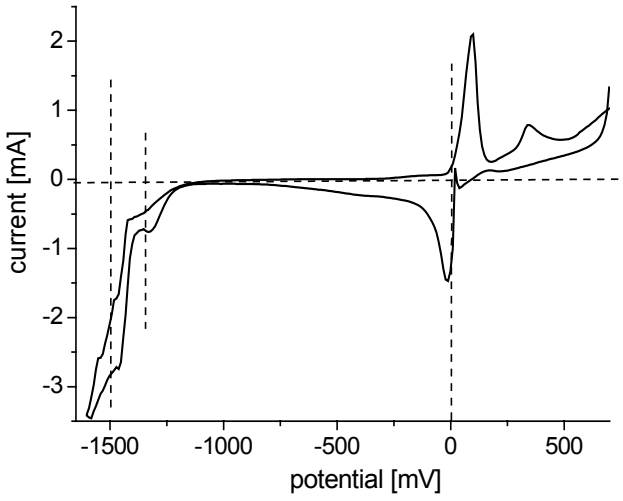

Fig. 3: Cyclovoltammogram of UO_2CO_3 in Na_2CO_3.

REFERENCES

[1] Grenthe, I. *et al.* (1992) *Chemical Thermodynamics of Uranium,* Elsevier Sci.Publ., Amsterdam.
[2] Tutschku, J. *et al*. (2003) *Report FZR-400*, p. 13.

UV-vis measurements of uranium(VI) and uranium(IV) in concentrated chloride solution prepared with the electrochemical cell

J. Tutschku, C. Hennig, G. Geipel, G. Bernhard

ABSTRACT. The formation of uranium chloride complexes in aqueous solution was observed by UV-vis spectroscopy. In solutions with high cloride concentrations water molecules are exchanged by the halide anion in the aquo shell of uranium. The reduction of uranium(VI) to uranium(IV) was performed in the electrochemical cell in order to prepare EXAFS measurements.

The behavior of uranium chloride in solution was investigated by UV-vis spectroscopy. With increasing concentration of chloride the solvation of uranium in different oxidation states was investigated.

EXPERIMENTS. LiCl was added to UO_2Cl_2-solutions until saturation was achieved. In preliminary tests the concentration range of the chloride was estimated and solutions with 1, 2, 3, 4, 6, 9 M LiCl were prepared.
The complex formation between uranium and chloride occurs only at high chloride concentration. For the investigation of complex formation by UV-vis and EXAFS we used three solutions with different LiCl concentrations.

The compositions of the solutions were adjusted to
3 M, 6 M, 9 M LiCl
0.01 M UO_2Cl_2
0.1 M HCl
The saturation of LiCl is 9.63 M.
A low pH is necessary for the solubility of U(IV).

The reduction of uranium(VI) to uranium(IV) was carried out in a special electrochemical cell, developed in the Institute of Radiochemistry [1].
In the reduction experiments, the stability of the reference electrode was not sufficient. Therefore, the reference electrode was freshly prepared for each experiment.
During the reduction the start current was about 1 mA. This high current results from a higher solubility of AgCl which can be observed by a grey deposit on the Pt-electrode. However, the reduction of uranium is not influenced which can be verified by UV-vis spectroscopy showing decreasing uranium(VI) and increasing uranium(IV) bands.

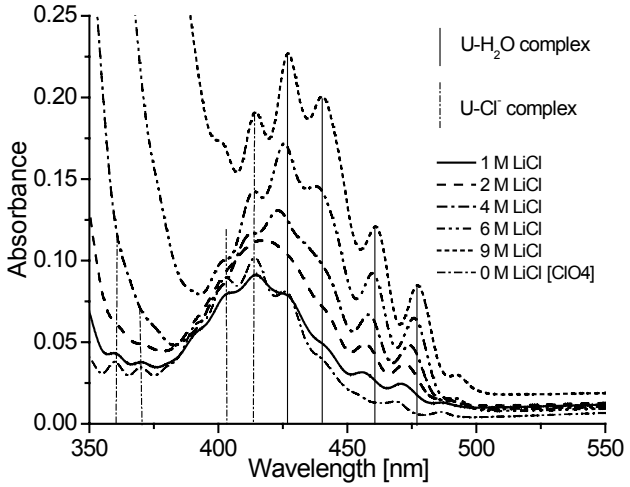

Fig. 1: UV-vis spectra of U(VI) in LiCl solutions of different concentrations.

RESULTS. In order to estimate the integration of chloride ions in the solvation shell of uranium, the UV-vis spectra of the uranium(VI) solutions containing different chloride concentrations are shown in Fig. 1. The bands representing uranium(VI) are shifted to longer wavelengths. Additionally, new bands at 460 nm and 475 nm appear. Their intensities correlate with increasing chloride ion concentration. Thus, these bands are assigned to chloride complexes of uranium(VI).
In order to compare the solvation effect of uranium(VI) and uranium(IV), the curves of completely reduced uranium solutions are assembled in Fig. 2.
With increasing chloride ion concentration a new band appears at 670 nm. It belongs to the bonding between U(IV) and chloride.

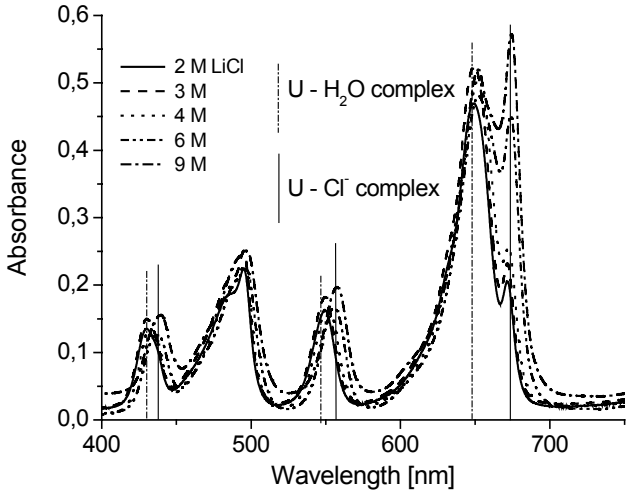

Fig. 2: UV-vis spectra of U(IV) in LiCl solutions of different concentrations.

REFERENCES

[1] Tutschku, J. *et al*. (2003) *Report FZR-400*, p. 13.

Generation of U(IV) colloids

S. Weiß, K. Opel, H. Zänker

ABSTRACT. The experimental setup and methods for the electrochemical generation of U(IV) colloids and for the delivery of colloid samples to the cell for laser-induced breakdown detection (LIBD) are described.

Uranium(IV) compounds exhibit very low solubilities and the reported data are uncertain [1]. Our study was aimed at the preparation of fresh U(IV) colloids and their detection by LIBD in order to determine the solubility of U(IV) [2]. Similar experiments have already been published for Th(IV) [3].
The generation of the colloids was accomplished as a two step procedure:

(1) Reduction of U(VI) to U(IV),

(2) Titration of the U(IV) solution.

BACKGROUND. The access of dust or other particles to the solutions had to be carefully avoided. Whenever possible, equipment made of perfluoroalkoxy-copolymer (PFA) was used. This fluoropolymer resin is known for its smooth surface and low rate of colloid generation. Most of the work was done in a glove box with nitrogen atmosphere.
The high-purity water (Membrapure) used in the experiments was boiled for 1 h in dust free environment in order to expel carbonate and oxygen.
For the pH determinations, a combined glass electrode (WTW) with a 3 M NaCl electrolyte solution was used. It was calibrated against standard solutions of the composition x M $HClO_4$/(0.2 – x) $NaClO_4$ (x = 0.001 – 0.1).
The titration vessel (volume 500 ml) was thermostated at 25 °C. The solutions were continuously stirred.
A replaceable top equipped with inlets for a Pt wire, manual sampling tube, pneumatic LIBD sampling tube, pH electrode and an anode compartment/salt bridge enabled high versatility. The current source was a Digistant 4462 galvanostat (Burster).
The U(VI) solutions were prepared by the dissolution of UO_3 in perchloric acid. $NaClO_4$ served as the background electrolyte. An ionic strength of 0.2 M $HClO_4$/$NaClO_4$ was adjusted and the initial pH was < 1. The blank of the colloid concentration was checked by LIBD before the experiments started.

REDUCTION. The anode compartment with the Pt wire was inserted into the vessel and filled with a 0.2 M $NaClO_4$ solution. The anode compartment was a glass tube with a frit (pore size G 2) as the diaphragm. For experimental setup see Fig. 1A. It took 1 – 2 weeks to reduce 350 ml of the solution at a current of 52 mA, depending on the U(VI) concentration. The progress of the reduction was monitored by two different methods: UV/VIS-spectroscopy (presence of U(IV)) and TRLFS (absence of U(VI)).

COULOMETRIC TITRATION. The salt bridge (filled with 0.2 M $NaClO_4$) was inserted into the vessel. It was made of glass and had two diaphragms (frits with pore size G 2). The anode was a calomel electrode. For experimental setup see Fig. 1B. The titrations were done at a current of 0.001 – 1 mA and took 3 – 4 weeks per sample.

SAMPLING PROCEDURE. The first step was purging the tubes and cuvette outside the glove box with nitrogen. Samples for LIBD were transported by a peristaltic pump into a flow-through cuvette. Measurements were done in the static mode, i. e. without sample flow during the measurement. The samples were pumped out of the vessel into the cuvette but did not pass the pump (pneumatic sampling; only air passed the pump). Therefore no particle contamination from abrasion of the tube in the pump could occur. After measurement, the samples were pumped back into the vessel and the cuvette was flushed with 500 ml of water and dried with nitrogen for 1 hour.

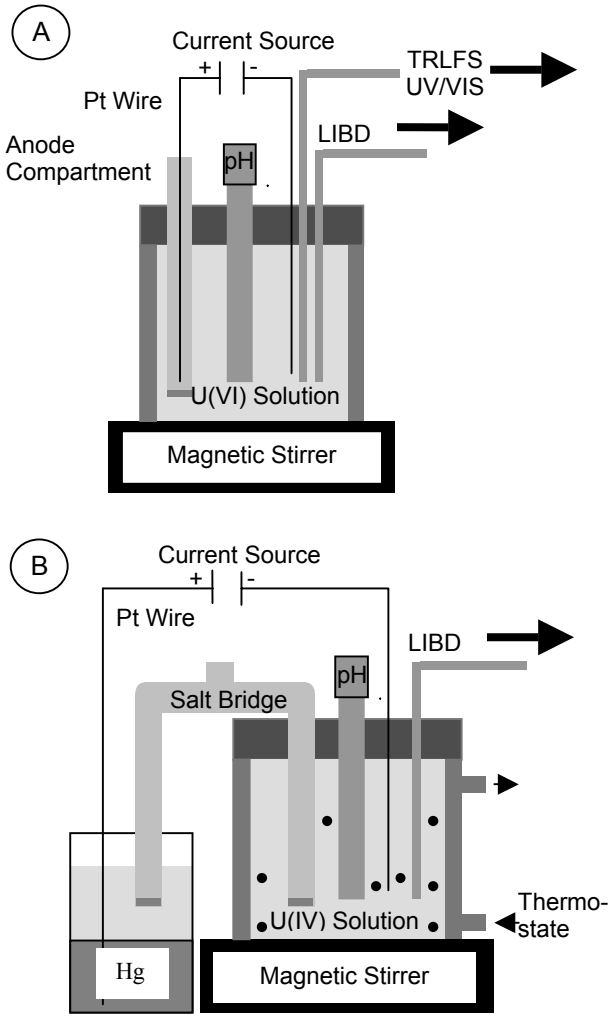

Fig. 1: Experimental setup of (A) reduction of U(VI) solutions and (B) coulometric titration of U(IV) solutions.

REFERENCES

[1] Silva, R. J. *et al.* (1995) *Radiochim. Acta* **70/71**, 377-396.
[2] Opel, K. *et al.* this report, p. 14.
[3] Bundschuh, T. *et al.* (2000) *Radiochim. Acta* **88**, 625-629.

Detection of uranium colloids under anoxic conditions by Laser-Induced Breakdown Detection (LIBD)

K. Opel, S. Hübener, S. Weiß, H. Zänker, G. Bernhard

ABSTRACT. Freshly prepared colloidal particles of U(IV) are detected by LIBD. The pH at the onset of colloid detection is used to re-evaluate the solubility product of U(IV) hydroxide.

Uranium, among other actinides, plays an important role in the long-term safety assessment of nuclear waste repositories. Furthermore, it is naturally present in former uranium mines and might contaminate aquifers when these mines are flooded. The correct determination of the thermodynamic solubility of uranium is essential for the geochemical modeling of these scenarios.

EXPERIMENTAL. The preparation of the U(IV) colloids and the sampling method are described in detail in [1]. A uranium concentration of 10^{-4} M was chosen. The basics of LIBD are explained in [2], the LIBD setup established at the IRC is presented in [3]. Sample solutions were investigated at laser pulse energies of 1.5 mJ. One thousand laser pulses were applied three times on each sample. The mean value of the measured breakdown probability at each pH was calculated and used to detect the onset of colloid formation.
The distribution of breakdown events in the focal area of the laser beam was also determined by LIBD to evaluate the mean size of the formed colloids [cf. 2].

RESULTS. Fig. 1 shows the dependency of the breakdown probability on the pH of the solution. The colloidal impurities in ultrapure water cause a background of the breakdown probability of some 4 %, this level is marked by a dashed line. The breakdown probability remains below the background level up to a pH of 2.55. It shows a steep slope at this point, *i.e.* a significant amount of colloids was generated and the solubility product of uranium(IV) hydroxide had been exceeded.

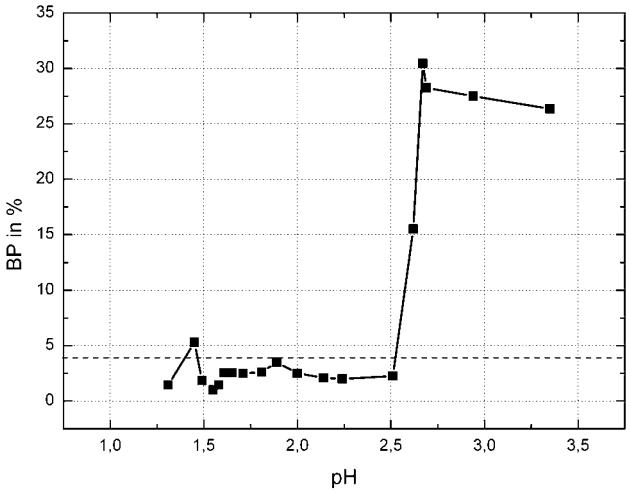

Fig. 1: Dependency of breakdown probability on pH in a 10^{-4} M U(IV) solution.

The solubility product of $U(OH)_4$ under the given conditions is calculated by equation (1).

$$K'_S = [U^{4+}][OH^-]^4 \quad (1)$$

To obtain a value which is comparable to published solubility products, the following facts have to be taken into account:
- U(IV) has a strong tendency to hydrolyse. Therefore not all U(IV) is in solution as U^{4+} but in the form of U(IV) hydroxo complexes. This is corrected by calculating the speciation of U(IV) using the respective hydrolysis constants from a recent review by Neck and Kim [4].
- The investigations were carried out in a solution containing 0.2 M $HClO_4/NaClO_4$. The calculated solubility product under these conditions has to be corrected to I=0 using the specific ion interaction theory (SIT) described in the NEA-TDB [5].

Under these circumstances, log K^0_S for uranium(IV) hydroxide is calculated to be –54.3 at zero ionic strength. This value is in good agreement with the value of –54.5 published in the review by Neck *et al.* [4]. Data in [4] are based on the results of solubility experiments but the contribution of colloids was not quantified in these experiments.
A similar study on thorium colloids [6] indicated a dependency of the solubility of the actinide on the particle size. The colloidal phase is better soluble than the bulk of the solid. In the case of thorium, a shift of the solubility product by about one order of magnitude resulted. Our focal lengths obtained by LIBD indicate that the formed colloids have a particle size that also needs to be taken into account when calculating the solubility product. Such corrected calculations are under way.
Presently it is assumed that the formed colloids consist of amorphous uranium(IV) hydroxide. The existence of other solids, e.g. microcrystalline UO_2, is also imaginable and has to be examined by other methods (XRD, EXAFS).
Furthermore, it is necessary to repeat the measurements for different concentrations of U(IV) to confirm the independence of K^0_S on the selected uranium concentration.

REFERENCES

[1] Weiß, S. *et al.* this report, p. 13.
[2] Walther, C. *et al.* (2002) *Nucl. Instr. Meth. Phys. Res. B* **195**, 374-388.
[3] Hübener, S. *et al.* (2003) *Report FZR-400*, p.46.
[4] Neck, V. *et al.* (2001) *Radiochim. Acta* **89**, 1-16.
[5] Grenthe, I. *et al.* (1992) *Chemical Thermodynamics of Uranium,* Elsevier Science Publ., Amsterdam.
[6] Bundschuh, T. *et al.* (2000) *Radiochim. Acta* **88**, 625-629.

Study on colloidal FeOOH particles

S. Weiß, H. Zänker

ABSTRACT. The formation and aging of colloidal FeOOH after the titration of a $FeCl_3$ solution with NaOH to pH 2.5 was investigated.

Due to the low solubility of Fe^{3+} in aqueous solution, colloidal states of polymerized ferric ions occur already at pH values ≤ 2.5. The colloids have been considered to be akaganeite-like in the presence of chloride [1].

EXPERIMENTAL. A solution of 10 mM $FeCl_3 \cdot 6H_2O$ was titrated with NaOH under vigorous stirring to a pH of 2.5 within 5 minutes. Photon correlation spectroscopy (PCS) on samples taken after several time intervals was done on a BI-90 instrument (Brookhaven). Furthermore, samples were taken at several times after NaOH addition for ultracentrifugation at 40,000 rpm (285,000 x g at r_{max}). Centrifugation at this acceleration results in the removal of the iron particles > 10 nm, but leaves most of the smaller ones behind in the supernatant.

RESULTS. Fig. 1 shows that the scattered light intensity dramatically increased by the NaOH addition. Afterwards it went through a minimum. The pH showed a steady decline after its maximum of 2.5. The count rate (CR) decrease can easily be explained by a decrease in particle size as Fig. 2 indicates. A particle size of about 10 nm was found after 31 h. The slow CR increase after its minimum at 31 h can be explained by a slight increase in particle size (Fig. 2). This particle growth is also demonstrated by a rise of the Fe fraction removable by ultracentrifugation (Tab. 1). XRD on a pellet from the ultracentrifugation (sample after 264 h) revealed that akaganeite (β-FeOOH) was the pre-vailing structure of the colloids.

DISCUSSION. Three types of particles play a role in FeOOH colloid behavior:

(a) Very small subunits (1.6 nm in the case of akaganeite [2]).
(b) Relatively compact aggregates of these subunits of linear or branched coordination (tens to several hundreds of nanometers) [2].
(c) Flocks, i. e. large associations of the type (b) particles which have low diffusion coefficients and tend to precipitate [1, 2].

The behavior of the colloids in our experiment seems to be attributable to two competing processes:

(i) The rise in pH leads to the formation of large amounts of type (a) subunits. However, these subunits still contain relatively few hydroxyle ions in the beginning. The latter can be due to a relatively low degree of polymerization, a high electrical charge (the subunits are polycations) or the build-in of Cl^- ions (note that the formation of the subunits mainly occurs by the hydrolysis of the $FeCl^{2+}$ complex, cf.[2]). The subunits form stable type (b) aggregates of about 10 nm. They slowly alter further by progressive polymerization, reduction of charge by OH^- uptake and exchange of Cl^- for OH^-. All this results in the increase of the hydrolysis ratio, $n = OH^-/Fe$, of the particles. It is discernible by a steady decrease of the pH of the liquid phase (Fig. 1).

(ii) Disturbed states are induced by NaOH addition. The flocculation threshold ($n \sim 2.7$; cf. [2]) is locally approached and a fraction of the Fe(III) (about 16%; see Tab. 1) forms large objects that are similar to type (c) associations ("flock-like" particles). However, these inhomogeneities relax within several hours to days. Relaxation is supported by the pH decrease (Fig. 1).

Before the CR minimum at 31 h, the behavior of the colloids is governed by process (ii), i. e. the dissaggregation of the flock-like objects. This is indicated by a steep CR decrease (Fig. 1) and a decrease in particle size (Fig. 2). After the CR minimum, the behavior is controlled by a slow growth process (Fig. 1, Fig. 2, Tab. 1). It may be a growth of the type (b) aggregates due to the capture of additional type (a) subunits. Another explanation might be Ostwald ripening of the type (a) subunits.

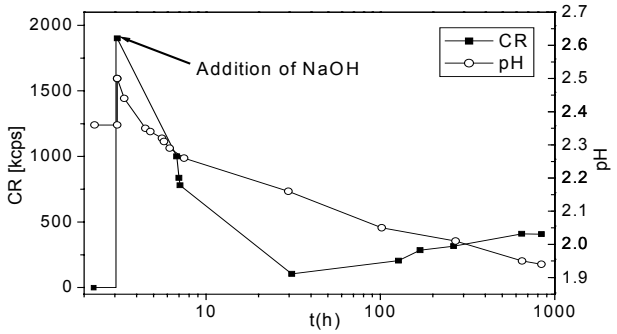

Fig. 1: Scattered light intensity (count rate, CR) and pH after addition of NaOH.

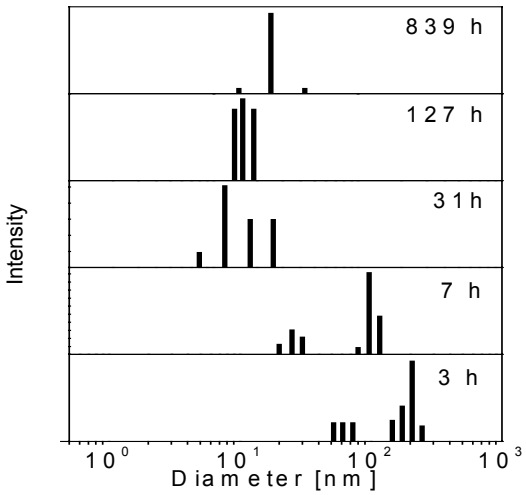

Fig. 2: Particle size distribution at several times after the addition of NaOH.

Tab. 1: Fraction of iron removable by centrifugation at 40,000 rpm (particles > 10 nm).

Time after NaOH addition [h]	Removable Fe fraction [%]
3	16
96	19
264	30
648	41

REFERENCES

[1] Schwyn, B. (1983) PhD thesis, ETH Zürich.
[2] Tchoubar, D. *et al.* (1991) *Langmuir* **7**, 398-402.

Formation of iron-containing colloids by the weathering of rock material

H. Zänker, T. Arnold, G. Hüttig

ABSTRACT. The direct formation of iron-containing secondary mineral colloids at the mineral-water interface by the weathering of rock material is an alternative to the well-known mechanism of colloid formation in the bulk of water bodies. Also colloids produced by this mechanism can significantly influence the transport of contaminants such as actinides.

EXPERIMENTAL. The formation of colloids during the weathering of ground phyllite was investigated. Tab. 1 gives the mineralogical composition of this phyllite. The rock material was jaw-crushed and sieved. The fraction of 63 to 200 µm was used. An amount of 24 g of ground phyllite was suspended in 600 mL of Milli-Q water. The material was "pre-washed" two times by centrifugation and resuspension. The pre-washed suspension was then shaken at a frequency of 280 min^{-1} for 87 h (oxic conditions, pH = 8.4). Aliquots of the suspension were centrifuged at different centrifugal accelerations between 500 x g and 46,000 x g for 1 h. Well-defined volumes of the supernatant were removed with a pipette and analyzed by light scattering, ICP-MS, and AAS. From the centrifugal acceleration and the mineral density, the maximum hydrodynamic diameter of mineral particles still present in the supernatant can be calculated (see Tab. 1 in [1]). A comparison of the measured removal of the chemical elements from the solutions with such calculations provides information on the chemical composition of the particles and the particle size in the sample. A size range of 10^1 to 10^2 nm is covered by the 500 x g to 46,000 x g centrifugations.

RESULTS. The chemical elements can be assigned to three groups: Group 1: Ca, Na, Group 2: Al, Fe, Si, Mn, Y and Group 3: K, Mg. The group 1 elements cannot be reduced by centrifugation. They occur as truly dissolved species. The concentrations of the group 2 elements behave similar to the scattered light intensity. They decrease on centrifugation, i.e. they are primarily in a colloidal form. The behavior of the group 3 elements lies in-between; a small fraction of them is removable by centrifugation, another fraction is not. These elements occur in both dissolved and colloidal forms. Column 2 of Tab. 2 gives the concentration differences between the supernatants of the 500 x g and the 46,000 x g centrifugations, $c_{500xg} - c_{46000xg}$. These differences represent the concentration and chemical composition of the 10^1 to 10^2 nm colloids. However, differentiation between primary and secondary mineral colloids is necessary. Indicators of primary mineral colloids are K, Mg and Na (these elements are very unlikely to form secondary minerals under the given conditions; any colloid-borne fractions of them in the samples should result from primary minerals, i.e. from unweathered phyllite constituents). K is indicative of muscovite, Mg of chlorite and Na of albite (cf. Tab. 1). The concentrations of the colloid-borne Al, Fe and Si can be "corrected" for their fractions caused by the primary minerals chlorite, muscovite and albite using the stoichiometric ratios between K, Mg, Na and Al, Fe, Si of these minerals (Tab. 1). Column 3 of Tab. 2 gives the results after this correction. Large amounts of colloids of the 10^1 to 10^2 nm size class were found in the suspension of ground phyllite after a weathering time of 87 h. The solution concentration of the secondary mineral colloids was as high as 10 mg/L. The mineralogical composition of the secondary mineral colloids is assumed to be:

Aluminum: Aluminosilicates, amorphous $Al(OH)_3$, gibbsite,
Silicon: Aluminosilicates, possibly iron silicates and iron-alumino silicates,
Iron: Ferrihydrite, possibly iron silicates and iron-alumino silicates,
Manganese: Manganese oxyhydroxides.

The colloids were stable over longer periods of time, even under the conditions of a highly concentrated suspension of ground rock.

CONCLUSIONS. The direct formation of iron-containing secondary mineral colloids at the mineral-water interface by the weathering of rock material is an alternative to the well-known mechanism of colloid formation in the bulk of water bodies as for instance in natural mixing zones. This direct mechanism is of relevance for colloid production during the weathering of freshly crushed rock in the unsaturated zone such as crushed rock in mine dumps. It can significantly contribute to the overall colloid inventories of natural oxic waters. Iron-containing colloids produced by this mechanism can influence the transport of contaminants such as actinides since they have a large specific surface area and a high sorption affinity.

Tab. 1: Mineralogical composition of the investigated phyllite.

Mineral	Chemical Formula	Conc. [vol.%]
Quartz	SiO_2	48
Chlorite	$(Mg_{2.4}Fe_{2.2}Al_{1.4})[Si_{2.5}Al_{1.4})O_{10}/(OH)_8$	25
Muscovite	$KAl_2(OH)_2AlSi_3O_{10}$	20
Albite	$NaAlSi_3O_8$	5
Opaq. min.	-	2

Tab. 2: Differences c500xg – c46000xg for the colloid-borne elements without and with correction for the calculated inventories of unreacted rock constituent colloids (average of the results of two parallel experiments).

Element	Concentration $c_{500xg} - c_{46000xg}$ [mg/l]	
	without correction	with correction
Al	9.41	2.95
Fe	4.27	2.76
K	2.55	-
Mg	0.73	-
Mn	0.073	0.073
Si	10.8	4.5
Y	0.002	0.002
Sum	27.8	10.3

REFERENCES

[1] Zänker, H. (2003) *Report FZR-400*, p. 48.

Colloid-chemical characterization of nanoparticles formed by $[Ti_2W_{10}PO_{40}]^{7-}$ and chitosan

W. Richter, H. Zänker, P. Krotká[1], Z. Matějka[1], A. Röllich[2], H. Stephan[2]

[1]Institute of Chemical Technology, Prague, Czechia; [2]Institute of Bioinorganic and Radiopharmaceutical Chemistry, Dresden, Germany

ABSTRACT. Nanoparticles formed of the Keggin type cluster anion $[Ti_2W_{10}PO_{40}]^{7-}$ with the polysaccharide chitosan have been characterised by photon correlation spectroscopy (PCS), scanning electron microscopy SEM, filtration and centrifugation experiments. Experimental results indicate the formation of particles in the range from 40 to 300 nm.

Organic modification of polyoxometalates (POMs) appears highly attractive to develop metallic drugs [1]. Thus, starch and liposome encapsulated POMs show suitable biocompatibility, enhanced chemical stability and improved antitumoural activity [2, 3]. Recently, we found that $[Ti_2W_{10}PO_{40}]$/chitosan associates have efficiently been incorporated by tumour cells [4]. Chitosan is a linear polysaccharide composed of randomly distributed ß-(1-4)-linked D-glucosamine (deacetylated unit) and N-acetyl-D-glucosamine (acetylated unit). Low molecular weight chitosan is well-soluble in water. However, when $K_7[Ti_2W_{10}PO_{40}]$ (POM1) is added, nanoparticles may be formed. In this paper, we want to report on the colloid-chemical characterization of these particles.

EXPERIMENTAL. Chitosan (YC-100, $M_r \sim 10^4$ g/mol) was supplied by YDC company (Seoul, South Korea). The experiments were carried out with two solutions: solution A (50 mg/l chitosan and $1 \cdot 10^{-4}$ M POM1) and solution B (500 mg/l chitosan and $1 \cdot 10^{-4}$ M POM1). Both solutions were diluted with water by a factor of 10. These diluted solutions were investigated by photon correlation spectroscopy, PCS (BI-90, Brookhaven Instruments), filtration (Nuclepore filters, Costar), centrifugation (Avanti J-20 XP, Beckman), scanning electron microscopy (Hitachi S-4800) in order to determine their content of colloidal particles and to identify the particle size. The centrifugates, filtrates and filter cakes were analyzed by ion chromatography (Jasco), TOC-analyser Multi NC and inductively coupled plasma mass spectrometry, ICP-MS (Elan 9000, Perkin Elmer).

RESULTS. The filtration experiments of the solutions suggested that all particles are smaller than 1 µm. Fig. 1 shows an SEM micrograph of the deposits on a 100-nm filter confirming the existence of particles of the 100-nm size range. PCS measurements in the solution revealed the presence of colloid particles of 40 to 300 nm in diameter. Fig. 2 shows the particle size distribution from solution A received by PCS measurement analyzed by the CONTIN method [5]. Centrifugation experiments were performed with both solutions: Solution A with an excess of POM1 and solution B with an excess of chitosan. The preparative Beckman centrifuge was used as an "analytical" centrifuge in this experiment according to the procedure described in [6].

As one can see, comparable size distribution of particles has been found (cf. Table 1). This finding points to the formation of well-defined associates between chitosan and POM1. The cell uptake of the cluster anion $[Ti_2W_{10}PO_{40}]^{7-}$ is remarkably enhanced in the case of these nanosized associates (causing higher anti-tumoral activity).

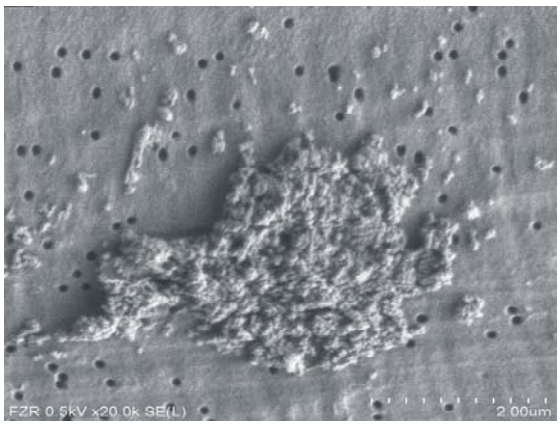

Fig. 1: Scanning electron micrograph of $[Ti_2W_{10}PO_{40}]$/chitosan associates (filter pores = 100 nm).

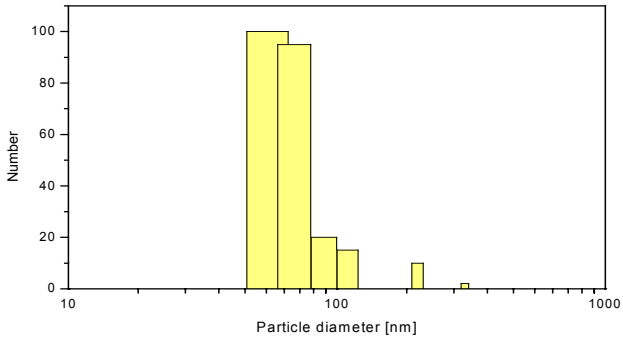

Fig. 2: Particle size distribution as obtained by photon correlation spectroscopy (PCS) for solution A.

Tab. 1: Particle size distribution as obtained by centrifugation assuming that the density of the particles averages 1.1 g/cm^3.

Particle size class [nm]	Frequency [mass %]	
	Solution A	Solution B
> 370	0.8	2.1
370 .. 224	9.7	2.4
224 .. 132	18.1	18.2
132 52	25.6	37.3
< 52	45.8	40.0

REFERENCES

[1] Rhule, J. T. *et al.* (1998) *Chem. Rev.* **98**, 327-357.
[2] Wang, X. *et al.* (2003) *Dalton Trans.,* 957-960.
[3] Yang, Y. *et al.* (2004) *Trans. Metal Chem.* **29**, 96-99.
[4] Stephan, H. *et al.* (2005) *FZR–IBRC Annual Report 2004*, in press.
[5] Provencher, S.W. (1979) *Makromol. Chem.* **180,** 201-209.
[6] Zänker, H. (2003) *Report FZR-400*, p. 48.

Determination of the hydration number of the first solvation shell of Am^{3+}

G. Geipel, Th. Stumpf[1]

[1]Institute for Nuclear Waste Disposal, Karlsruhe, Germany

ABSTRACT. The fluorescence lifetime Am^{3+} species depends on the concentration of D_2O in the solution. This effect was used to re-establish an equation to use the fluorescence decay constant to calculate the number of water molecules in the first solvation shell.

The first studies about a relationship between the fluorescence decay constant and the number of water molecules in the salvation sphere were performed by Kimura and Choppin [1] for Cm^{3+} species. The fluorescence lifetime of UO_2^{2+}, Cm^{3+} and Eu^{3+} species is much longer than the fluorescence lifetime of the aquatic Am^{3+} species. It was described in the literature [2] to be $\tau_{1/2}$ = 24.6±0.6 ns. The authors [2] used laser pulses with a duration of about 15 ns (excimer laser) for excitation of the studied samples. Therefore it could be concluded that the measured fluorescence lifetime would be influenced by the duration of the excitation pulse. Additionally only four measurements were performed where water was partly exchanged by D_2O. In order to establish a somewhat better relationship between the fluorescence decay constant and the number of water molecules in the first salvation shell, the measurements were repeated.

EXPERIMENTAL. A basic solution of Am^{3+} in 0.1 M $HClO_4$ was diluted by increasing amounts of pure (99.9%) D_2O. The concentration of this basic solution was in the range of 1.0 x 10^{-5} M. The samples were excited with a 503.2 nm laser pulse generated by optical parametrical oscillation of a BBO-crystal, which is pumped by the third harmonic of a Nd:YAG laser (MOPO system, Spectra Physics). The pulse duration at the output is in the range of about 3 ns. The emitted fluorescence was measured by an intensified CCD camera system after spectral resolution. The exposure time of the camera was set to 500 ns and a delay increment of 10 ns was used (exception pure aquatic solution: 5 ns). The fluorescence Spectrum was measured in the range 625 nm to 770 nm, corresponding to the maximum of the fluorescence emission at around 690 nm ($^5D_1$ => $^7F_1$). The applied laser energy was adjusted to 4.4 ± 0.1 mJ and 40 shots were collected for each spectrum. At each delay time 5 spectra were averaged.

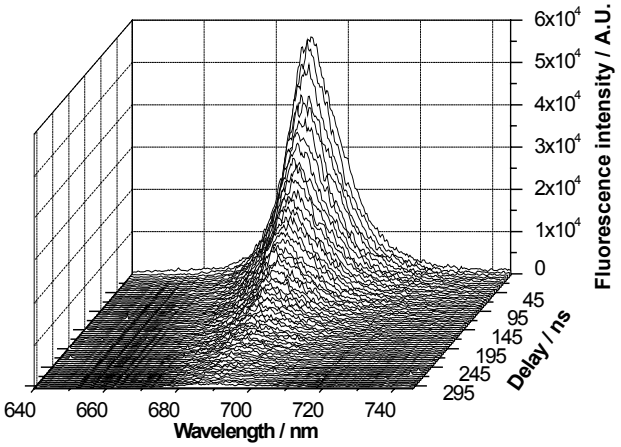

Fig. 1: Time-resolved fluorescence spectrum of Am^{3+} in 75% D_2O.

RESULTS AND DISCUSSION. In Fig. 1 a typical time-resolved fluorescence spectrum is shown. Clearly the emission at 690.8 nm can be observed.

From the dependence of the signal integrated in the complete measured wavelength range on the delay time the fluorescence lifetime was calculated (Fig. 2). The obtained fluorescence decay constants (1/τ) are summarized in table 1.

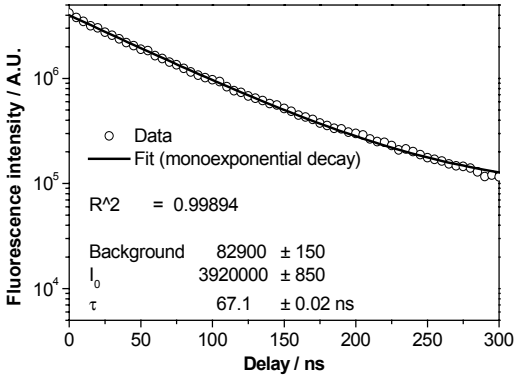

Fig. 2: Fluorescence decay of the spectrum in Fig. 1.

Tab. 1: Fluorescence decay constants as function of the D_2O concentration.

% D_2O	n_{H_2O}	k_{obs} / s^{-1}
0	9	4.57 x 10^7
25	6.75	3.60 x 10^7
40	5.4	2.91 x 10^7
50	4.5	2.58 x 10^7
62.5	3.375	2.07 x 10^7
70	2.7	1.72 x 10^7
75	2.25	1.49 x 10^7
87.5	1.125	1.16 x 10^7
93.75	0.563	8.76 x 10^6
100	0	6.20 x 10^6

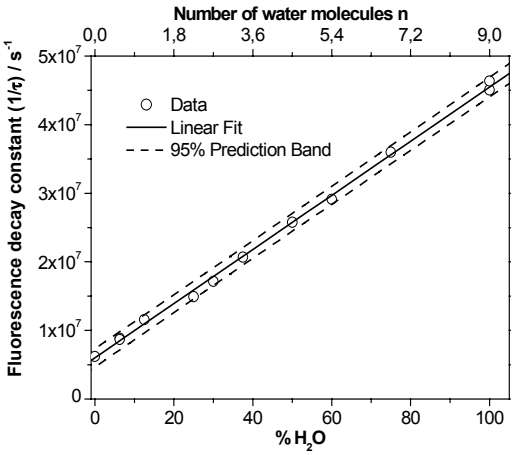

Fig. 3: Fluorescence decay as function of the water concentration for Am^{3+}.

According to Fig. 3 we establish the following relationship (1):

$$n_{H_2O} = 2.27 \cdot 10^{-7} \times k_{obs}(\mathrm{Am}) - 1.32 \qquad (1)$$

REFERENCES

[1] Kimura, T.; Choppin, G. (1994) *J. Alloys Comp.* **213/214**, 313-317.
[2] Kimura, T.; Kato, Y. (1998) *J. Alloys Comp.* **271-273**, 867-871.

Neptunium(V) reduction by various natural and synthetic humic substances

K. Schmeide, G. Geipel, G. Bernhard

ABSTRACT. The time dependence of the reduction of Np(V) to Np(IV) by natural and synthetic humic substances was studied under anaerobic conditions between pH 3.5 and pH 9.

Synthetic humic acid (HA) model substances with distinct redox properties [1] have shown higher Fe(III) and U(VI) redox capacities compared to natural Aldrich HA [1]. In this work, the stability of Np(V) in contact with various natural and synthetic humic substances is studied.

EXPERIMENTAL. Synthetic HA type Cat-Gly (oxidation product from catechol and glycine), type Hyd-Glu (oxidation product from hydroquinone and glutamic acid) and type Hyd-Glu-PB (HA with blocked phenolic/acidic OH groups) [1] were applied together with natural humic substances Aldrich HA (AHA) and Kranichsee FA (KFA) [2]. Experimental conditions: $[Np]_{tot} = 1 \cdot 10^{-4}$ M, [HA] = 100 mg/L, I = 0.1 M ($NaClO_4$), pH 3.5-9.0, N_2 atmosphere, exclusion of light.

RESULTS. The reduction of Np(V), determined by liquid-liquid extraction with 2-thenoyltrifluoroacetone, is shown in Figs. 1 and 2. The synthetic HA type Cat-Gly and Hyd-Glu show a stronger Np(V) reduction compared to the natural humic substances AHA and KFA.

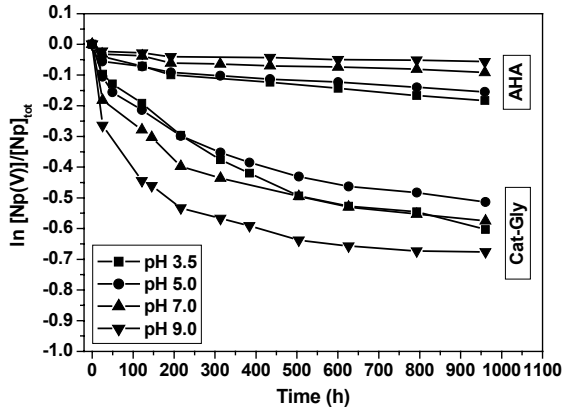

Fig. 1: Reduction of Np(V) to Np(IV) by HA type Cat-Gly and AHA.

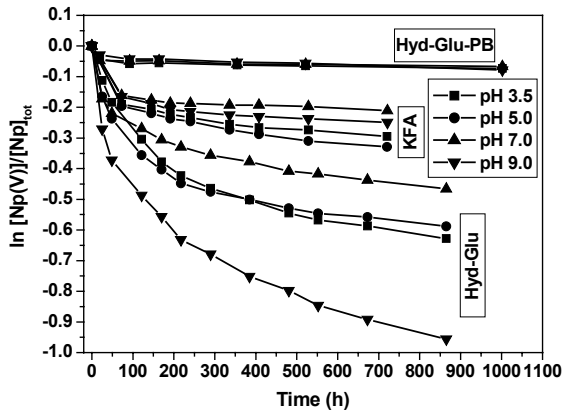

Fig. 2: Reduction of Np(V) to Np(IV) by HA type Hyd-Glu, HA type Hyd-Glu-PB and KFA.

The strongest Np(V) reduction is found for the HA type Hyd-Glu at pH 9. After 865 h (36 d) 62% of the Np(V) is converted to Np(IV). Also in case of HA type Cat-Gly, the strongest Np(V) reduction is found at pH 9 (961 h (40 d), 49% Np(IV)). The redox capacity, which decreases in the sequence synthetic HA > KFA > AHA, can be correlated to the phenolic/acidic OH group contents of the humic substances which are compiled in [3]. A comparable correlation between the phenolic/acidic OH group content of various synthetic and natural HA and their Fe(III) and U(VI) redox capacities was observed in [1].

To verify the influence of phenolic/acidic OH groups on the redox behavior of humic substances, the synthetic HA with blocked phenolic/acidic OH groups of type Hyd-Glu-PB was applied. The amount of Np(IV) formed by the modified HA type Hyd-Glu-PB is very small compared to the strong Np reduction by the unmodified HA type Hyd-Glu (Fig. 2). This again shows that the phenolic/acidic OH groups play a major role for the redox behavior of humic substances.

Laser-induced photoacoustic spectroscopy (LIPAS) was applied for direct spectroscopic detection of Np species in the sample solutions. Exemplary for all samples the spectrum of Np(IV,V)/HA type Cat-Gly equilibrated at pH 3.5 is shown in Fig. 3. As expected the spectrum shows the Np(IV) humate complex at 967 nm together with the NpO_2^+ aquo ion at 980 nm. In addition, in all LIPAS spectra obtained from solutions equilibrated between pH 3.5 and pH 9, a further peak at about 1018 nm is observed which cannot be assigned to a certain Np species so far.

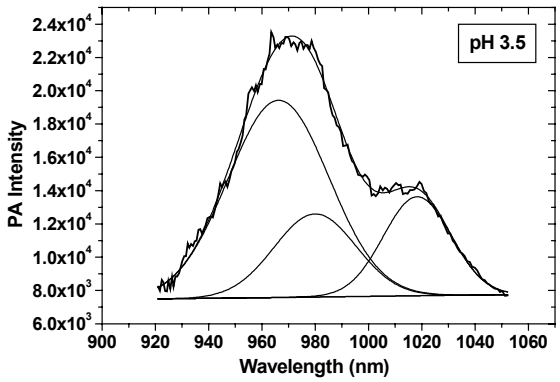

Fig. 3: Photoacoustic spectrum of Np(IV,V)/HA type Cat-Gly.

By application of the synthetic HA with distinct redox properties actinides can be stabilized in lower oxidation states, e.g. in complexation and sorption studies.

ACKNOWLEDGEMENTS. This work was supported by the BMWA (No. 02E9673) and the EC Commission (No. FIKW-CT-2001-00128).

REFERENCES

[1] Sachs, S. *et al.* (2004) *Report FZR–399*, pp. 9-25.
[2] Schmeide, K. *et al.* (1998) *FZKA 6124*, pp. 161-195.
[3] Schmeide, K. *et al.* (2005) *FZKA 7070*, in press.

Complex formation of neptunium(V) with 4-hydroxy-3-methoxybenzoic acid studied by Time-Resolved Laser-Induced Fluorescence Spectroscopy with ultra-short laser pulses

D. Vulpius, G. Geipel, L. Baraniak, G. Bernhard

ABSTRACT. The complex formation of neptunium(V) with 4-hydroxy-3-methoxybenzoic acid (vanillic acid) was studied by time-resolved laser-induced fluorescence spectroscopy with ultra-short laser pulses using the fluorescence properties of 4-hydroxy-3-methoxybenzoic acid. A 2:1 complex of neptunium(V) with 4-hydroxy-3-methoxybenzoic acid was found. The formation constant of this complex was determined to be log β_{210} = 7.33 ± 0.10 at an ionic strength of 0.1 mol/l ($NaClO_4$) and at 21 °C.

In a previous contribution [1] we reported on our studies of the excited-state proton transfer of several hydroxybenzoic acids. We ascertained that these reactions have to be considered at the fluorescence spectroscopic determination of complex formation constants. Now, we have found that 4-hydroxy-3-methoxybenzoic acid (vanillic acid) does not undergo excited-state reactions at pH values above 5. Thus, expensive kinetic calculations are not necessary. Therefore, we studied the complex formation of neptunium(V) with 4-hydroxy-3-methoxybenzoic acid at pH 6.00.

RESULTS. The fluorescence spectra of 4-hydroxy-3-methoxybenzoic acid as a function of the neptunium(V) concentration at pH 6.00 are shown in Fig. 1. After correcting the inner filter effects [2], the graphical analysis of the logarithmic mass action law results in a slope of 1.97 ± 0.03 (see Fig. 2), which indicates a metal-ligand ratio of 2:1 in the complex. This fact is also confirmed by the Stern–Volmer plot (see Fig. 3). All results are summarized in Tab. 1. Consequently, the formation constant log β_{210} of the complex is 7.33 ± 0.10 at an ionic strength of 0.1 mol/l ($NaClO_4$) and at 21 °C.

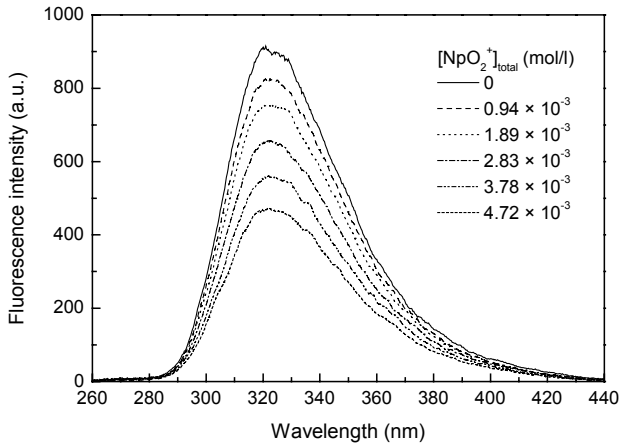

Fig. 1: Fluorescence spectra of 4-hydroxy-3-methoxybenzoic acid (VNA) as a function of the neptunium(V) concentration recorded 125 ps after reaching the fluorescence maximum ([VNA] = 1.0×10^{-4} mol/l, I = 0.1 mol/l ($NaClO_4$), pH = 6.00 ± 0.05, t = (21 ± 1) °C).

ACKNOWLEDGEMENTS. This study was supported by the Deutsche Forschungsgemeinschaft under contract no. BE 2234/3-1 and BE 2234/3-2.

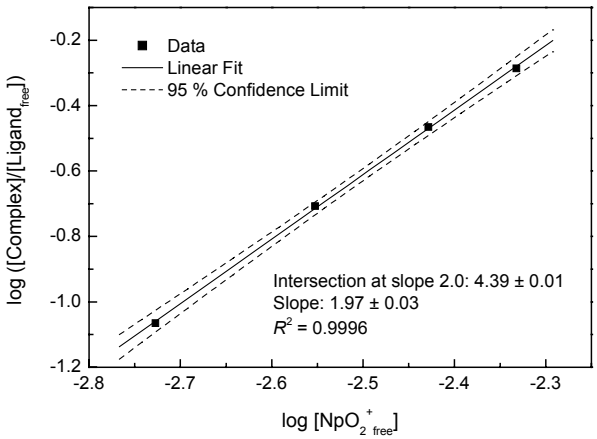

Fig. 2: Graphical analysis of the logarithmic mass action law for the complex formation of neptunium(V) with 4-hydroxy-3-methoxybenzoic acid started from the fluorescence spectra in Fig. 1.

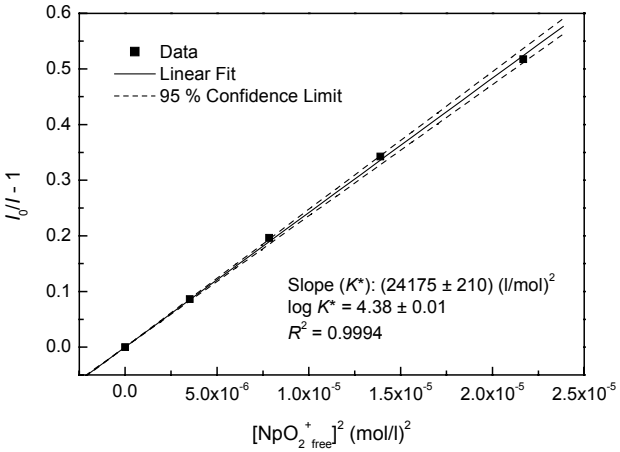

Fig. 3: Stern–Volmer plot for the complex formation of neptunium(V) with 4-hydroxy-3-methoxybenzoic acid started from the fluorescence spectra in Fig. 1.

Tab. 1: Results of the fluorescence spectroscopic determination of the stability constant of the 2:1 complex of neptunium(V) with 4-hydroxy-3-methoxybenzoic acid at an ionic strength of 0.1 mol/l ($NaClO_4$), at a pH value of 6.00 ± 0.05 (corresponds to $-\log [H^+] = 5.94 \pm 0.05$), and at (21 ± 1) °C. The indicated uncertainties result for log K* from the calculation modus and for log K and log β_{210} from the law of error propagation and correspond to the standard deviation multiplied by 1.96.

	Graphical analysis of the MAL[(a)]	Stern–Volmer plot	Numerical analysis of the MAL[(a)]
log K*	4.39 ± 0.01	4.38 ± 0.01	4.39 ± 0.02
log K	−1.55 ± 0.10	−1.55 ± 0.10	−1.55 ± 0.10
log β_{210}	7.33 ± 0.10	7.33 ± 0.10	7.33 ± 0.11

(a) MAL = Mass action law.

REFERENCES

[1] Vulpius, D. *et al.* (2004) *Report FZR–400*, p. 8.
[2] Gauthier, Th.D. *et al.* (1986) *Environ. Sci. Technol.* **20**, 1162–1166.

Formation of stable Cu(II)-complexes with dendritic oxybathophenanthroline ligands

H. Stephan[1], G. Geipel, G. Bernhard, U. Hahn[2], F. Vögtle[2]

[1]Institute of Bioinorganic and Radiopharmaceutical Chemistry, Dresden, Germany; [2]University of Bonn, Bonn, Germany

ABSTRACT. Hydrophobic dendritic oxybathophenathroline ligands (generation 0…4) have been synthesized. The complexation behaviour towards Cu(II) has been studied using liquid-liquid extraction experiments and time-resolved laser-induced fluorescence spectroscopy (TRFLS). The formation of 1:3 complexes (metal:ligand) having high stability has been proven in organic media.

Derivatives of 1,10-phenathroline and its metal complexes are of considerable interest in bioinorganic chemistry, biology and medicine [1]. In this nexus, dendritic modification (Scheme 1) is gaining in importance opening the way of tailoring complexation and solubility behaviour. Ruthenium(II) complexes containing dendritic 4,7-bis(benzyloxy)-1,10-phenanthroline show interesting luminescence and redox properties [2]. Octahedral assemblies can be obtained by coordination of phenanthroline ligands having branched units in the 3,8-position with certain metal ions [3]. Recently, bischelates of dendritic 2,9-disubstituted phenanthroline derivatives with copper(I) have been described [4].

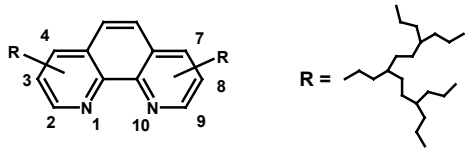

Scheme 1: Suitable positions for dendritic modification of 1,10-phenanthroline.

Here, we want to report the complexation behaviour of dendritic oxybathophenanthroline ligands towards copper(II).

RESULTS AND DISCUSSION. Dendritic oxybathophenanthroline ligands from zero to the fourth generation (cf. Scheme 2; only generation 1 is shown) were synthesized by addition of 2 equiv. of the corresponding dendritic benzylbromides to 1 equiv. deprotonated 4,7-bis(4´-hydroxyphenyl)-1,10-phenanthroline (NaH) dissolved in DMF.

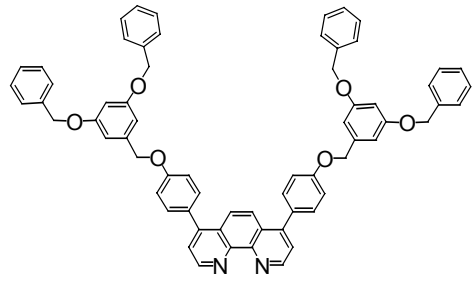

Scheme 2: Dendritic oxybathophenanthroline ligand (generation 1).

Liquid-liquid extraction studies in the system $Cu(NO_3)_2$ / MES-NaOH buffer (pH = 5.3) / ligand / $CHCl_3$ using ^{64}Cu for the determination of copper concentration have been performed. The higher the generation of the dendritic ligand the higher the extraction efficiency of Cu(II) clearly indicating a dendritic effect. The results obtained from liquid-liquid extraction point to fast kinetics of complexation and the formation of 1:3 complexes (Cu(II):ligand) in the organic phase. This finding has been corroborated by spectroscopic investigations using TRLFS experiments. Spectroscopic titration of dendritic ligands with copper(II) gives the evidence of clean 1:3 complex formation for all dendritic ligands investigated. It can be seen from Fig.1 that the intensity of the emitted fluorescence signal of the dendritic ligand (excitation wavelength: 266 nm) is reduced with increasing copper concentration. At the stoichiometry of 1:3 (Cu(II):ligand) the fluorescence of the ligand is almost disappeared pointing to the formation of highly stable Cu(II) complexes in the organic media.

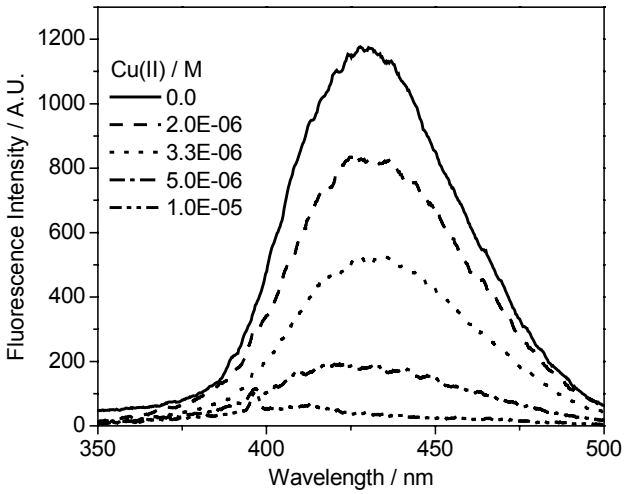

Fig. 1: Time resolved fluorescence spectra of oxybathophenanthroline ligand (generation 1) in dependence of $Cu(CF_3SO_3)_2$ concentration in $CHCl_3$.

The results obtained for the copper complexation with hydrophobic dendritic ligands have been encouraged us to develop water-soluble analogues having PEG arms as branching units in view of binding the diagnostically and therapeutically relevant radioisotopes ^{64}Cu and ^{67}Cu.

REFERENCES

[1] Luman, C. R.; Castellano, F. N. (2004) In: *Comprehensive Coord. Chem.*, *Vol. 1,* 25-39.
[2] Serroni, S. *et al.* (1994) *Gazz. Chim. Ital.* **124**, 423-427.
[3] Tor, Y. (2003) *C. R. Chim.* **6,** 755-766.
[4] Gumienna-Kontecka, E. *et al.* (2004) *Inorg. Chem.* **43**, 3200-3209.

Study of complexation behavior of a hexadentate bispidine derivative towards neptunium

T. Suzuki[1], G. Geipel, A. Rossberg, H.Stephan[2], S. Juran[2], P. Comba[3]

[1]The University of Kitakyusyu, Fukuoka, Japan; [2]Insitute of Bioinorganic and Radiopharmaceutical Chemistry, Dresden, Germany; [3]Department of Inorganic Chemistry, Heidelberg, Germany

ABSTRACT. EXAFS measurements on Np-bispidine complexes were carried out at BM20 at the ESRF. The EXAFS spectra of the three samples ($5.0x10^{-4}$ mol/L) were measured in fluorescence mode with a 13-element Ge solid-state detector.

Hexadentate bispidine ligands N2Py4 (Fig. 1) having amine and pyridine nitrogen as donor atoms show interesting complexation behavior [1]. Such ligands seem to be very promising in view of lanthanides/actinides separation. In this nexus, it is desirable to have the information about the binding pattern formed for lanthanides and actinides. Here, we want to report the complexation behavior of the hexadentate bispidine ligand N2Py4 towards neptunium.

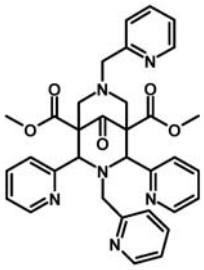

Fig.1: Structure of hexadentate bispidone (N2Py4).

EXPERIMENTAL. The metal:ligand ratios and pH values of the studied samples are summarized in Table 1. The concentration of the metal was adjusted to $5.0x10^{-4}$ mol/L. The measurements were performed at the ROBL Beamline at the ESRF. For EXAFS the fluorescence signal at the Np-L_{III} edge was used.

Tab. 1: Metal:ligand ratio and pH of the samples.

Sample	Np	Ligand (N2Py4)	pH
Np4-01	1	2	4
Np4-02	1	1	3
Np4-03	1	2	2

RESULTS AND DISCUSSION. The EXAFS spectra and the corresponding Fourier transformations (FT) are shown in Fig. 2. The resulting structural parameters are summarized in Table 2. In the samples at pH 4 and pH 3 a residual was found which can be interpreted as a radial Np–O distance at 2.15 ± 0.02 Å.

For the sample at pH 4 an additional peak at 4.6 Å arises in the FT. This backscatter contribution was not found in the other two samples. The structural parameters of this sample were fitted again and the signal is assigned to a Np–Np interaction with a distance of 4.86 ± 0.02 Å (Table 2 last line). For the complex formed at pH 4 a polynuclear complex is suggested.

The formed complexes in the samples at pH 2 and 3 are assigned to be a mononuclear. For the sample at pH 2 the fit could be improved by inclusion of two carbon atoms (Table 3). For this sample and possibly also for pH 3 the proposed structure of the formed complex is shown in Fig. 3. The results support the suggestion on strong complex formation between actinyl ions and bispidone.

REFERENCES

[1] Bleiholder, C. *et al.* (2005) *Inorg. Chem.,* in press.

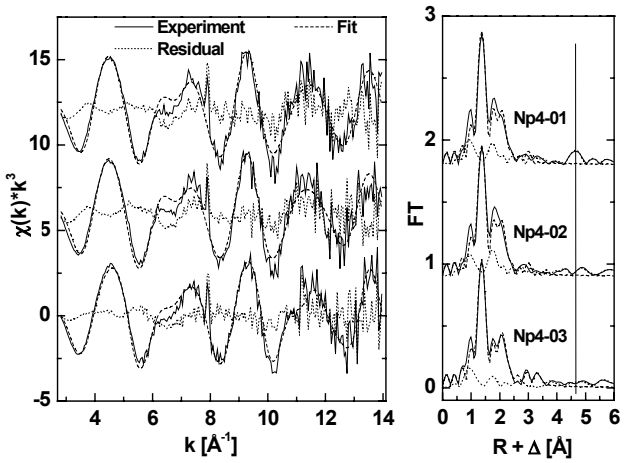

Fig. 2: EXAFS Spectra and FT's including the adjustment and residuals of the studied Np-(N2Py4)-complexes.

Tab. 2: EXAFS structural parameters for the fit in Fig. 2.

	Np-O_{axial}	Np-$Atom_{equatorial}$		
	R [Å]	Atom	N	R [Å]
pH 4	1.824(2)	N	4.9(6)	2.525(6)
pH 3	1.829(2)	N	4.7(5)	2.520(5)
pH 2 2.8-14	1.824(2)	N C_1 C_2	3.3(4) 3(1) 5(2)	2.528(5) 3.49(2) 3.69(1)
pH 4	1.825(3)	N Np	5.7(6) 1	2.515(6) 4.86(1)

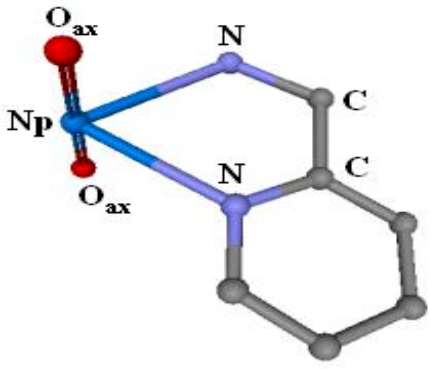

Fig. 3: Structural fragment of a hypothetical mononuclear Np-complex as found for sample at pH 2. Atoms of minor relevance to the ligand are not shown.

Complex formation of curium with adenosine 5'-triphosphate (ATP) studied by TRLFS

H. Moll, G. Geipel, G. Bernhard

ABSTRACT. Three Cm-ATP species, $M_pH_qL_r$, could be identified from the fluorescence emission spectra: CmH_2ATP^+, CmHATP, and $CmATP^-$. The formation constants of these complexes were determined to be $\log \beta_{121} = 16.86 \pm 0.09$, $\log \beta_{111} = 13.23 \pm 0.10$, and $\log \beta_{101} = 8.19 \pm 0.16$.

ATP is the major source of energy for cellular reactions. The amount of adenosine phosphates in living systems is in the 2-10 millimolar concentration range [1]. The fact that a special ATP-synthesizing enzyme has been located in membrane systems of cells [2] points to the importance of ATP for biosorption processes of actinides on cell membranes of microbes, *e.g.*, the biosorption process of Cm(III) on *D. äspöensis* [3]. The complex formation constants with trivalent actinides are unknown up to now.

EXPERIMENTAL. Adenosine 5'-triphosphate disodium salt was purchased from ACROS ORGANICS (analytical grade). The experiments were performed under N_2 atmosphere at 25 °C. As a background electrolyte 0.154 M NaCl was used. [Cm(III)] was set to $3x10^{-7}$ M. [ATP] was varied between $3x10^{-7}$ and $1.5x10^{-4}$ M. The pH was varied between 1.5 and 7.0. Time-resolved laser-induced fluorescence spectroscopy (TRLFS) was performed using a flash lamp pumped Ti:sapphire laser (Elight, Titania). Details on the experimental set-up are given in [3].

RESULTS. Fluorescence emission spectra of $3x10^{-7}$ M Cm(III) with $3x10^{-6}$ M ATP in 0.154 M NaCl in the pH range 1.5 to 7.0 are shown in Fig. 1

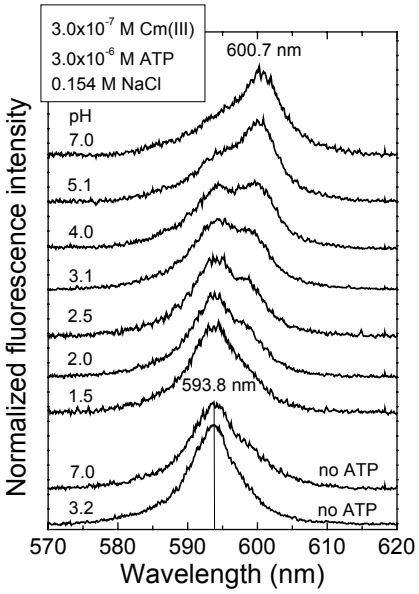

Fig. 1: Fluorescence emission spectra of $3x10^{-7}$ M Cm(III) in 0.154 M NaCl solution containing $3x10^{-6}$ M ATP at various pH; the spectra are scaled to the same peak area.

The Cm^{3+} aquo ion is characterized by a fluorescence emission band maximum at 593.8 nm. When adding ATP and changing the pH to 7.0, there is a pronounced red-shift of the emission, 6.9 nm, as a result of the complex formation. The series of samples at pH 4.5 revealed one Cm(III) peak with a maximum at 600.4 nm at ATP concentrations above $3x10^{-6}$ M. At pH 6.5 the peak maximum is shifted to 601.8 nm at ATP concentrations above $1.2x10^{-5}$ M. This might indicate the formation of different Cm-ATP species.

To describe the complex formation reactions in the system Cm(III)-ATP, we applied the factor analysis program code SPECFIT [4]. Input parameters for the data fitting were the known total concentrations of Cm^{3+}, ATP, the pH of each sample, and the protonation constants for ATP published in [5]. As result we derived a chemical model describing the ongoing processes in the Cm(III)-ATP system. It could be demonstrated that predominantly 1:1 complexes of the type $M_pH_qL_r$ (see Fig. 2) were formed under the given experimental conditions [6].

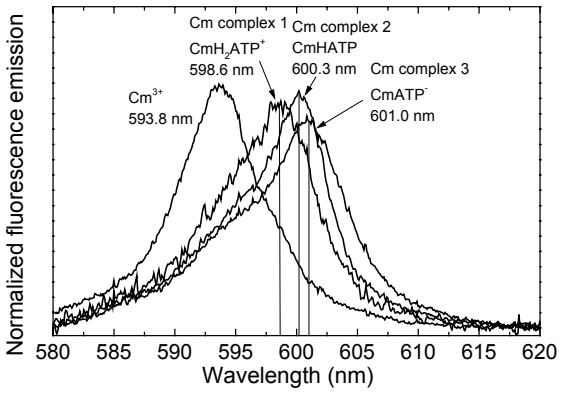

Fig. 2: TRLFS spectra of the single components in the Cm-ATP-system as derived by SPECFIT.

The dependencies found in the TRLFS data could be expressed by the following equilibria:

$$Cm^{3+} + ATP^{4-} + 2H^+ \leftrightarrow CmH_2ATP^+ \quad (1)$$

$$Cm^{3+} + ATP^{4-} + H^+ \leftrightarrow CmHATP \quad (2)$$

$$Cm^{3+} + ATP^{4-} \leftrightarrow CmATP^- \quad (3)$$

Formation constants for reactions (1) to (3) were calculated as $\log \beta_{121} = 16.86 \pm 0.09$, $\log \beta_{111} = 13.23 \pm 0.10$ and $\log \beta_{101} = 8.19 \pm 0.16$, respectively. In test solutions with an excess of ATP greater than 1:500 the TRLFS spectra give evidence for the existence of a further Cm-ATP species, presumably a 1:2 complex.

ACKNOWLEDGEMENTS. This work is supported by the BMWi (no. 02E9491).

REFERENCES

[1] Shanbhag, S.M. *et al.* (1987) *Inorg. Chim. Acta* **139,** 119-120.
[2] Purves, W.K. *et al.* (2003) *Life: The Science of Biology,* 7th Edition, Sinauer Associates, Inc. Publishers, Sunderland, MA, USA.
[3] Moll, H. *et al.* (2004) *Environ. Sci. Technol.* **38**, 1455-1459.
[4] Binstead, R.A. *et al.* (2003) SPECFIT Global Analysis System Version 3.0.34.
[5] Oscarson, J.L. *et al.* (1995) *J. Solution Chem.* **24**, 171-200.
[6] Moll, H. *et al.* (2005) *Inorg. Chim. Acta*, in press.

Investigation of the complex formation of uranium with selected amino acids using UV-vis absorption spectroscopy

A. Günther, G. Geipel, G. Bernhard

ABSTRACT. We studied the complexation of uranium (VI) with the amino acids glycine and cysteine by UV-vis spectroscopy at pH 3. The identified 1:1 and 1:2 complexes showed absorption bands shifted to higher wavelength compared to the free uranyl ion. The formation constants were calculated.

For determination of the uranium speciation in biosystems like plants and bacteria we investigate the interaction of uranium(VI) with biorelevant model compounds. The amino acids have several functional groups in the fundamental chain or the side chains, which can bind uranium.

EXPERIMENTAL. The absorption experiments of the uranium/glycine and uranium/cysteine systems were performed using a CARY5G UV-vis-NIR spectrometer (Varian Co.). The measurements were performed on $1 \cdot 10^{-3}$ M uranium perchlorate. The concentration of the amino acids varied between 0 and $3 \cdot 10^{-1}$ M. All absorption spectra were measured at an ionic strength of I = 0.5 M
($NaClO_4$) and at pH 3.

RESULTS. Fig. 1 shows the absorption spectra of uranium(VI) as a function of the total glycine concentration at pH 3 as an example. The spectra are background-corrected.

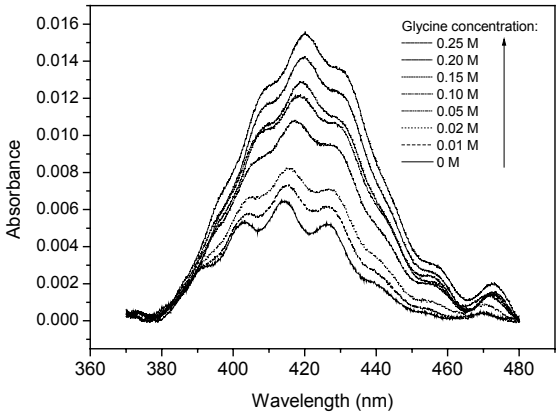

Fig. 1: UV-vis spectra of uranium(VI) as a function of the glycine concentration at pH 3.

The investigated uranium/amino acids systems show an increase in absorption and a red shift of the absorption maxima compared to the free uranyl cation. This indicate the formation of uranyl complex species with this amino acids. 81.4 % of glycine and 92.3 % of cysteine are present as zwitter-ion at pH 3. The reaction of UO_2^{2+} with the amino acids can be written as:

$$UO_2^{2+} + x\ {}^{+}NH_3(R)COOH^{-} \overset{\log \beta_{1x}}{\Rightarrow} [UO_2(NH_3(R)COO)_x]^{2+}$$

Using the infomation of the deprotonation constants of the –COOH group and the $–NH_3^+$ group [1] we determinated the stoichiometry of the formed uranyl complexes with the factor analysis program SPECFIT [2].
We found two species, a 1:1 and a 1:2 complex in both U(VI)/amino acid systems. The complex formation constants in the uranium/glycine system are $\log\beta_{11} = 1.91 \pm 0.09$ for UO_2Gly^{2+} and $\log\beta_{12} = 2.62 \pm 0.11$ for $UO_2(Gly)_2^{2+}$. In a first calculation we determined $\log\beta_{11} = 1.41 \pm 0.09$ for UO_2Cys^{2+} and $\log\beta_{12} = 2.35 \pm 0.07$ for the second species $UO_2(Cys)_2^{2+}$. They are smaller than the constants of the glycine species.

Tab. 1: Main absorption bands of the complex species in comparison to the bands of free uranyl at pH 3.

UO_2^{2+}	391	402	414	427	439
UO_2Gly^{2+}	394	405	417	429	442
$UO_2(Gly)_2^{2+}$	398	409	420	433	444
UO_2Cys^{2+}	394	405	417	429	441
$UO_2(Cys)_2^{2+}$	397	408	420	432	444

The absorption maxima of the first complex are shifted by about three nm and those of the second complex by about six or seven nm in comparison to the bands of the free uranyl cation (Tab. 1). An example of the deconvolution of a measured sum spectra is shown in Fig. 2.

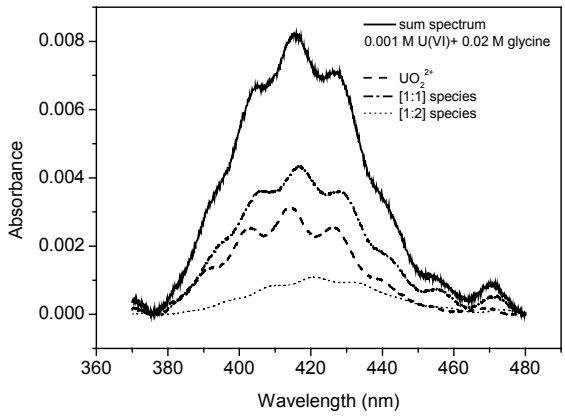

Fig. 2: Spectra of the single components of U(VI)/glycine system.

Furthermore, the 1:1 and 1:2 uranyl complexes of glycine and cysteine have a significantly higher absorbance at the selected wavelength in comparison to the free uranyl ion (Tab. 2).

Tab. 2: Molar extinction coefficients [L mol^{-1} cm^{-1}] of uranium (VI) species at different wavelengths.

	402 nm	414 nm	420 nm	433 nm
UO_2^{2+}	5.2	6.5	4.9	3.1
UO_2Gly^{2+}	6.8	8.9	8.7	6.2
$UO_2(Gly)_2^{2+}$	10.6	17.6	22.1	18.9
UO_2Cys^{2+}	8.7	10.6	9.8	6.2
$UO_2(Cys)_2^{2+}$	11.3	16.9	19.6	15.4

ACKNOWLEDGEMENTS. The autors thanks T. Birk for the preparation of the complex solutions.

REFERENCES

[1] Smith, R.W. ; Martell, A.E. (1998) *NIST Standard Reference Database 46 - Version 5.0.*, Gaithersburg.
[2] *SPECFIT 32* (2003) Spectrum Software – Associates.

Solving the structure of aqueous U(VI)-salicylate at pH 6 with Monte-Carlo Target Transformation Factor Analysis (MCTFA)

A. Rossberg, A.C. Scheinost

ABSTRACT. The structure of U(VI)-salicylate (SAL) complexes in aqueous solution is only poorly understood, because conventional EXAFS analysis methods failed. We use a novel approach, Monte-Carlo Target Transformation Factor Analysis (MCTFA) with multiple scattering paths to solve the structure of the 1:2 $UO_2SAL_2^{2-}$ complex at pH 6.

An aqueous solution of 0.05 M U(VI) and 0.1 M SAL was prepared from stock solutions of $UO_2(NO_3)_2$ and $C_6H_4(OH)CO_2Na$ under N_2 atmosphere to exclude CO_2. The pH was adjusted to 6 with NaOH. According to thermodynamic calculations only the $UO_2SAL_2^{2-}$ complex should be present at this pH. U-L_{III} edge EXAFS spectra were recorded in transmission mode at RT. Theoretical scattering phases and amplitudes functions were calculated self consistent with FEFF8.02 based on the XRD data of a solid U(VI)-SAL complex [1].

In the first step of MCTFA [2], an approximated structure of the $UO_2SAL_2^{2-}$ complex is determined. Two SAL ligands were considered in agreement with the calculated speciation. In addition one water molecule was included in the model. We used experimentally determined Debye-Waller factors for the backscattering ligand atoms. All important 3- and 4-legged multiple scattering (MS) paths up to an effective path length of 4.8 Å were considered. The approximated structure of the $UO_2SAL_2^{2-}$ complex based on the SAL structure [3] is shown in Fig. 1 together with the experimental and the theoretical EXAFS spectra.

We assume that the resulting asymmetric U–O distances of the functional groups (bidentate carboxylate and 6-membered carboxylate-phenol ring, Fig. 1) arise from the uncertain ligand stucture. According to XRD-derived structures of similar U(VI) compounds for one coordinated ligand, the U–O distances (O coordinated) should be approximately symmetrical. Therefore, we shifted the SAL ligands to achieve symmetrical U–O distances of 2.30 Å for the 6-membered ring structure, and 2.47 Å for the single carboxylate group.

In the second step of MCTFA, the estimated ligand structure was replicated 40 times to get a statistical distribution of complex structures to simulate the structural disorder. The bond angles and the interatomic distances between the ligand atoms, which are involved in important MS paths, were refined. Now 40 x 21 = 840 ligand atoms are moved and are constrained partly by the simultaneously calculated MS paths.

After 40.000 movements of the atoms (11 hours on a Pentium© IV processor), both the structure of the ligand and the total complex were refined (Fig. 2). The achieved theoretical spectrum of the U(VI)-SAL complex is in excellent agreement with the experimental spectrum. Small deviations are due to experimental error (noise) and the common problem of the B-spline fitting in the EXAFS data treatment or atomic EXAFS (Fig. 2, R < 1.4 Å).

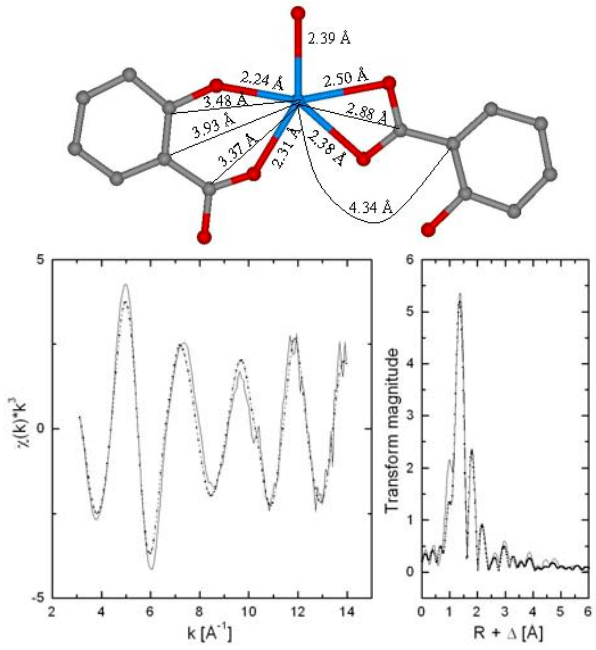

Fig. 1: Approximated structure of $UO_2SAL_2^{2-}$ after the first MCTFA step. Top: estimated complex structure, bottom: experimental (full line) and theoretical EXAFS spectra (dotted line).

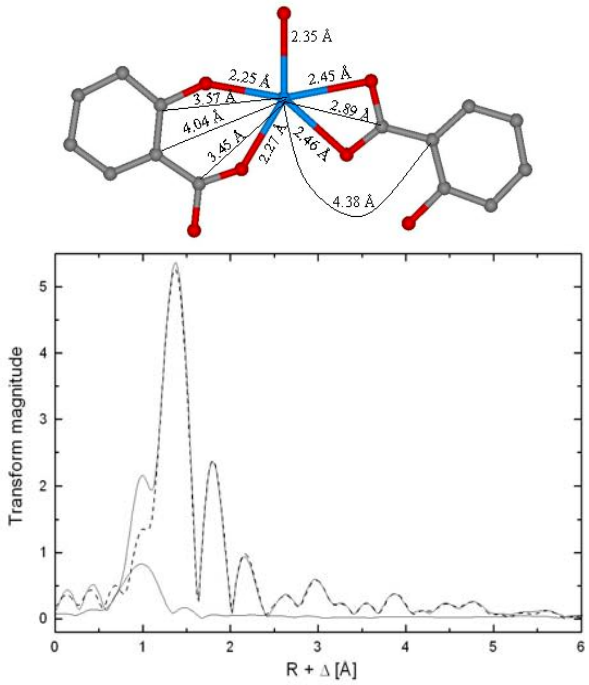

Fig. 2: Refined structure of $UO_2SAL_2^{2-}$ after the second MCTFA step. Top: refined complex structure, bottom: Fourier transform of the experimental (full line) and theoretical EXAFS spectra (dotted line) and the residual (thin line).

To the best of our knowledge, this is the first time that the structure of an aqueous U(VI) salicyate complex could be reliably solved, thereby improving our understanding of the interaction of U(VI) with humic acids and other natural organic matter on the molecular level.

REFERENCES

[1] Nassimbeni, L.R. *et al.* (1976) *Inorg. Chim.Aacta* **20**, 149-153.
[2] Rossberg, A. *et al.* (2005) *Physica Acta,* in press.
[3] Alcock, W. *et al.* (1989) *Acta Cryst*. **C45**, 719-721.

Testing the performance of EXAFS Monte-Carlo Target Transformation Factor Analysis (MCTFA) for aqueous U(VI)-protocatechuate complex mixtures

A. Rossberg, A.C. Scheinost

ABSTRACT. MCTFA is a new tool for the three-dimensional modeling of EXAFS spectral mixtures. Here we demonstrate that MCTFA reliably solves the structure of a U(VI)-ligand complex from EXAFS spectral mixtures with the high noise and limited k-range typical for dilute samples.

A common problem in actinide aqueous chemistry is the simultaneous presence of structurally different complexes. Up to now it was not possible to determine their structure with EXAFS, if neither the relative concentrations of the complexes in the mixtures were known nor the spectra of the complexes were available. Quite often, however, the structure of the uncomplexed ligands is available from crystal structure databases. In this case, MCTFA is able to derive the structure of the complexes from the spectral mixtures [1]. Here we test this newly developed method using (theoretically calculated) mixtures between two different U(VI) protocatechuate (PC) complexes, where the searched complex contributes ≤ 70 % to the sum spectrum.

In complex 1, U(VI) is bidentately coordinated to the carboxylate group of three PC (structural fragment Fig. 1, bottom left). In complex 2, U(VI) forms a five-membered ring with the two deprotonated phenolic OH groups of two PC (structural fragment Fig. 1, bottom right). For our test, we calculated the spectra of mixtures based on the previously determined bond distances and Debye-Waller factors of complex 1 and 2 using FEFF (Fig. 2) [2]. We added artificial noise and restricted the k-range to simulate EXAFS spectra of diluted samples. A test with such simulated spectra has two advantages over tests with real spectra: first, the source and the magnitude of the error in the data is known and can be modified, and second, one is able to measure the quality of the result. Note that the spectra of the pure species (complex 1, complex 2 in Fig. 2) are shown for comparison only, but were not used for MCTFA.

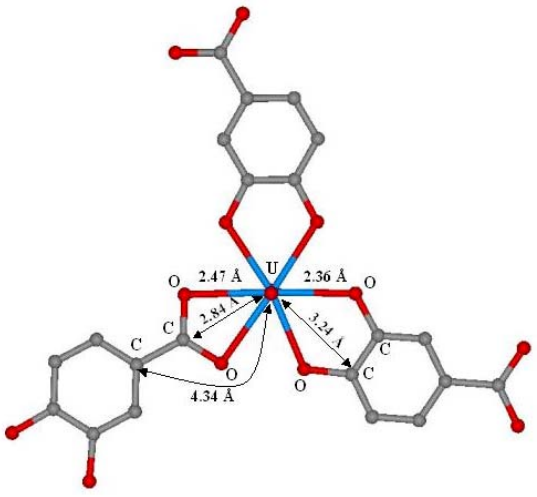

Fig. 1: Structural model for the calculation of theoretical back-scattering phase and amplitude functions with FEFF.

The MCTFA procedure, which is described in detail in [1], consists of two steps. First, an initial approximate for the pure spectrum and the structure of complex 1 is derived.

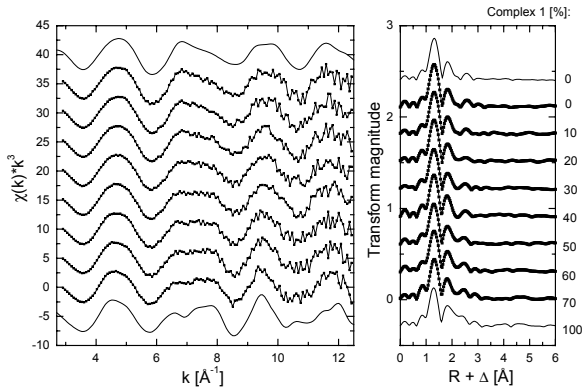

Fig. 2: Theoretical U-L_{III} edge EXAFS spectra of the U(VI)-PC complexes (top and bottom) and their mixtures with added artificial noise (dotted line).

Second, this initial structure is replicated n-times to create a large ensemble of molecules. Then, the structural disorder (σ^2) of each ligand atom and the atomic distances are refined. The purpose of this second step is not only to determine the exact arrangement of U in relation to the ligand, but also to refine the structure of the ligand itself, which may distort due to the metal-ligand interaction. In Fig. 3 we show the result of our test: the isolated spectrum and the derived structure of complex 1 agree well with the structural fragment of complex 1 (Fig. 1), which was used to create the spectral mixtures. Hence MCTFA was successful, even though EXAFS data quality was limited (small k-range, large noise).

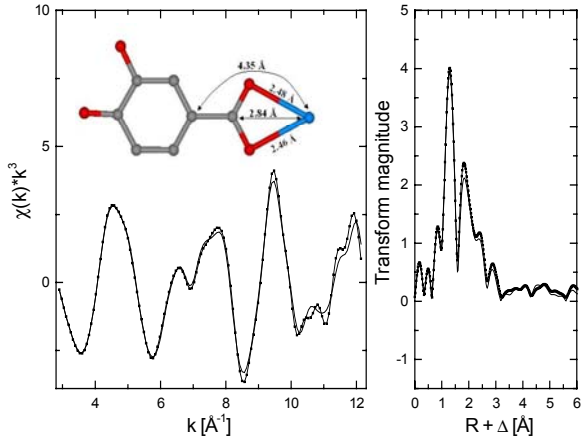

Fig. 3: Line – spectrum of complex 1, dotted line – spectrum of complex 1 isolated from the spectral mixtures.

REFERENCES

[1] Rossberg, A. *et al.* (2005) *Physica Acta,* in press.
[2] Rossberg, A. *et al.* (2003) *Anal. Bioanal. Chem* **376**, 631-638.

New MS Windows™-based software to control LIPAS experiments

M. Eilzer

ABSTRACT. For the laser-induced photo acoustic spectroscopy (LIPAS) a new up to date program software was developed.

Up to now for laser-induced photo acoustic spectroscopy (LIPAS) only a relative old under MS-DOS operating control program was used. Together with reprogramming the software, one aim was to convert the old MS-DOS based program to the Microsoft Windows operating system. This should be done to increase the programs performance and to use the software with actual computers.
The new program controls the Laser System (MOPO), the energy-meter and the oscilloscope [1]. All measured values will be stored, calculated and displayed graphically as a spectrum. The user interface should be as easy and as intuitive as possible. Due to the use of windows standard elements, this aim was reached easily.
The existing LIPAS software was programmed with Basic. This available code could be used as a template for the new software design. Now, it is programmed with Visual C++ Version 7. For this software, a basic dialog application acts as framework.
Two main classes were designed. First, the CGPIB class, to encapsulate all PC device related communication functions. This class provides basic and some special communication functions for the peripheral devices. Secondly, the CDiaGraph class. This class provides a two dimensional point or line diagram, for displaying the recorded spectrum. It contains only simple graphic routines, to support a wide range of different operating system versions.
While developing these classes, attention was paid on the software portability. So, now it is possible to use these functions and classes in other projects without major changes. With the program it is also possible to read previously recorded files and display the datasets on the screen.
The calculation of wavelength is integrated in the software, when the LIPAS is performed in the NIR-Range (> 730 nm = Idler Mode). This allows the use of the complete available wavelength range, without any external calculations.

RESULTS. An application was created, which has an ergonomic and easy user interface. During the measurements the actual values will be displayed online on the screen as a spectrum. The values will be stored automatically to a file. The format of the stored data is a proprietary ASCII text. These files can be opened and analyzed with other software programs like Excel, Origin or GRAMS-3D. The new software allows the online observation of the spectrum during the measurement via network connection.

Fig. 1: Np(IV) / Np(V)-humate in the NIR-region (The spectrum is mirrored.)

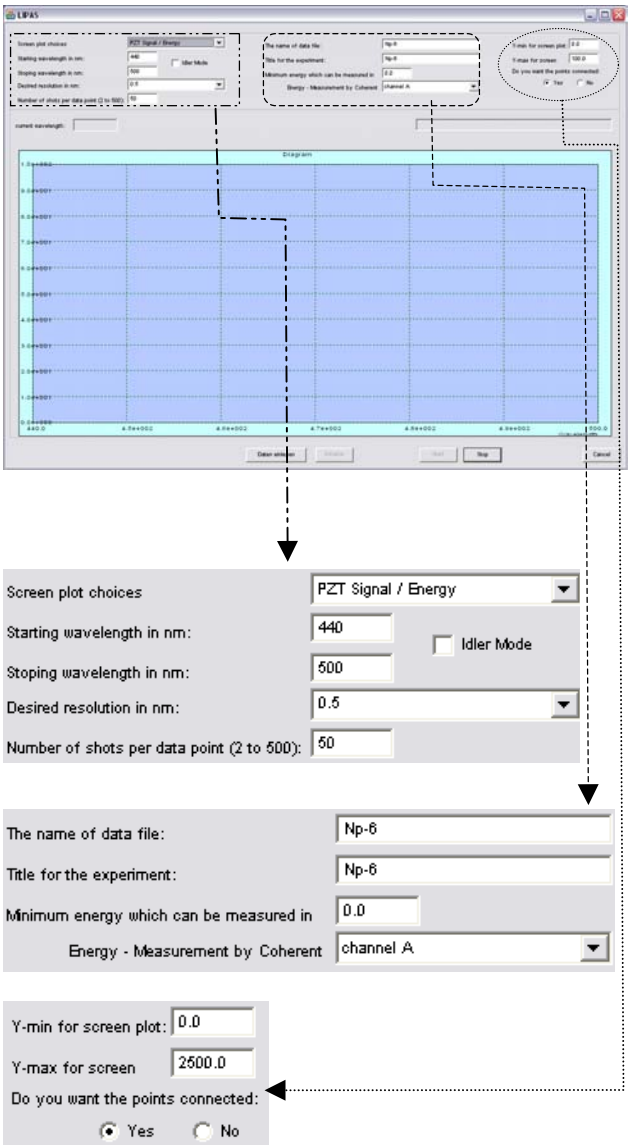

Fig. 2: Program software.

REFERENCES

[1] Geipel, G. *et al.* (1998) *Radiochim. Acta* **82**, 59-62.

Part 2:

Actinides in bio-systems

Interaction of uranium with S-layer protein of *Bacillus sphaericus* JG-A12 in aqueous solution

K. Muschter, H. Foerstendorf, J. Raff

ABSTRACT. The interaction of uranium with the S-layer protein from *Bacillus sphaericus* JG-A12 in aqueous solution was investigated by reaction-induced ATR-FT-IR spectroscopy using a dialysis flow cell. Indications for the deprotonation of carboxyl groups, the formation of uranium hydroxo nanocomplexes and uranium phosphates were found.

The surface layer (S-layer) protein from the uranium mining waste pile isolate *Bacillus sphaericus* JG-A12 is able to accumulate heavy metal ions such as uranium [1]. The combination of the attenuated total reflection (ATR) technique with reaction-induced infrared difference spectroscopy can provide spectra of samples in an aqueous medium without the limitation of total absorption [2]. From these spectra it is expected to derive the molecular interactions of the sorption processes.

EXPERIMENTAL. The infrared experiments were performed with the home-built dialysis flow cell shown in Fig. 1, which is attached to a diamond ATR-unit (crystal diameter: 4 mm; 9 internal reflections). For the infrared experiments 30 µl of the protein suspension (6 mg/ml S-layer, pH 4) was pipetted directly onto the ATR-crystal. After the flow cell was mounted with an appropriate dialysis membrane (MWCO 50 kDa) the liquid exchange between the suspension and the external flow solution (0.2 ml/min) occurs exclusively *via* diffusion through the membrane (Fig. 1). Equilibration of the whole cell with 0.1 M NaCl (pH 4) is necessary to obtain a constant background which was verified by continuously recording baselines. The sorption process was induced by a solution of UO_2Cl_2 ($[UO_2^{2+}] = 10^{-3}$ M; pH 4). The difference spectra were calculated from single beam spectra (128 scans) which were recorded continuously during the sorption process. Two different S-layer preparations were investigated. S1 is the native S-layer isolated according to the method described in [3]. S2 was additionally chemically modified with a 22-fold increased content of phosphate groups to allow to study the influence of phosphate groups on the binding of UO_2^{2+}. The modification was implemented by activation of phosphothreonine using 1-Ethyl-3-(N,N´-di-methyl-aminopropyl)-carbodiimide (EDC) [4] and zero-crosslinking to the S-layer protein.

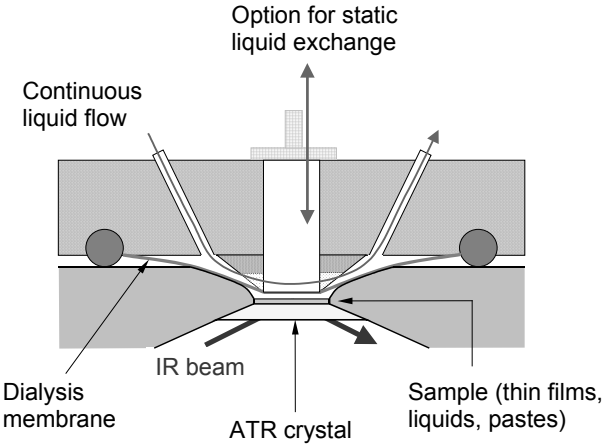

Fig. 1: Schematic cross-section of the ATR-dialysis flow cell.

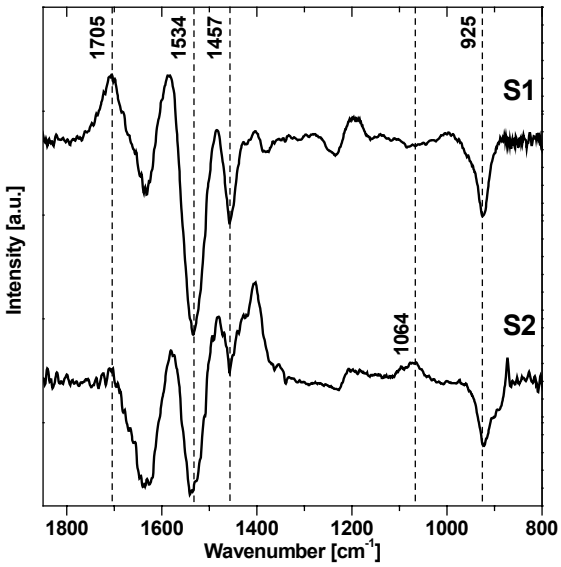

Fig. 2: FT-IR difference spectra of the sorption process of uranium on the S-layer protein of *Bacillus sphaericus* JG-A12 in a native solution (S1) and a solution with increased content of phosphate groups (S2).

RESULTS. In Fig. 2 the infrared difference spectra of the studied S-layer solutions are shown. The positive and negative bands in the infrared difference spectra represent the different states of the sample in the absence and in the presence of uranium, respectively. In the spectra the antisymmetric stretching vibration of the uranyl cation ν_{as} (UO_2^{2+}) can be seen at 925 cm^{-1}. The positive band at 1705 cm^{-1} represents protonated carboxyl groups of the protein which are obviously deprotonated in the presence of uranium. Consequently the negative bands at 1534 and 1457 cm^{-1} are tentatively assigned to carboxylate groups. However, from measurements of pure solutions of uranium chloride at pH 4 contributions of products of hydrolysis processes in the same wavenumber range can not be ruled out. The hydrolysis of the uranium oxo-hydroxo complexes might be facilitated by a specific molecular environment formed by the S-layer molecule. It can be supposed that the overall structure of the protein provides distinct cavities where the formation of uranium hydroxo nanocomplexes is preferred. This could explain the high affinity of the S-layer to heavy metal species.
Surprisingly, the difference spectrum of the phosphate enriched S2 is in general accordance to the spectrum of the native protein. Only around 1064 cm^{-1} an additional band shows up in the S2-spectrum. Since in this spectral region phosphate groups normally absorb this feature may represent the UO_2^{2+}-phosphate interactions.

REFERENCES

[1] Selenska-Pobell, S. *et al.* (1999) *FEMS. Microbiol. Ecol.* **29**, 59-67.
[2] Foerstendorf, H. *et al.* (2003) *Report FZR-400* p. 12.
[3] Raff, J. (2002) PhD thesis, University of Leipzig.
[4] Hoare, D.G. *et al*. (1967) *J. Biol. Chem.* **242**, 2447-2453.

Interactions of the S-layer of *Bacillus sphaericus* JG-A12 with palladium and formation of Pd-nanoclusters

K. Pollmann, M. Merroun, J. Raff, K. Fahmy[1], C. Hennig, A.C. Scheinost, S. Selenska-Pobell
[1]Institute of Nuclear and Hadron Physics, Dresden, Germany

ABSTRACT. The surface layer (S-layer) of the uranium mining waste pile isolate *Bacillus sphaericus* JG-A12 binds Pd(II) very efficiently, and Pd(0) nanoclusters are formed in the presence of H_2. The Pd binding sites in the protein were investigated by EXAFS analyses, ATR-FT-IR difference spectroscopy and by N-terminal sequencing of protein fragments.

The cells of the uranium mining waste pile isolate *Bacillus sphaericus* JG-A12 are enveloped by a proteinaceous paracrystalline surface layer (S-layer) [1]. Previous analyses demonstrated that the S-layer is capable of binding heavy metals making this protein interesting for bioremediation [1]. In addition, Pd(II) from an aqueous solution of Na_2PdCl_4 is bound by the S-layer very efficiently. In the presence of a reducing agent Pd(0) nanoclusters are formed, which are highly interesting for technical applications such as the development of novel catalysts.
We investigated the interactions of the S-layer of the strain *Bacillus sphaericus* JG-A12 with Pd(II) by using EXAFS and Fourier-transform infrared (FT-IR) analyses and identified probable Pd(II) binding sites by N-terminal sequencing of protein fragments resulting from the digestion of the native and the metallized proteins.

EXPERIMENTAL. S-layer proteins of the strains *Bacillus sphaericus* JG-A12 and NCTC 9602 were purified and recrystallized as described previously [1]. For metallization, the proteins were incubated with an aged solution of 2 mM Na_2PdCl_4 (pH = 3.1) and H_2 was added as a reducing agent to form Pd-nanoclusters. EXAFS analyses were used to study the interactions of the S-layer protein with Pd(II) and to characterize the Pd-nanoclusters. ATR-FTIR difference spectra were recorded as described previously [2]. pH changes were induced by buffer exchange in the upper compartment of the ATR-cell.

RESULTS. Palladium K-edge EXAFS spectra and the corresponding Fourier transforms (FT) of $[PdCl_4]^{2-}$ bound to the S-layer protein of *B. sphaericus* JG-A12 and of the formed Pd-nanoclusters are shown in Fig. 1. The coordination of Pd(II) to oxygen indicates that most likely carboxyl groups are involved in Pd-binding. The size of the formed Pd-nanoclusters was estimated to 0.8-1.0 nm from the Pd-Pd coordination numbers.
The pH induced changes of IR-absorption spectra of the S-layer protein due to the protonation of its carboxyl groups are shown in Fig. 2A. Metallization of the protein prevents the IR-spectral changes (Fig. 2B), indicating that the carboxyl groups are blocked for protonation by complexation with Pd(II). Furthermore, the metal-protein interactions stabilize the protein structure [2].

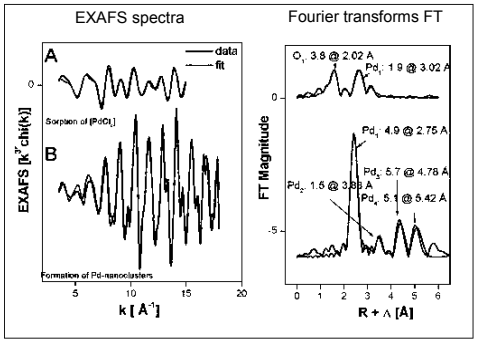

Fig. 1: Pd K-edge EXAFS spectra. **A:** Sorption of $[PdCl_4]^{2-}$ by the S-layer of *B. sphaericus* JG-A12; **B:** Formation of Pd-nanoclusters on the S-layer of *B. sphaericus* JG-A12 after addition of H_2.

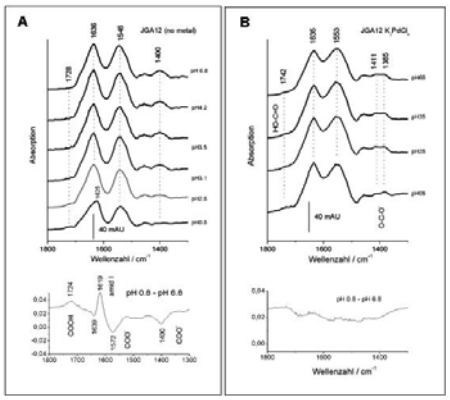

Fig. 2: **(A)** pH-dependent IR absorption spectra of S-layers prepared from *B. sphaericus* JG-A12. (**A**) Resuspended S-layers. **(B)** Pd-metallized S-layers in suspension.

Digestion of purified S-layer protein of *B. sphaericus* JG-A12 and NCTC 9602 with the endoproteinase Glu-C, which cleaves between -Asp-P1'- and -Glu-P1'-, gave 5 (Fig. 3) or 9 (data not shown) fragments, respectively. The proteinase was not able to digest the Pd-metallized protein due to the blockage of the carboxyl groups by the metal (Fig. 3). The locations of the cleavage sites and therefore the probable metal binding sites in the protein were determined by N-terminal sequencing of the protein fragments. These sites are preferentially found in the central (JG-A12) and the C-terminal (9602) regions.

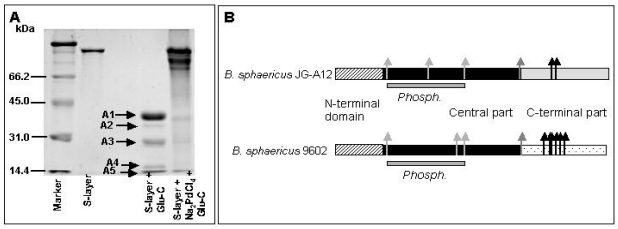

Fig. 3: **(A)** SDS-Gel: Native and palladized S-layer proteins of *B. sphaericus* JG-A12 were digested with Glu-C.
(B) Localization of Glu-C cleavage sites in the S-layer proteins of *B. sphaericus* JG-A12 and NCTC 9602 are indicated by arrows.

ACKNOWLEDGEMENTS. This study was supported by the grants DFG/SE 671/7-2 (DFG), 7531.50-03.0370-01/5 (SMWK), and GRD1-2001-40424 (EC). We thank R. Getzlaff, I. Plumeier (GBF Braunschweig).

REFERENCES

[1] Raff, J. (2002) *Report FZR–358*.
[2] Savchuk, O. *et al.* (2004) *Report FZR–401*, p. 47.

XAS characterization of gold nanoclusters formed by cells and S-layer sheets of *B. sphaericus* JG-A12

M. Merroun, A. Rossberg, A.C. Scheinost, S. Selenska-Pobell

ABSTRACT. Cells and S-layer sheets of *B. sphaericus* JG-A12 were used as templates for the deposition of metallic gold nanoclusters by reduction with H_2. Gold L_{III}-edge XAS measurements confirmed the formation of Au(0) nanoclusters in both cases. However, cells reduced 67% of Au(III) to Au(0), whereas S-layers reduced only 37%.

The area of nanotechnology encompasses the synthesis of nanoscale matter, the understanding and the utililization of their often exotic physicochemical and optoelectronic properties, and the organization of nanoscale structures into predefined superstructures. Thus nanotechnology promises to play an increasingly important role in many key technologies of the new millenium. As for the synthesis of nanoparticles, there is an ever-growing need to develop clean, non-toxic, and environmentally friendly ("green chemistry") synthetic procedures. Consequently, researchers in the field of nanoparticle preparation have been looking at biological systems for inspiration. In this work, we studied structures of the gold nanoparticles formed on cells and S-layer protein sheets of *B. sphaericus* JG-A12 by using X-ray absorption spectroscopy (XAS).

EXPERIMENTAL. *B. sphaericus* cells were grown in a batch culture to mid exponential phase and harvested by centrifugation at 10.000 rpm for 30 min. The preparation of S-layer protein was perfomed as described in [1]. To metallize *B. sphaericus* JG-A12 cells and S-layer, 40 ml of Gold(III) solution ($HAuCl_4$ x $3H_2O$) was poured into 55 ml serum bottles, and O_2 was eliminated by bubbling N_2 through the solution for 15 min. The reduction of Au(III) to Au(0) was then induced by adding H_2 gas.

RESULTS. Gold K-edge EXAFS spectra of cells and S-layers of *B. sphaericus* JG-A12 in the absence and presence of H_2 are shown together with Au reference compounds in Fig. 1.
Using XANES spectroscopy and Iterative Target Test Factor Analysis [2] we found that in the presence of H_2 cells and S-layer of the bacterium are able to reduce 67 % and 37 % of Au(III) to Au(0), respectively. The Fourier Transform (FT) peaks of metallic Au were attributed to 4 Au-Au shells with distances of 2.87, 4.06, 4.98 and 5.68 Å. The Au-Au coordination number of the first shell of the biocomponent (CN=6-7) are smaller than that of the measured gold metal foil (CN=12). Using the cubic (FM3-M) structure of elemental gold, one can calculate that an average CN number of 6-7 corresponds to an average cluster diameter of 7 to 9 Å. The formation of gold nanoparticles by the cells and S-layer is confirmed by UV-vis spectroscopy: an absorption band at 540 nm arises from the excitation of surface plasmon vibrations and is responsible for the ruby-red color of gold nanoparticles.
In addition to these Au-Au shells, an Au-O/N/C contribution at 2.01 Å was detected in the EXAFS spectra which corresponds probably to Au bound to surface functional groups of the cells and S-layer.

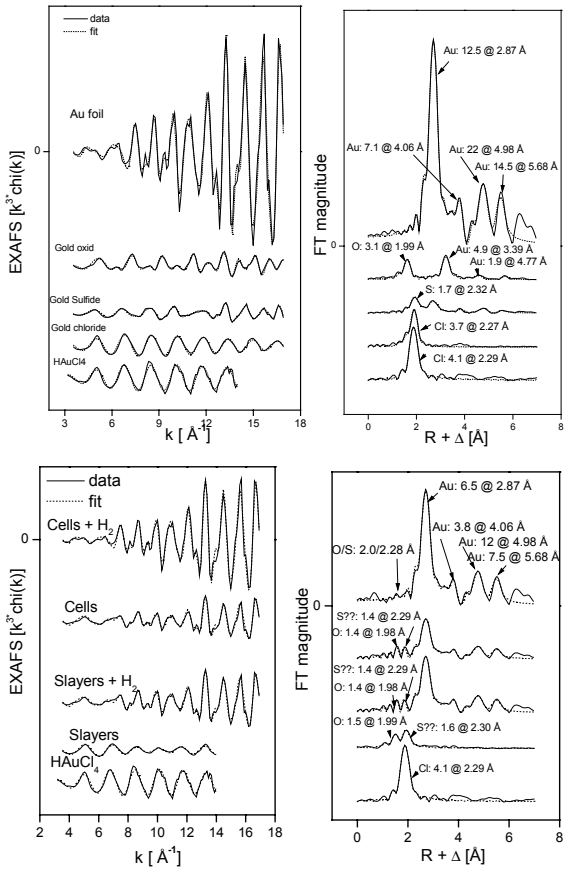

Fig. 1: Au K-edge EXAFS spectra and their FT of Au complexes and nanoclusters formed by cells and S-layer of *B. sphaericus* JG-A12. For comparison, the spectra of some gold references are shown.

In the absence of an reducing agent, results by factor analysis suggested a mixture of about 35 % Au(0) and 65 % Au(III) in the cell sample and of only 10 % A(0) in the S-layer sample. This difference may be explained by reduction of Au by cells with sulfur surface groups, which are absent in the S-layer of *B. sphaericus* JG-A12. The EXAFS spectra of the cell sample contain in addition to the Au-Au shells also contributions from backscattering of light atoms like oxygen, nitrogen or carbon at bond distances of 2.01 Å and 2.29 Å. Theses atoms belong most likely to functional group of the biocomponents, therefore suggesting specific sorption of gold.

ACKNOWLEDGEMENTS. This work is supported by SMWK Grant N° 7531.50-03.0370-1/5.

REFERENCES

[1] Raff, J. (2002) *Report FZR-358*.
[2] Rossberg, A. *et al.* (2003) *Anal. Bioanal. Chem.* **376**, 631-638.

Analysis of the S-layer protein of *Bacillus sphaericus* JG-A12 by two-dimensional polyacrylamide gel electrophoresis

D. Regenhardt, J. Raff, K. Pollmann, S. Selenska-Pobell

ABSTRACT. Two-dimensional gel electrophoresis demonstrates that the proteinaceous surface layer of *B. sphaericus* JG-A12 contains an unusually high number of isoforms. This is an indication for post-translational modifications. The exact number and role of the latter are under investigation.

As many other organisms from the domains of *Bacteria* and *Archaea* the uranium mining waste pile isolate *B. sphaericus* JG-A12 possesses a surface layer protein as the outermost cell structure. The S-layer protein represents up to 15 % of the total protein of the cell [1], contains a high amount of acidic amino acids and a low theoretical isoelectric point (pI) [2], that are typical features for S-layer proteins [3]. The two-dimensional polyacrylamide gel electrophoresis (2-D PAGE) is used in proteome projects to provide a global view of the proteins expressed in cells or tissue types under defined conditions. Also for the work with purified proteins it is a powerful tool to obtain additional information, especially with regard to post-translational modifications and isoelectric point determination of the proteins, an option missing in the one-dimensional polyacrylamide gel electrophoresis (1-D PAGE).

EXPERIMENTAL. The isolated and recrystallized S-layer protein of *B. sphaericus* JG-A12 was separated by 1-D and 2-D PAGE. For the first dimension 30 µg of S-layer protein was separated by isoelectric focusing (IEF) with immobilized pH gradients (IPG strips, Biorad). The strips were actively rehydrated for 12 h at 50 V together with the sample in rehydration buffer (7 M urea, 2 M thiourea, 4 % CHAPS, 20 mM Tris base, 30 mM DTT, protease inhibitor cocktail, 0.2 % Biolyte, bromphenolblue). The focusing was obtained on a PROTEAN II Cell (Biorad) by application of 50 V for 1 Vh, 300 V for 185 Vh, 1000 V for 1000 Vh, 4000 V for 5000 Vh and then maintained constant at 4000 V for a total of 19 kVh. For the second dimension the gels were equilibrated for two intervals of 13 min in equilibration solution (6 M urea, 30 % glycerol, 2 % SDS, 50 mM Tris base, pH 8.8). For the first step 2 % DTT was added to the solution that was replaced by 2.5 % iodacetamide in the second round. The strips were then applied on 10 % polyacrylamide minigels using Tris/Glycine/SDS buffer and separated at 90 V for 3 h. After the electrophoresis gels were stained with Collodial Coomassie brilliant blue dye (CBB G-250) and analyzed.

RESULTS. The 1-D PAGE shows the mature S-layer protein of *B. sphaericus* JG-A12 with a molecular weight of 126 kDa (Fig. 1, arrow).
The protein profile resulting from a 2-D PAGE of the purified S-layer protein is given in Fig. 2. The S-layer protein possesses an unusually high number of isoforms (chain of spots indicated by the arrows) showing differences in their isoelectric points. The observed isoelectric points of the isoforms are ranging from 4.95 to 6.5 but show no differences in molecular weight. The most basic spot is more than 1.4 pI units higher than the theoretical isoelectric point of the mature S-layer protein (pI 5.1) and the most acidic is 0.15 pI units lower.

DISCUSSION/OUTLOOK. The variations of the pIs are most likely due to post-translational modifications such as phosphorylations [4], rather than introduction of high molecular weight groups (e. g. glycan groups) that would change the molecular weight of the protein. Recently the multiplicity in pI isoforms was also described for the S-layer protein EA1 of *B. anthracis* [5].
The exact nature and the role of the observed isoelectric isoforms of the S-layer protein have not yet been studied in detail. Efforts to map the modifications of *B. sphaericus* JG-A12 S-layer protein are in progress in our laboratory.

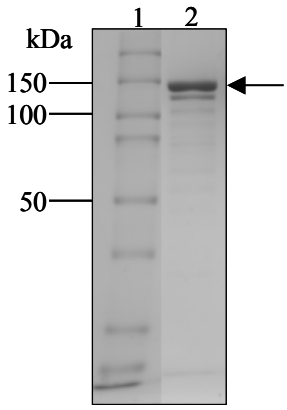

Fig. 1: SDS PAGE of the S-layer protein *of B. sphaericus* JG-A12 (lane 2). The arrow indicates the mature form of the protein. The molecular mass standard proteins are shown in lane 1.

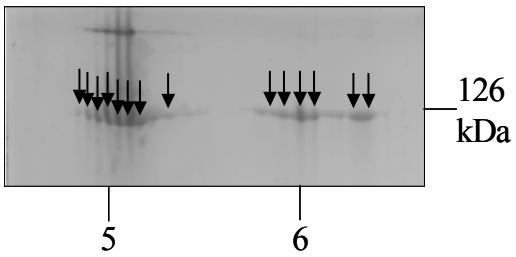

Fig. 2: Separation of the S-layer protein of *B. sphaericus* JG-A12 (enlarged part of a 2-D gel). The protein was subjected to IEF on a 5-8 narrow range IPG strip followed by SDS PAGE. The arrows indicate the different isoforms of the S-layer protein.

ACKNOWLEDGMENTS. This work is supported by the SMWK Grant N^{o} 7531.50-03.0370-1/5.

REFERENCES

[1] Boot, H. *et al.* (1999*) Mol. Microbiol*. **21**, 1117-1123.
[2] Pollman, K. *et al.* (2005) *Appl. Environ. Microbiol.*, submitted.
[3] Sleytr, U.B.; Beveridge, T. (1999) *Trends Microbiol*. **7**, 253-260.
[4] Umeyama, T. *et al.* (2002) *Appl. Microbiol. Biotechnol.* **59**, 419-425.
[5] Chitlaru, T. *et al.* (2004) *Proteomics* **4**, 677-691.

Selective immobilization of uranium from weakly contaminated waters by *Bacillus sphaericus* based biocers

J. Raff, S. Selenska-Pobell

ABSTRACT. We investigated uranium (U) removal from four different tap water samples spiked with 30 µg/L U and from a Hungarian mineral water with an indigenous U content of 142 µg/L using immobilized *Bacillus sphaericus* JG-A12 cells (biocers). More than 99% of dissolved U was removed from the tap water samples. From the heavy metal containing and highly saline Hungarian water, 86% of U and 76% of Zn were removed by selective binding to the biocers.

In previous studies we investigated the selective and reversible binding of uranium (U) by *B. sphaericus* JG-A12 cells, spores and the surface layer (S-layer) protein [1, 2]. Since pure biomass is not suitable for cleaning water, we used sol-gel techniques to produce biological ceramics (biocers). Either cells, spores or S-layer protein of *B. sphaericus* JG-A12 were embedded in a porous silicate matrix [2, 3]. Sorption experiments using free and immobilized biocomponents of JG-A12 showed that the immobilization has no impact on the binding capacity of the cells and S-layer. Biocers of cells had even higher binding capacities than the S-layer biocer or the spore biocer. In all these previous experiments, U concentrations in the mg/L range were employed. Hence our objective was to extend these previous studies to much lower U concentrations in the µg/L range.

EXPERIMENTAL. *B. sphaericus* JG-A12 cells were grown in nutrient broth (NB) to the late logarithmic growth phase. After washing the cells were immobilized using sol-gel techniques [2, 3]. For the sorption experiments 500 ± 0.1 mg biocers or xerogel were equilibrated at pH 7.5, transferred to 35 ml water samples and shaken for 48 h at 30 °C. Four tap water samples from different regions in Germany, supplemented with 29.5 ± 0.6 µg/L U, and one Hungarian mineral water sample with a U content of 142.3 ± 1.3 µg/L were used. The pH values vary from 7.4 to 8.5. The content of Ag, Al, As, B, Ba, Br, Cd, Co, Cr, Cu, Fe, Hg, Mg, Mn, Ni, Pb, Se, Sb, Sr, U and Zn was measured before and after the incubation with xerogel or biocer and also in reference tubes after incubation by inductive coupled plasma mass spectroscopy (ICP-MS). In addition, the carbonate concentration was measured in all samples.

RESULTS. The five water samples had a substantial variation of carbonate content. Sample W1 contains 216, W2 220, W3 59.9, W4 86.9 and W5 905 mg/L carbonate. Sample W5 has in addition high heavy metal concentrations and is highly saline. As shown in Fig. 1 and Tab. 1, U uptake from tap water (W1 to W4) was more than 98.5 % (xerogel) or 99.1 % (biocer). Uranium uptake from the mineral water was 86.6 % (xerogel) or 85.7 % (biocer). Sorption experiments with sample W5 proved the selective binding of U and Zn. In contrast, the binding capacity and selectivity of Al, As, Cu, Cr, Pb and Sb are dependent on the content of other metals and on the overall ionic strength. Although the results in this work show almost equal binding capacities of xerogel and cell-biocer for U, former experiments with U concentrations of 214.2 mg/L demonstrated significant higher binding capacity for the cell-biocer [2]. To develop improved cleanup strategies for drinking water, future work will focus on the surface layer protein of *B. sphaericus* JG-A12, since this is more suitable for hygienic reasons. Furthermore, the binding capacity and binding selectivity of S-layers can be improved by genetic modifications [4].

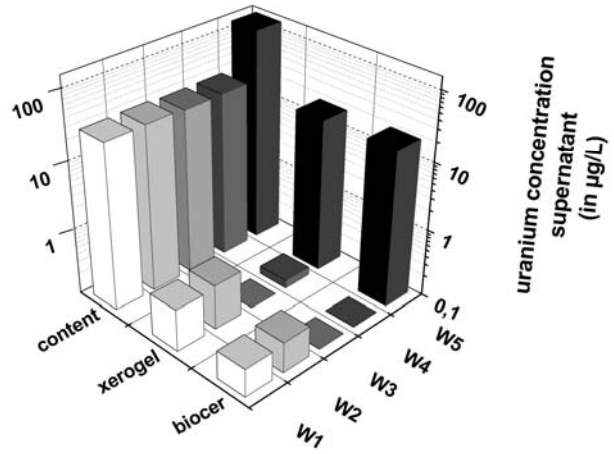

Fig. 1: Removal of uranium from different water samples by xerogel or cell-biocer.

Tab. 1: Immobilization of heavy metals with more than 50 % removal in µg/L. Al, Sb are not present in W2, Al, As and Sb not in W3 as well as Al and As are not in W4.

water sample	element	content	supernatant xerogel	supernatant biocer
W1	Al	53.33±1.72	1.63±0.31	< 0.5
	As	0.26±0.10	0.19±0.07	< 0.1
	Pb	0.28±0.05	0.12±0.02	0.12±0.01
	U	29.73±0.13	0.42±0.12	0.26±0.04
	Zn	120.00±0.82	3.40±0.16	1.66±0.45
W2	As	0.50±0.06	0.40±0.06	< 0.1
	Cu	594.33±15.63	72.43±1.74	19.13±0.53
	Pb	0.80±0.29	0.09±0.03	0.15±0.03
	U	30.33±0.54	0.66±0.30	0.28±0.01
	Zn	48.67±3.51	3.09±1.49	2.27±0.28
W3	Cr	1.15±0.14	< 0.5	< 0.5
	Cu	8.17±0.13	4.35±0.18	2.36±0.13
	Pb	8.00±0.18	0.18±0.02	0.26±0.02
	U	28.80±0.37	0.08±0.01	0.08±0.01
	Zn	12.30±0.36	< 1	< 1
W4	Cu	145.33±1.70	16.77±0.97	5.07±0.36
	Pb	0.31±0.10	< 0.05	< 0.05
	Sb	0.24±0.02	< 0.05	< 0.05
	U	29.10±0.37	0.13±0.05	0.083±0.018
	Zn	75.00±0.42	< 0.5	< 0.5
W5	U	142.33±1.25	19.07±2.92	20.37±2.05
	Zn	33.03±2.78	9.64±2.11	7.89±0.73

ACKNOWLEDGEMENTS. This work was founded through project DFG SE 671/7-2 from German Research Community (DFG). We thank U. Soltmann (GMBU, Dresden) for the biocer preparation, U. Schaefer and D. Birnstein for the ICP-MS and carbonate analyses.

REFERENCES

[1] Selenska-Pobell, S. *et al.* (1999) *FEMS. Microbiol. Ecol.* **29**, 59-67.
[2] Raff, J. *et al.* (2002) *Chem. Mater.* **15**, 240-244.
[3] Soltmann, U. *et al.* (2002) *J. Sol Gel Sci. Technol.* **26**, 1209-1212.
[4] Pollmann, K. *et al.* (2005) *Appl. Environ. Microbiol.*, submitted.

Interaction of actinides with *Desulfovibrio äspöensis* (DSM 10631^T). Part III: Neptunium

H. Moll, M. Merroun, S. Selenska-Pobell, G. Bernhard

ABSTRACT. We are presenting the first results on interactions of the sulfate-reducing bacterium (SRB) *D. äspöensis* with neptunium(V). From an aqueous solution of 9 µM Np(V) supplemented with 10 mM lactate, cells of this strain removed 59 % of the Np(V) within 72 h of incubation at pH 6.

In continuation of our project exploring the interaction of the SRB *Desulfovibrio äspöensis* with selected actinides in different oxidation states, U(VI) [1] and Cm(III) [2], we are reporting the first results obtained with Np(V). The total number of SRB in the Äspö aquifer was measured to be within the range of 10^1 to 10^3 cells mL^{-1} [3]. Motamedi and Pedersen could recover a new SRB-strain called *D. äspöensis* from a depth of 600 m at the Äspö site [4]. Little is known about bacterial interactions of Np(V) with microbes. Np(V) forms only weak complexes with ligands and is thought to be non-sorptive.

EXPERIMENTAL. The Gram-negative strain *D. äspöensis* was grown to the mid-exponential phase as described in [2]. The collected biomass was 0.95 ± 0.25 $g_{dry\ weight}$/L. The molecular analysis of the *D. äspöensis* cultures was performed using ARDREA as described in [2].

RESULTS. In this study, we could show for the first time the removal of Np(V) from the solution due to the activity of *D. äspöensis* (Fig. 1-3). In all samples without cells, the Np concentrations measured by ICP-MS did not differ significantly from the initial values. Fig. 1 shows the results of the time dependent decrease of Np and U in the presence and absence of biomass at pH 6. The main Np(V) removal occurred after the first 72 h. Whereas steady state conditions are reached after 168 h. In contrast to these results, uranium interacts with the biomass in a faster way. Furthermore, we observed a stronger interaction of U with the biomass compared to Np. Interestingly, we found no difference in the amount of accumulated Np by the biomass in the presence or the absence of U in the test solutions. This might indicate the occurrence of different binding places and/or binding modes for Np and U on the cell envelope of *D. äspöensis*.

From the time dependences shown in Fig. 1 one might conclude that probably two different processes occur after adding the biomass.

The pH is one factor limiting the Np removal efficiency. A slight increase from 63 to 77 % was observed when the pH changed from 5.95 to 7.70, respectively (Fig. 2).

Besides the pH, the Np concentration in solution is another limiting factor of the removal efficiency (Fig. 3). Only at low $[Np(V)]_{initial}$, 2.15 mg/L, a removal efficiency above 50 %, 63 % (1.21 $mg/g_{dry\ weight}$), could be achieved. Whereas at $[Np(VI)]_{initial}$ of 28.68 mg/l, the removal efficiency decreased to a level of 9.9 % (3.89 $mg/g_{dry\ weight}$).

The determination of the speciation of the bound Np, *e.g.* by NIR spectroscopy, is difficult due to the low amount of Np associated with the biomass.

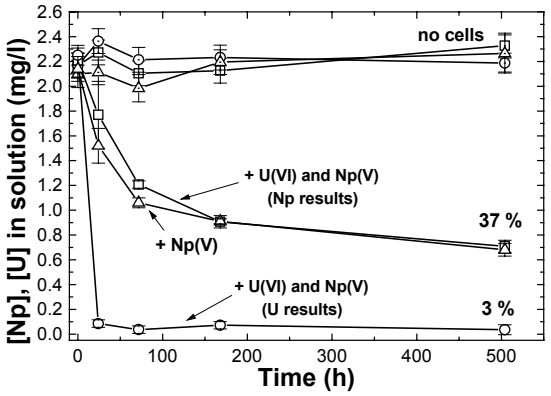

Fig. 1: Decrease of the U(VI) and Np(V) concentration ($[U(VI)]_{initial}$: 2.25 mg/L, $[Np(V)]_{initial}$: 2.21 mg/L) in solution as a function of the contact time.

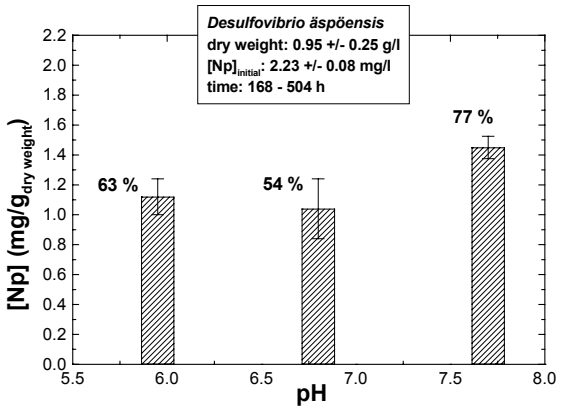

Fig. 2: Total amount of Np(V) removed from the solution by *D. äspöensis* as a function of pH.

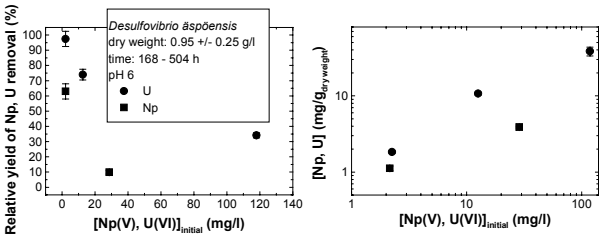

Fig. 3: Removed neptunium/uranium from the solution in the presence of *D. äspöensis* at pH 6.

ACKNOWLEDGEMENTS. This work is supported by the BMWi (no. 02E9491).

REFERENCES

[1] Moll, H. *et al.* (2003) *Report FZR–373*, pp. 31-32.
[2] Moll, H. *et al.* (2004) *Environ. Sci. Technol.* **38**, 1455-1459.
[3] Pedersen, K. (2000) *SKB Technical Report TR-00-04*.
[4] Motamedi, M. *et al.* (1998) *Int. J. Syst. Bacteriol.* **48**, 311-315.

Interaction of uranium with bacterial strains isolated from extreme habitats: EXAFS studies

M. Merroun, M. Nedelkova, M. Heilig, A. Rossberg, C. Hennig, S. Selenska-Pobell

ABSTRACT. EXAFS spectroscopy was used to investigate the U(VI) retention mechanism of five environmental isolates. At pH 2.9, all strains sorbed U(VI) by formation of a complex with organic phosphate groups. At pH 4.5, however, all strains precipitated uranium as a m-autunite-like phase.

Uranium is a long-living radionuclide that represents ecological and human health hazards. The mining and processing of uranium during the last decades for nuclear fuel and nuclear weapon production resulted in generation of significant amounts of radioactive wastes. It is critical that the uranium in these wastes has to be effectively immobilized in order to prevent ground water contamination. Microbial biosorption of U(VI) was proposed as one of the methods for uranium immobilization. In this paper, we investigate the coordination chemistry of uranium bound to different bacteria isolated from uranium mining wastes using Extended X-ray Absorption Fine Structure (EXAFS) spectroscopy.

EXPERIMENTAL. Bacterial cells grown to the late exponential phase were harvested by centrifugation (11000 rpm for 20 min at 4°C) and washed three times with 0.1 M $NaClO_4$ to remove the disturbing ingredients of the growth medium. The washed cells were resuspended and shaken for 48 h in 35 ml 10^{-3} M $UO_2(NO_3)_2$ x 6 H_2O resolved in 0.1 M $NaClO_4$, at two pH values of 2 and 4.5. After the uranyl contact, the cells were harvested and washed with 0.1 M $NaClO_4$. The pellet samples were dried in a vacuum incubator at 30°C for 24 h and powdered.

RESULTS. The X-ray absorption near edge structure (XANES) spectra (data not shown) of uranium complexes formed by different bacteria studied in this work contain an XANES peak at 17188 eV which has previously been attributed to uranium in the 6+ oxidation state. In addition, the intensity maximum for the absorption edge occurs at the position characteristic of U(VI). Both observation indicate that uranium is present in the samples as U(VI). The k^3-weighted χ spectra determined from EXAFS analyses of the uranium species formed at pH 2 and 4.5 are presented in Figure 1 along with the best fits obtained from the fitting procedure. The FT of the EXAFS spectra of the samples studied in this section at pH 2 and 4.5 show five significant peaks. The first two peaks arise from the scattering contribution of the axial oxygen atoms (O_{ax}) at 1.3 Å and the equatorial oxygen atoms (O_{eq}) at 1.8 Å. The U-O_{eq} bond distance is within the range of previously reported values for the oxygen atom of the phosphate bound to uranyl. The third and the fourth FT peak, which appear at 2.3 and 3 Å, are a result of the back-scattering from oxygen and phosphorous atoms, respectively.
This U-P distance is consistent with monodentate coordination of phosphate to the uranyl equatorial plane as in m-autunite. At pH 4.5, a fifth shell corresponds to U at distance of 5.20 Å. This distance is also present in m-autunite, suggesting that a similar phase (inorganic uranyl phosphate phase) was precipitated by the bacterial cells at

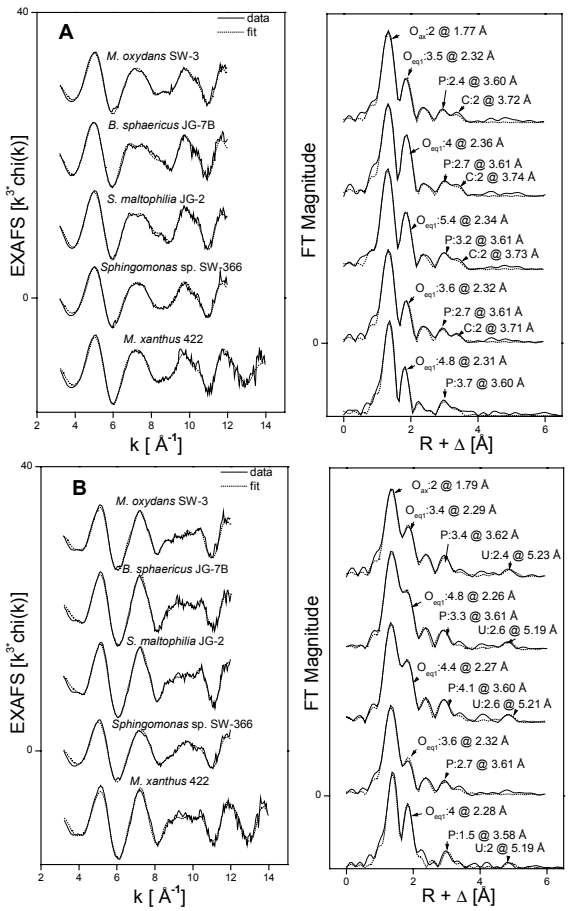

Fig.1: U L_{III}-edge EXAFS spectra and their corresponding FT of the U complexes formed by the uranium mining waste isolates at pH 2 (A) and 4.5 (B).

pH 4.5, probably due to the release of inorganic phosphates from the cells as result of the acid phosphatase activity. At pH 2, however, this peak is absent, but we could fit a contribution of U-C at a distance of 3.72 Å. This C atom most probably originates from the organic phosphate molecules of the cell surface which are implicated in the binding of uranium.

ACKNOWLEDGEMENTS. This work was supported by a grant 03I4004B from the Bundesministerium für Bildung und Forschung, Berlin, Germany.

Heterologous expression and modification of the S-layer protein gene of *Bacillus sphaericus* JG-A12

K. Pollmann, S. Selenska-Pobell

ABSTRACT. The S-layer protein gene of *Bacillus sphaericus* JG-A12 was cloned and heterologously expressed in *Escherichia coli*. A protein with Ni-binding capability was obtained by the addition of histidine residues to the N- and C-termini of the protein.

Previous analyses have shown that the outermost surface-layer (S-layer) of the cells of the uranium mining waste pile isolate *Bacillus sphaericus* JG-A12 is able to bind selectively and reversibly high amounts of heavy metals such as U, Pb, Cu, Al, Ga, and Cd [1]. The S-layer is composed of protein monomers with the ability to self-assemble into paracrystalline arrays. These special features of the S-layer stimulated the interest for biotechnological applications such as bioremediation [1].

The expression and purification of recombinant proteins facilitates the production and characterization of virtually any protein [2]. Among the various developed expression systems the use of *Escherichia coli* as host is the most important and hence most extensively studied. The purification of the produced recombinant proteins is essential for the characterization of the proteins, but remains still challenging. The use of affinity tags greatly simplifies the purification procedure. By this procedure, specific affinity tags such as histidine tags are added to the protein of interest. The 6xHis affinity tags facilitate binding to Ni-binding resins and allow the purification of the modified proteins by affinity chromatography.

In the present work the S-layer protein gene of the strain *Bacillus sphaericus* JG-A12 was cloned and heterologously expressed in *Escherichia coli*. The protein was modified by the addition of six histidine residues at the N- and C-termini. The Ni^{2+} binding capability of the histidine residues enabled the purification by Ni chelating chromatography. The obtained purified protein will be tested for its Ni^{2+}-binding capacity.

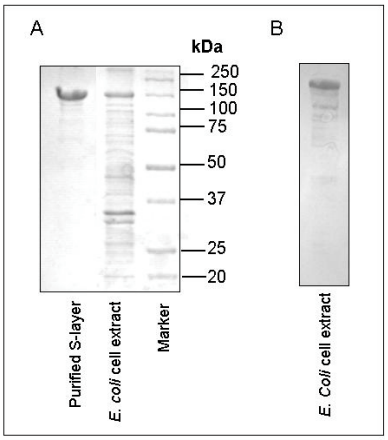

Fig. 1: **(A)** Heterologous expression and purification of the S-layer protein of *B. sphaericus* JG-A12 in *E. coli*. **(B)** Immunoblot assay of a cell extract of the *E. coli* mutant prepared after induction of the cells with IPTG. The Immunoblot assay was performed using S-layer protein specific antibodies.

EXPERIMENTS AND RESULTS. The S-layer protein gene of JG-A12 encoding the S-layer protein monomers was cloned in the vector pET30 Ek/Lic and heterologously expressed in *Escherichia coli* Bl21(DE3) (Novagen). Fig. 1 shows the expression of the protein by the *E. coli* mutant after induction with IPTG. The successful expression was confirmed by an immunoblot assay using S-layer protein specific antibodies. The addition of six histidine residues at both the N- and C-termini enabled the purification of the recombinant protein by Ni-chelating chromatography using a XK-26/20 column (Amersham) packed with Ni-Sepharose High-Performance (Amersham).

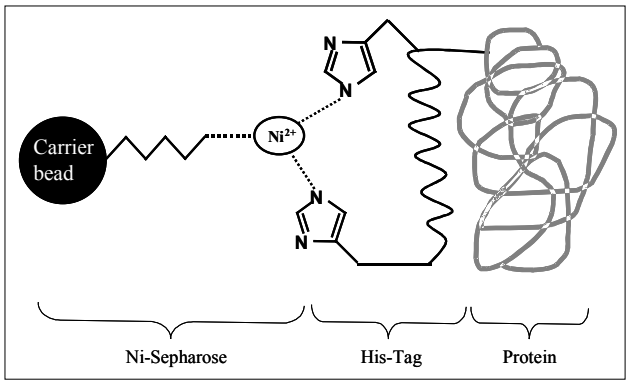

Fig. 2: Principle molecular mechanism of histidine binding to Ni-Sepharose. The nickel ion has a high affinity and specifity for His-tagged proteins, thus enabling the purification of the protein by Ni chelating chromatography.

The molecular mechanism of histidine binding to the Ni-resin is shown in Fig. 2. Histidine residues are well known for their strong interaction with Ni^{2+}. In order to elucidate the capabilities of the modified protein to bind Ni^{2+} ion from water, we will incubate the purified protein with different solutions of $NiCl_2$ and water contaminated with different heavy metal ions. The binding capacity will be compared with that of the S-layer proteins purified from *Bacillus sphaericus* JG-A12.

ACKNOWLEDGEMENTS. This study was supported by grant DFG/SE 671/7-2 from DFG, Bonn, Germany, by grant 7531.50-03.0370-01/5 from SMWK, Dresden, Germany, and by EC grant GRD1-2001-40424.

REFERENCES

[1] Raff, J. (2002) *Report FZR–358*.
[2] QIAGEN (2003) *The QIAexpressionist. A handbook for high-level expression and purification of 6xHis-tagged proteins.* QIAGEN GmbH, Hilden, Germany.

Uranium speciation in two Freital mine tailing samples: 1. Sample characterization and selective sequential extractions

A.C. Scheinost, M. Leckelt, K. Krogner, R. Knappik[1]
[1]VKTA Rossendorf, Germany

ABSTRACT. We investigated two mine tailing samples from acidic ore extraction, which were buried for 30 years under several meters of mine and communal waste. In sample F1, U is predominantly water soluble and/or ion exchangeable, while in sample F3, U is predominantly hosted by recalcitrant solid phases.

During the uranium ore extraction, uranium is converted to from relatively insoluble U(IV) and U(VI) minerals to highly mobile U(VI) species. Contaminated mine waste piles and tailings and surrounding soils are usually covered by soil materials to reduce the Rn emission and radionuclide spreading by wind and water erosion. Under these conditions, microbial and surface-catalytic reduction may transform uranium back to more immobile, tetravalent or hexavalent species. The mechanisms and kinetics of this step are largely unknown, but are essential to predict the long-term risk of such deposits, as well as of nuclear waste repositories and of contaminated sites in general. Therefore, we investigated the uranium speciation in covered mine tailings by a combination of microspectroscopic and wet chemical approaches, which are fundamental to achieve reliable results [1-3]. The results are shown here and in the following reports.

EXPERIMENTAL. Total elemental concentrations were determined by ICP-MS after digestion in a microwave oven, and complemented by graphite furnace AAS and energy-dispersive XRF analysis (Spectro XLab 2000). Selective sequential extractions (SSE) included the following 6 steps [4]: **1.** Water soluble salts and exchangeable ions: 1 M NH_4NO_3. **2.** Weakly complexed ions (often specific sorption): 1 M NH_4OAc at pH 6.0**. 3.** Metals bound by Mn hydroxides: 0.1 M NH_2OH-HCl + 1 M NH_4OAc at pH 6.0 and 5.5, resp. **4.** Strongly complexed metals (bound to organic matter): 0.025 M NH_4-EDTA at pH 4.6. **5.** Metals bound by easily reducible Fe(III) minerals: 0.2 M NH_4-oxalate at pH 3.25. **6.** Metals bound by other reducible Fe(III) minerals: 0.1 M ascorbic acid + 0.2 M oxalate at pH 3.25. **7.** Recalcitrant minerals: Total – (sum of steps 1 to 6).

SAMPLES. Sediment cores were collected in 1992 at Absetzbecken 1 of the former Wismut operation site Freital near Dresden, Germany [5]. The mine tailings were in use from 1949 to 1960 for acid ore extraction wastes, and were covered from 1968 by communal waste and soil, followed by a second cover of mine waste. Samples F1 and F3 are from 5 m and 12 m depth (Table 1).
Pore waters of both samples were oxic. The high pH of F1 is associated with high Ca and S contents. The source of S could be both pyrite oxidation or the ore extraction. F1 has also much higher Cu, Zn and Pb concentrations. Uranium concentrations are high, suggesting a relatively inefficient ore extraction process.

EXTRACTION RESULTS. In the pH 8 sample (F1), the predominant part of U is highly mobile, while at pH 4 (F3), most U is strongly bound by one or several mineral phases. Other mobile metals include Ni, Cu and Zn, while Th and Pb are bound by mineral phases. Therefore, U, Ni, Cu and Zn are susceptible to leaching from these tailings.

Tab. 1: pH, Eh and elemental concentrations (mg/kg).

	F1	F3		F1	F3
pH/-	**8.0**	**4.0**			
Eh/mV	**450**	**500**	**Co**	45	37
U	**444**	**425**	**Ni**	193	115
P	651	597	**Cu**	**682**	349
S	**25900**	5433	**Zn**	**876**	294
Cl	52	127	**As**	254	177
K	27950	33500	**Se**	15	16
Ca	**12390**	1261	**Hg**	3	3
Mn	71	135	**Pb**	**1410**	128
Fe	21950	26800	**Th**	16	27

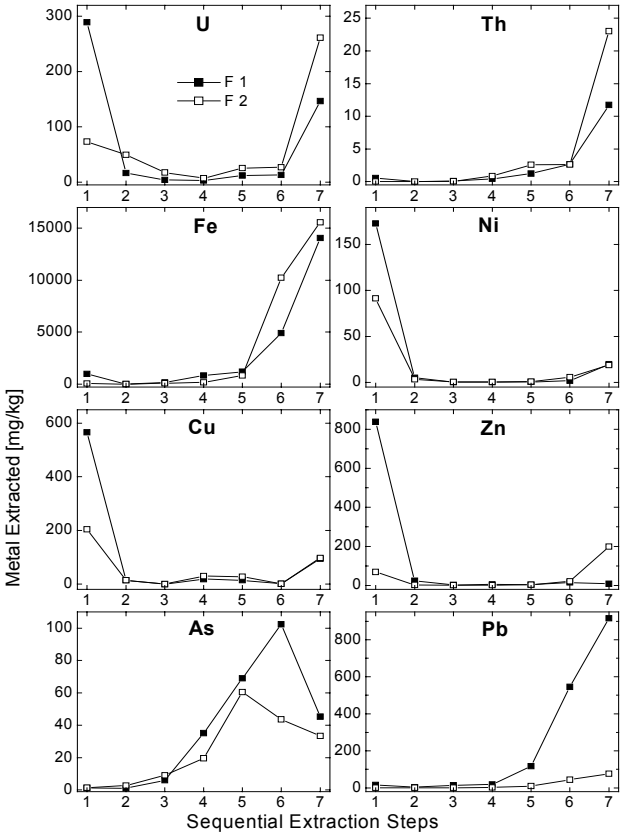

Fig. 1: Selective sequential extraction results.

REFERENCES

[1] Hunter, D. B. *et al.* (1998) *J. Radioanal. Nuclear Res.* **234**, 237-242.
[2] Morris, D. E. *et al.* (1996) *Environ. Sci. Technol.* **30**, 2322-2331.
[3] Catalano, J. G. *et al.* (2004) *Environ. Sci. Technol.* **38**, 2822-2828.
[4] Zeien, H. *et al.* (1989) *Mitt. Dtsch. Bodenkundl. Ges.* **59**, 505-510.
[5] Knappik, R. *et al.* (1996) *Migrationsverhalten von Radionukliden in Tailings unter besonderer Berücksichtigung des Oxidationspotentials in alten Tailingsablagerungen,* VKTA Rossendorf.

Uranium speciation in two Freital mine tailing samples: 2. Synchrotron µ-XRF

A.C. Scheinost, A. Somogyi[1], G. Martinez[1]
[1]European Synchrotron Radiation Facility, Grenoble, France

ABSTRACT. We investigated two mine tailing samples from acidic ore-extraction, which were buried for 30 years under several meters of mine and communal waste. In sample F1 (pH 8), U predominates homogeneously distributed at relatively low concentrations (mg/kg) in aggregates with a diameter of tens to hundreds of µm, where it is associated with K and 3d metals. In sample F3, U is highly enriched in local spots (g/kg) with distinct elemental compositions suggesting a variety of U and U-containing minerals.

Soil and sediment samples often consist of minerals and aggregates of mineral assemblies in the micrometer range. Hence probing samples with micrometer resolution allows to select single mineral grains, or at least aggregates consisting of a smaller number of different minerals than the bulk sample. While definitive mineral identification depends on µ-XRF (see following page) or µ-XAS, elemental maps and the inherent information on elemental correlations give first indications for metal species [1]. This may be especially true if elemental composition is as rich as that of the two investigated Freital mine tailing samples, which reflect the rich mineralogy of the Saxonian Erzgebirge (see preceeding page).

EXPERIMENTAL. Micro-XRF was performed on beamline ID-22 (ESRF), using KB-mirrors to focus the beam size to 2 x 6.7 µm^2. Spectra were collected with a SiLi detector. Clay-sized samples were sprinkled on Kapton tape. Elemental maps were produced from 2-dimensional micro-XRF arrays by deconvolution of the fluorescence lines with AXIL (University of Antwerp).

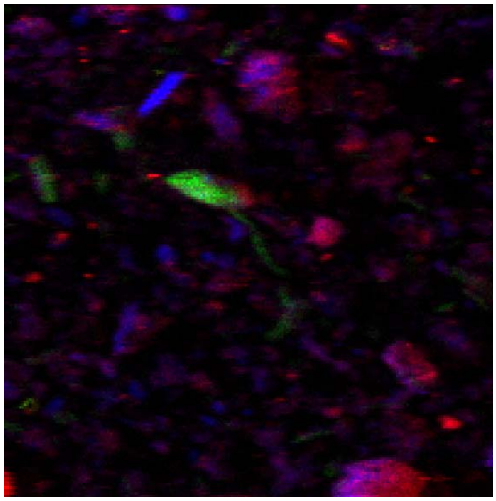

Fig. 1: F1 µ-XRF map (400x400 µm^2). U (red), K (blue), S (green).

RESULTS. In the pH 8 sample (F1), closely associated U and Cu (U/Cu, r = 0.84) occur predominately in K-rich aggregates with a diameter of tens to hundreds of µm, creating purplish hues in Fig. 1. U concentrations in these regions are in the mg/kg range, suggesting either minerals where U is not a substantial component or U sorption complexes. In addition, U occurs as small crystals without any other heavier (≥ Si) elements (red dots), presumably uranium oxides. Elongated areas with close association of Ca and S suggest gypsum (green hues), blue regions may indicate feldspar minerals.

In the pH 4 sample (F3), U does not show strong correlations with other elements across the whole map (Fig. 2, 3), indicating a more varied mineralogy or sorption complexes. In two larger aggregates, U (and Cu, Z, Ni) are again associated with K. However, other U-rich areas are associated with V (purplish regions), Cu (yellow) or Ca (not shown). Again, in some small spots U is not associated with other elements ≥ Si. In general, U concentrations are often in the g/kg range suggesting the presence of U minerals.

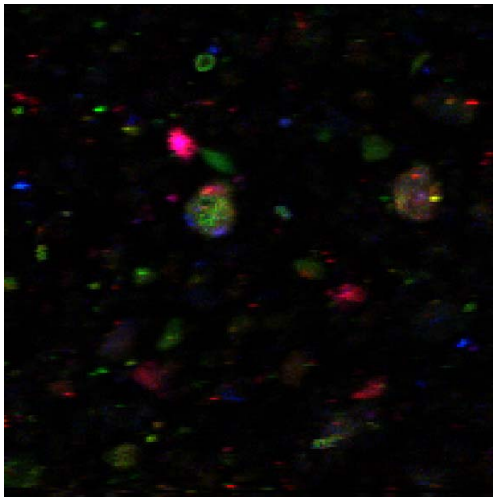

Fig. 2: F3 µ-XRF map (400x400 µm^2). U (red), Cu (green), V (blue).

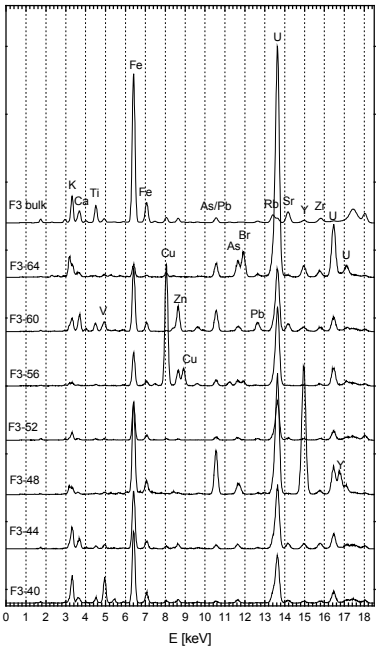

Fig. 3: XRF spectra of the bulk sample (top) and of selected micro-spots.

REFERENCES

[1] Roberts, D.R. *et al.* (2002) *Environ. Sci. Technol.* **36**, 1742-1750.

Uranium speciation in two Freital mine tailing samples: 3. Synchrotron μ-XRD

A.C. Scheinost, C. Hennig, A. Somogyi[1], G. Martinez[1]
[1]European Synchrotron Radiation Facility, Grenoble, France

ABSTRACT. We used synchrotron μ-XRD to investigate single particles of both samples. In sample F1 (pH 8), U is associated with the layer silicates muscovite, illite and kaolinite. The Selective Sequential Extraction (SSE) results suggest sorption to rather than inclusion by these minerals. In sample F3 (pH 4), U is hosted by a variety of minerals, including coffinite, uraninite, uranyl hydroxide, and vanuralite, in addition to sorption by layer silicates. Our results suggest that a large amount of U remained mobile in the tailings.

In spite of their environmental relevance, only few studies succeeded to reliably identify uranium species in contaminated soils and sediments. Hunter and Bertsch [1] found uranyl hydroxide phases and U(VI) associated with organic matter and amorphous Fe oxides in soils at the Savannah River DOE site. Morris *et al.* [2] found autunite- and schoepite-like phases in soils of the Fernald (Ohio) site. Roh *et al.* [3] found schoepite, uranophane, coffinite, U-Ca-oxide and U-Ca-phosphates at the Oak Ridge (Tennessee) site. Catalano *et al.* [4] found boltwoodite in sediments at the Hanford (Washington) site. Here we present the first study on U speciation at a former WISMUT (Germany) uranium mining and extraction site.

EXPERIMENTAL. μ-XRD was performed on beamline ID-22 at the ESRF. The beam was focused by KB mirrors to achieve a spot size of 2 x 6.7 μm^2 on the samples. μ-XRD were collected with a CCD camera positioned 60 mm behind the sample and normal to the incident beam. An incident energy of 18 keV, corresponding to a wavelength of 0.6887 Å was used. Samples were prepared by sprinkling 1-2 mg of the clay-sized mine tailing deposits onto Kapton tape. The camera images were converted to powder patterns with Fit2D (A. Hammersley, ESRF) and then analyzed by the search software EVA (Siemens).

RESULTS. The bulk mineral composition of both samples consists of quartz and phyllosilicates; F1 shows also gypsum and F2 also feldspar (Table 1). In F1, μ-XRD revealed in addition to the bulk minerals jarosite, but no U minerals. Together with the large amount of exchangeable U (see SSE results) and its diffuse distribution within K-rich aggregates, this suggests that most U is sorbed onto the edge sites of phyllosilicates. At pH 8, high [HCO_3^-] would prevent U(VI) sorption due to formation of neutral aqueous carbonato complexes, but [HCO_3^-] is low with < 0.5 mg/L [5], hence does not contradict the suggested sorption. μ-XRF suggested also a minor amount of U oxide, which was not detected by μ-XRF. The large secondary gypsum precipitates found in this sample contain only a very minor amount of U, hence are no sink for U.
In F3, the U minerals coffinite, uraninite, uranyl hydroxide and vanuralite were found. From the oxic redox potential in both samples, we conclude that the two U(IV) minerals uraninite and coffinite are remainders of the mined uranium ore, suggesting incomplete extraction. In addition, U was associated with phyllosilicate minerals suggesting again sorption. The prevalence of U in recalcitrant phases is in line with the SSE results. The low pH of 4 would prevent specific sorption to edge sites of phyllosilicates, while sorption to permanent-charge phyllosilicates like montmorillonite is possible. However, the latter minerals could not be identified, because their diagnostic region (d-spacing > 12 Å) was not achieved by our technique.
The results demonstrate that a substantial amount of U remained in the buried tailings as relatively mobile, adsorbed U(VI) species. To prevent groundwater contamination, it is therefore of paramount importance to prevent any leaching through the covered mine tailings.

Tab. 1: μ-XRD results.

Sample	Main elements	Identified phases
F1-bulk		Quartz (Qz), muscovite, (illite), kaolinite, gypsum
F1-d1100	S, Fe, As, Pb, Bi, U, Y/Rb, Zr	(Qz), muscovite, (jarosite)
F1-d014-00	S, K, Fe, Ni, Cu, Zn, Pb, U	(Qz), kaolinite, muscovite, jarosite
F1-d014-01	d014-00	(Qz), kaolinite, muscovite, jarosite
F1-d014-02	d014-00 +Ti	kaolinite, muscovite, (illite), jarosite
F1-d014-03	d014-00 +Ti	(Qz), kaolinite, muscovite, jarosite
F1-d014-07	d014-00 +Ca +Ti	(Qz), kaolinite, muscovite, (illite) , gypsum, jarosite
F1-d014-08	d014-00 +Ca +Ti	(Qz), kaolinite, muscovite, (illite) , gypsum, jarosite
F1-d014-09	d014-00 +Ca +Ti	(Qz), kaolinite, muscovite, gypsum, jarosite
F3-bulk		Qz, microcline, kaolinite, muscovite, (illite)
F3-d040	K, V, Fe, U	Qz, muscovite, (illite), hematite, **vanuralite** ($Al(UO_2)_2V_2O_8(OH)\cdot 11H_2O$)
F3-d044	K, Ca, Fe, U	Qz, muscovite , (**uraninite), (uranyl hydroxide)**
F3-d048	K, Fe, As, U, Y	(Qz), hematite, **uraninite**, xenotime
F3-d052	K, Fe, U	muscovite, (illite), **uraninite, uranyl hydroxide**
F3-d056	Fe, Cu, Cr, U	(Qz), muscovite, (illite)
F3-d060	K, Ca, Ti, V, Fe, Zn, As, Pb, U	(Qz), muscovite, (illite)
F3-d064	K, Ca, Fe, Br, U	Qz, **coffinite**

REFERENCES

[1] Hunter, D. B. *et al.* (1998) *J. Radioanal. Nuclear Res.* **234**, 237-242.
[2] Morris, D. E. *et al.* (1996) *Environ. Sci. Technol.* **30**, 2322-2331.
[3] Roh, Y. *et al.* (2000) *Soil Sediment Contam.* **9**, 463-486.
[4] Catalano, J. G. *et al.* (2004) *Environ. Sci. Technol.* **38**, 2822-2828.
[5] Knappik, R. *et al.* (1996) *Migrationsverhalten von Radionukliden in Tailings unter besonderer Berücksichtigung des Oxidationspotentials in alten Tailingsablagerungen*, VKTA Rossendorf.

Bacterial community changes after addition of U(VI) to a U mining waste pile sample

A. Geißler, S. Selenska-Pobell, M. Leckelt, K. Krogner, A.C. Scheinost

ABSTRACT. A sample from the uranium mining waste pile Haberland containing originally 40 mg/kg of U was supplemented with 58 mg/kg of U(VI). Selective sequential extraction analysis showed that most of the added U(VI) remained as weakly complexed species. The growth of several *Pseudomonas*, *Arthrobacter* and *Geobacter* populations was stimulated by the addition of U(VI).

Bacteria have developed different mechanisms to tolerate the presence of uranium or to even make use of U(VI) as terminal electron acceptor in anaerobic respiration [1]. Therefore, they play a major role in the biogeochemical cycling of this element and can be used for the bioremediation of uranium contaminated sites. In order to understand how U(VI) influences and interacts with bacterial communities which are indigenous for such sites a sample called JG35 which was collected from the uranium mining waste pile Haberland situated near the town of Johanngeorgenstadt in Germany was analyzed before and after supplementation with U(VI). The latter was added in a form of uranyl nitrate (pH 4.0) to 15 g of the JG35 sample in a plastic tube and incubated for four weeks in dark at 10 °C. The bioavailability of the originally present and of the added uranium was assesses by selective sequential extraction (SSE) analysis according to Zeien and Brümmer [2]. Information about the bacterial community structures of the original sample (JG35), containing 40 mg/kg U, and of the supplemented with 59 mg/kg U(VI) sample (JG35+U1) was derived via the 16S rDNA retrieval [3].

It is evident from the results presented in Fig. 1 that after four weeks of incubation most of the U(VI) added was extracted from the JG35+U1 sample by the second step with 1 M NH_4Oac (pH 6), indicating that U was predominantly weakly complexed. A small amount of U(VI) was also bound by Mn(hydr)oxides (step 3) and by Fe(hydr)oxides of low crystallinity (step 5). A higher concentration near the U(VI) inflow suggests strong retention of uranium by the sample.

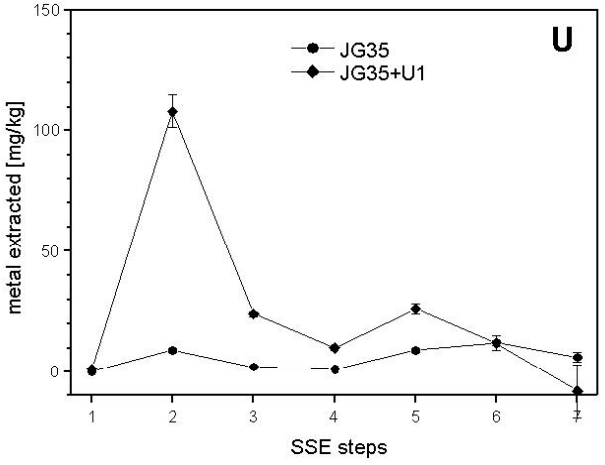

Fig. 1: SSE analysis of the untreated sample JG35 and of the sample with added U(VI), JG35+U1.

The 16S rDNA retrieval revealed that representatives of the *Holophaga/Acidobacterium* phylum and of α-Proteobacteria are dominating the bacterial community of the JG35 sample (not shown). This finding is in agreement with our previous studies on bacterial diversity of other equally polluted samples collected from the same site [4]. The predominant bacterial populations in the community of the sample JG35+U1 were analyzed after 4 weeks of incubation with U. No *Holophaga/Acidobacterium* and only a few α-Proteobacteria were retrieved. Instead, sequences of γ-*Pseudomonas*, *Arthrobacter*, and *Geobacter* spp. were found (Fig. 2). This is in line with the high potential of *Pseudomonas* spp. to accumulate and/or to reduce U(VI) [5]. Interestingly, the natural bacterial community of the most contaminated (108 mg/kg U) sample collected from the same site was also enriched with γ-*Pseudomonas* [4]. *Arthrobacter* spp. have been frequently observed in different extreme, heavy-metal contaminated environments, which suggests the potential to resist heavy metals [6]. *Geobacter* spp. are able to reduce and immobilize a large number of metals and radionuclides [1].

This work demonstrates for the first time a response of a natural bacterial community of a particular environment to the addition of U(VI). Further monitoring of the bacterial community structure changes and also of the formation of different U complexes in the JG35+U samples, after longer incubation with U, is of great importance for understanding the processes induced by U(VI) in the studied environment (work in progress in our laboratory). Such experiments may help to improve our knowledge about the role of bacteria in the geochemical cycle of U.

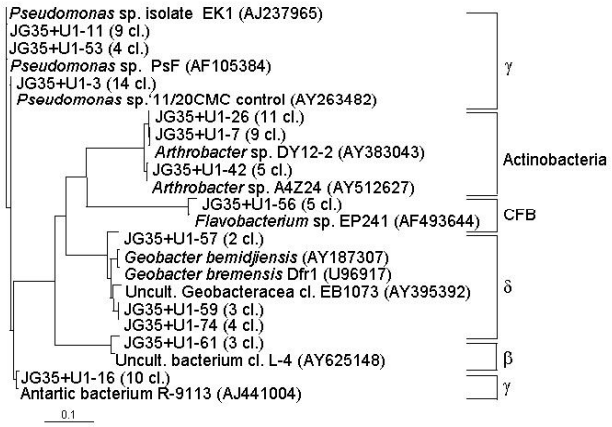

Fig. 2: Predominant bacterial populations in sample JG35+U1.

REFERENCES

[1] Lovley, D.R. (1993) *Annu. Rev. Microbiol.* **47**, 263-290.
[2] Zeien, H.; Brümmer, G.W. (1989) *Mitt. Dtsch. Bodenkundl. Ges.* **59**, 505-510.
[3] Geißler, A. (2003) *Report FZR-377*.
[4] Selenska-Pobell, S. *et al.* (2005) In: *Perspectives in Environmental Microbiology*, Elsevier Sci. Publ., Amsterdam, in press.
[5] McLean, J. *et al.* (2001) *Appl. Environ. Microbiol.* **67**, 1076-1084.
[6] Hanbo, Z. *et al.* (2004) *FEMS Microbiol. Ecol.* **49**, 333-341.

Autotrophic bacterial diversity in waters of the Siberian deep-well monitoring site Tomsk-7

M. Nedelkova, S. Selenska-Pobell

ABSTRACT. The diversity of autotrophic bacteria was studied in deep underground waters near the radioactive waste injection site Tomsk-7 by using the RubisCO molecular approach. Some of the retrieved sequences were affiliated with RubisCO genes of Proteobacteria, which are related to those identified previously in the same samples via the 16S rDNA retrieval. Furthermore, the method revealed the presence of other autotrophic organisms, which were not identified by the 16S rDNA approach.

Autotrophic microorganisms have been identified in different subsurface and deep-sea habitats [1, 2]. They may play an important role in such oligotrophic environments, where carbon dioxide is the primary carbon source. The enzyme responsible for the CO_2 fixation is RubisCO, which occurs in four forms. The most extensively studied is the RubisCO form I, which is divided into green-like and red-like groups. It is widely distributed within plants, algae and the most photo- and chemoautotrophic bacteria.

EXPERIMENTAL. The autotrophic bacterial diversity was studied in water samples collected from depths of 290 to 324 m at the monitoring site S15 near the city of Tomsk, Russia. The biomass from the samples was concentrated via consequent filtration on a glass fiber filter and on two filters with pore sizes of 0.45 μm and 0.22 μm. Total DNA was isolated from the whole biomass collected on all three filters for the S15A sample and separately for each of the filters for the S15B sample. In order to achieve more detailed characterization of the indigenous autotrophic bacteria at that site, primer pairs developed by Alfreider [1] and Nanba [3] specific for RubisCO form I were used and clone libraries for the S15A and S15B samples were generated.

RESULTS. The phylogenetic tree presented in Fig. 1 summarizes the results from affiliation of the deduced amino acid sequences of the RubisCO I clones. Forty-seven green-like RubisCO genes were retrieved by the Alfreider primers in the S15B sample. All of them, represented by S15BAlf1 clone, were almost identical with the RubisCO gene of the *Hydrogenophilus thermolutheolus*, a facultative chemolithoautotroph from the β-subclass of Proteobacteria. Interestingly, in our previous study of the same sample, applying the 16S rDNA approach [4], 30 % of the clones were related to a β-proteobacterial species. One additional clone S15BNan3 from the green-like group was identified with the Nanba primers in the S15B sample as well. In the S15A sample only six green-like RubisCO clones were retrieved by using the two primer pairs.

A total of thirty-six red-like RubisCO I genes were identified using the Nanba primer pairs. Almost all of them were similar between the S15A and S15B samples. More than half of the clones clustered with the RubisCO gene of the ammonia-oxidizing *Nitrosospira* sp. 40KI from the β-subclass of Proteobacteria [5]. Other group of clones from the two samples were similar to the RubisCO genes of *Xantobacter flavus* and *Ralstonia eutropha.* The sequence of the individual clone S15BNan30 affiliated with the RubisCO gene of *Sinorhizobium meliloti*. The individual clone S15ANan17 clustered with an uncultured bacterium from volcanic deposit [3].

The identification of facultative chemolithoautotrophic bacteria from the *Ralstonia* and *Sinorhizobium* genus is in agreement with our 16S rDNA analysis of that samples [4]. Interesting is the result that more than 80 % of the sequences were affiliated with RubisCO genes of different species from the β – subclass of Proteobacteria. The latter were earlier estimated also as predominant in the studied sample applying the 16S rDNA approach.

In this work mainly β – Proteobacteria were identified by using the RubisCO I retrieval. However, three more forms of the RubisCO gene (II, III and IV) were found in several other bacterial groups. Our first analyses based on a RubisCO II approach demonstrate presence of other additional autotrophic bacteria in the sample S15A.

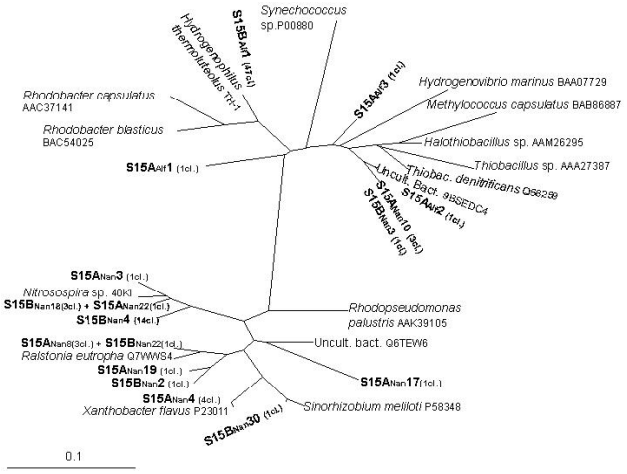

Fig.1: The green-like and red-like RubisCO clones identified at the S15 site. The number of clones is given in brackets.

ACKNOWLEDGEMENTS. This work was partly supported by grant FIKW-CT-2000-00105 "BORIS" from the EU.

REFERENCES

[1] Alfreider, A. *et al*. (2003) *Microb. Ecol*. **45**, 17-328.
[2] Elsaied and Naganuma (2001) *AEM* **67**, 1751-1765.
[3] Nanba, K., *et al.* (2004) *AEM* **70**, 2245-2253.
[4] Nedelkova, M. *et al.* (2005) In: *Underground Injection Science and Technology*, Elsevier Sci. Publ., Amsterdam, in press.
[5] Utäker, J. *et al.* (2002) *J. Bact*. **184**, 468-478.

Differences between planktonic and biofilm-associated bacterial communities in drain waters of the uranium mill tailings Königstein

K. Flemming, S. Selenska-Pobell

ABSTRACT. Biofilms formed on several bioceramic filters used for cleaning heavy metal polluted waters were analyzed and compared with the bacterioplankton of the same waters. Our analyses indicate that the biofilms were specifically enriched with bacteria which were not predominant in the plankton fraction.

EXPERIMENTAL. Molecular analysis was performed of microbial diversity in one water sample (E-318) collected in October, 2003 from the U mill tailings Königstein and of the biofilms (BFs) formed on three *B. sphaericus* based bioceramic (biocer) filters [1] prepared for water purification. Biofilm BF-F2 was formed on a biocer soaked in 1L of the E-318 water for 8 weeks, biofilm BF-M1u - on a biocer through which original E-318 water was flowing for 4 weeks in August, 2003. The third biofilm (BF-S3) was loaded with E-318 water in a similar way as BF-M1u, but in June, 2003 and than stored at 4 °C for one month before analysis. The U content in the waste water was about 4 mg/L. Molecular analyses were based on the 16S rDNA retrieval by using the PCR primer pair 7F - 1513R [2, 3].

RESULTS. The following 16S rDNA clone libraries were constructed: **E-318,** representing the planktonic microbial populations; **BF-F2**, **BF-M1u,** and **BF-S3**, representing the bacterial populations of the corresponding biofilms (see Table 1).

Tab. 1: Structure of the studied bacterial communities.

Bacterial group	Populations sizes in % found in:			
	E-318	BF- F2	BF-M1u	BF-S3
α-Proteobacteria	7	9	3	6
β-Proteobacteria	7	74	32	9
γ-Proteobacteria	13	-	24	-
ε-Proteobacteria	44	-	-	-
CFB[1]	29	14	17	30
Holophaga/Acidobacteria	-	-	16	24
Clostridium sp.	-	-	-	22
Cyanobacteria/Chloroplasts	-	3	8	-
GNSB[2]	-	-	-	4.5
Candidate Division OP11	-	-	-	4.5

[1]-*Cytophaga/Flavobacterium/Bacteroides*, [2]-Green non-sulfur bacteria.

It is evident from the data presented in the table 1 that the microbial composition of the three biofilms is highly specific and differs significantly from that of the planktonic community of the **E-318** water. However, representatives of three bacterial groups, namely of **α-** and **β-Proteobacteria,** and also of **CFB** were identified in all of the samples studied.

α-Proteobacteria: The number and the size of the retrieved bacterial populations of this subdivision were relatively small in all samples. In the case of the **E-318** plankton and of the **BF-M1u**, which was immediately analyzed after its loading with continuously running fresh E-318 water, mainly populations of closely related purple non-sulfur photosynthetic bacteria were identified. In the case of the **BF-F2** which was developed on a biocer via static incubation in 1L of E-318 water as well as in the case of the **BF-S3** which was stored at 4 °C before analyses, mainly biofilm-specific perchlorate-reducing and nitrifying-denitrifying α-Proteobacteria were identified.

β-Proteobacteria: The size and the structure of the retrieved β-proteobacterial populations varied very strongly between the samples. In the case of **E-318** only a few oligotrophic and chemoautotrophic populations of this subdivision were identified. In contrast, **BF-M1u** was highly enriched with 16S rDNA sequences of arsenite-oxidizing and also of other bacteria with undefined function which were previously retrieved in soil samples of the U mill tailings Gittersee [2, 3]. The highest number of β–proteobacterial 16S rDNA sequences was found in **BF-F2**. According to our analysis this biofilm was strongly enriched with members of the metal-resistant *Ralstonia* species, with denitrifying Fe-oxidizing bacteria, and also with several small groups of oligo- and autotrophic bacteria. The retrieved rDNA sequences in the **BF-S3** were limited to only one group of oligotrophic N_2-fixing bacteria found also in the **BF-F2.**

CFB: The **E-318** sample contained mainly 16S rRNA genes of *Sphingobacterium*, which belongs to the biggest fresh water cluster of **CFB** [4], whereas the biofilm samples contained mainly 16S rDNA sequences of biofilm-specific bacteria, such as those retrieved formerly in nitrogen and phosphor removing biofilms (**BF-M1u**), arsenite-oxidizing biofilm (**BF-F2**), and in the uranium contaminated aquifer (**BF-S3**).

Specific for the sample **E-318** was the high number of 16S rDNA sequences representing metal- and sulphate-reducing **ε-Proteobacteria** which were not identified in the biofilms. For **BF-M1u** and **BF-S3** *Holophaga/Acidobacterium* members were characteristic. 16S rDNAs of cyanobacteria and of chloroplasts of not yet cultured diatoms, identified earlier in an arsenite-oxidizing biofilm, were found in **BF-M1u** and **BF-F2.** Most specific for **BF-S3** was the enrichment with 16S rDNAs of *Clostridia*, GNSB, and also of the Candidate Division OP11.

Our results demonstrate significant differences between plankton and biofilm bacterial communities. This indicates that these communities are involved in different biogeochemical processes. The conditions of the biofilms formation strongly influence their structure and presumably their activity as well. Remarkably, some of the sequences retrieved in the biofilms were related to 16S rRNA genes identified previously in soil but not in water samples of different U wastes [2, 3]. The latter indicates that their bacterial hosts are involved in processes associated with the surfaces of the sediments but not with the plankton from where they were captured and amplified.

ACKNOWLEDGEMENTS. This study was supported by grant No. 03I4004B from the Bundesministerium für Bildung und Forschung, Berlin, Germany.

REFERENCES

[1] Raff, J. *et al.* (2003) *Chem. Mater.* **15,** 240-244.
[2] Selenska-Pobell, S. *et al.* (2001) *Int. J. Gen. Mol. Microbiol. Antonie van Leewenhuek* **79**, 149-161.
[3] Selenska-Pobell, S. (2005) In: *Perspectives of Environmental Microbiology*, Elsevier Sci. Publ., Amsterdam, in press.
[4] Glöckner, F. *et al.* (2000) *Appl. Env. Microbiol.* **66**, 5053-5065.

Development of microsensoric equipment and a simple rotating reactor for replicated biofilm studies on various rock-forming minerals

K. Großmann, T. Arnold

ABSTRACT. A special reactor, which provides optimal and near-natural growth conditions for bacteria, was developed for cultivation and microsensoric characterization of biofilms on rocks and rock-forming minerals.

Bacteria in nature usually do not occur as single individual cells but rather in large communities of bacteria glued together by Extracellular Polymeric Substances (EPS). Such aggregates are called biofilms. They may significantly influence the transport of heavy metals in the geosphere by changing the geochemical conditions within the biofilm or simply by adsorption of heavy metals onto biological surfaces. For the cultivation and study of these microbial communities, a variety of devices are available [1]. For our studies we use two different reactor systems: (1.) a simple flow-through cell reactor to obtain geochemical information within the biofilms by microsensors and (2.) a rotating annular bioreactor to generate thick biofilms.

SIMPLE FLOW-THROUGH REACTOR. To measure electrochemical conditions such as pH and Eh *in situ* within the biofilm and in the surrounding bulk solution we use the experimental setup shown in Fig. 1. The used reactor is a simple flow-through cell reactor. By using this reactortype we obtained a maximum biofilm thickness of 50 µm (Fig. 2). The sensors were provided from the "Kurt-Schwabe-Institut", Meinsberg, with tailor-made long and thin tips. The sensors were inserted through the nutrient solution into the biofilm via a micrometer screw. Independent from the insertion depth into the biofilm and the bulk solutions the measured pH and Eh values were very similar. These results, however, may be an artifact because the surrounding bulk solution may have entered the hollow space created by the retracting microsensor tip. To improve the situation the sensors will be minimized further, the insertion depth will be monitored by a lens system, and the measurement direction will be reversed.

ROTATING ANNULAR REACTOR. A rotating annular reactor is a system with a stationary outer and a rotating inner cylinder. This system provides a well mixed liquid phase, turbulent flow and constant shear fields and is suitable for cultivation of biofilms from flowing environments [2]. Lawrence *et al*. described the design of similar rotating annular reactors and by using it acquired bioflms of approximately 150 µm thickness. To increase our biofilm thicknesses obtained with the simple flow-through reactor we will use a bioreactor as shown in Fig. 3. For biofilm sampling, removable microscopic slides with affixed mineral platelets are placed in recessed slots on the outside of the inner cylinder. These slides can be removed via a port in the top of the reactor. The nutrient solution is pumped into the base of the reactor, triggering a circulation from bottom to top.

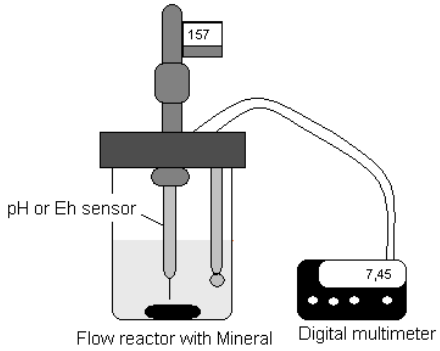

Fig. 1: Schematic diagram of the experimental design to measure the electrochemical conditions inside the biofilm.

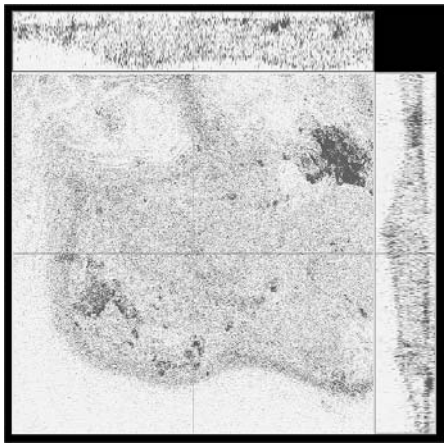

Fig. 2: *Pseudomonas aeruginosa* biofilm on a biotite surface. Main window shows a top view on and the right and top window shows a cross section of the biofilm with 25 µm thickness.

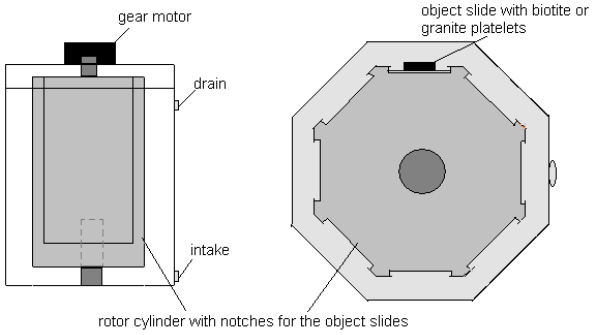

Fig. 3: Schematic diagram of the rotating annular reactor.

REFERENCES

[1] Caldwell *et al*. (1997) In: *Manual of Environmental Microbiology*, pp. 79–90, ASM Press, Washington, DC.
[2] Lawrence *et al.* (2000) *J. Microbiol. Methods* **42**, 215–224.

Part 3:

Interaction of actinides with solid phases

Study of the humic acid synthesis in the presence of kaolinite and of the U(VI) adsorption onto a synthetic humic substance-kaolinite sorbate

S. Sachs, G. Bernhard

ABSTRACT. The synthesis of humic acid M42 was studied in the presence of kaolinite to estimate its influence on the humic acid formation. The U(VI) sorption onto the obtained humic substance-kaolinite sorbate was determined depending on pH.

The risk assessment of future nuclear waste repositories requires knowledge on the migration behavior of actinides in potential host rock formations, which is significantly influenced by humic substances. Clay formations as possible host rocks are closely associated with natural organic matter. The immobilization as well as the release of humic substances by clays can influence the mobilization of actinide ions. Furthermore, clay minerals can affect the formation of humic acid-like melanoidins [1].
First studies were performed in order to determine the impact of kaolinite KGa-1b (Clay Mineral Society) on the formation of a synthetic humic acid (HA) and the U(VI) sorption on a synthetically obtained humic substance-kaolinite sorbate.

EXPERIMENTAL. HA type M42 was synthesized in a parallel batch starting from 16.5 g xylose, 11 g glutamic acid monohydrate and 150 mL water in the absence or presence of 2 g kaolinite KGa-1b (HA M42 and M42K, respectively). After reflux boiling (90 h, 80 °C), the HA-like products were isolated from both batches. A humic substance-kaolinite sorbate (M42-KS) was isolated from the batch synthesized in presence of kaolinite. The U(VI) sorption onto M42-KS was studied between pH 3 and 10 ($[UO_2^{2+}]$: $1 \cdot 10^{-6}$ M, I: 0.01 M $NaClO_4$, S/L: 4 g/L).

RESULTS. We isolated 196 mg HA M42 and 137 mg HA M42-K. The yield differences can be attributed to the adsorption of humic substances onto the kaolinite when present in the synthesis. The TOC content of the kaolinite sorbate M42-KS was determined with 24 mg C/g representing about 44 mg humic substances/g. Both HA show small differences in their elemental compositions (C, H, N, S) and functional group contents. Fig. 1 depicts the FT-IR spectra of both HA in comparison to that of kaolinite. Generally, both HA have comparable structural elements. However, IR absorption bands were detected in the M42-K spectrum (e.g., 3693, 3620, 1033, 1013, 541, 472 cm^{-1}) that point to the occurrence of kaolinite residues in this HA. Al and Si traces in the HA (determined by ICP-MS) support this observation. These results indicate that the presence of kaolinite during the synthesis mainly influences the HA yield and the elemental composition of the resulting HA (Al, Si content).
In Fig. 2 the U(VI) sorption onto M42-KS is shown in comparison to that onto kaolinite KGa-1b in absence and presence of ^{14}C-labeled HA M42 (^{14}C-M42) [2]. Between pH 3 and 6 the U(VI) sorption onto M42-KS is comparable to that of U(VI) onto KGa-1b in ^{14}C-M42 presence. The U(VI) adsorption is increased compared to that of the HA-free system which is ascribed to the sorption/association of HA on/with KGa-1b. Compared to the HA-free system, the U(VI) sorption onto M42-KS is significantly reduced between pH 6 and 8. This is in contrast to the ^{14}C-M42-KGa-1b system. Under these conditions

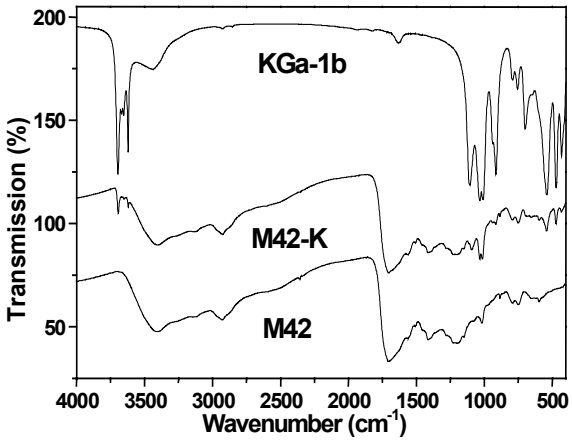

Fig. 1: FTIR spectra of HA synthesized in absence (M42) or presence (M42-K) of kaolinite KGa-1b in comparison to kaolinite KGa-1b (spectra are shifted along the y-axis.).

M42-KS releases HA, resulting in HA concentrations of about 35-50 mg/L which are significantly higher than in the ^{14}C-M42-KGa-1b system. Thus, the decrease in the U(VI) sorption can be explained by the formation of soluble U(VI)-HA complexes. A further reduction of the U(VI) sorption onto M42-KS was observed between pH 8 and 10. This behavior can be attributed to two overlapping processes: (i) the formation of soluble U(VI)-HA complexes and (ii) the formation of U(VI) carbonates which dominate the U(VI) sorption in the HA-free system in this pH range.

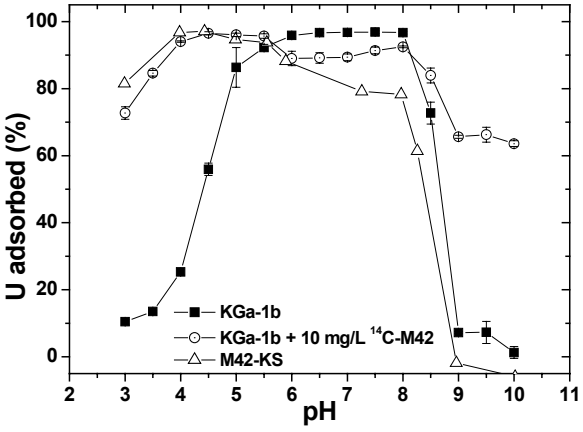

Fig. 2: U(VI) sorption onto the humic substance-kaolinite sorbate M42-KS and onto kaolinite (KGa-1b) in absence and presence of HA ^{14}C-M42 [2].

These first results indicate that the release of HA from HA-clay associates can significantly increase the mobilization of U(VI). In future studies, the U(VI) sorption onto M42-KS will be compared to that in the ^{14}C-M42-KGa-1b system, however, using higher HA concentrations.

ACKNOWLEDGEMENT. The German Federal Ministry of Economics and Labor funded this work (02E9673).

REFERENCES

[1] Taguchi, K. *et al.* (1986) *Org. Geochem.* **10**, 1081-1089.
[2] Křepelová, A. *et al.* this report, p. 50.

U(VI) sorption onto kaolinite in the presence and absence of humic acid (HA)

A. Křepelová, S. Sachs, G. Bernhard

ABSTRACT. In the present work the uranium(VI) sorption onto kaolinite was investigated in batch experiments as a function of the pH. Experiments were performed in the absence and presence of CO_2 with varying uranium concentration as well as ionic strength, as in the absence and presence of HA.

The migration behavior of actinides is influenced by humic acids, which affect the speciation of metal ions and thus, their migration in the environment. Within this work the influence of HA on the uranium sorption onto clay minerals was studied exemplary with kaolinite.

EXPERIMENTAL. The sorption experiments were performed at room temperature applying ^{14}C-labelled synthetic HA type M42 [1] and kaolinite KGa-1b from the Clay Minerals Society Source Clay Repository (Washington County, Georgia) [2]. Kaolinite suspensions were equilibrated for 72 hours and 4 – 5 weeks in the presence and absence of CO_2, respectively. The final concentrations of U(VI) and HA were $1 \cdot 10^{-5}$ M or $1 \cdot 10^{-6}$ M and 10 or 50 mg/L, respectively. The solid liquid ratio was 4 g/L and the ionic strength was 0.1 M or 0.01 M $NaClO_4$. The pH values were adjusted in the range from pH 3 to pH 10. The contact time was 60 hours. The samples were analyzed by LSC for the final HA concentration and by ICP-MS for the final U(VI) concentration.

RESULTS

Sorption of HA onto kaolinite:
The sorption of HA decreases with increasing pH values. This decrease is regarded as the result of the electrostatic repulsions between carboxyl groups of HA and the kaolinite surface. At pH > 3 carboxyl groups of HA are deprotonated resulting in a negative charge of the HA. The surface charge of kaolinite is considered to be also negative in this pH range (p.z.c. = 6.0 [3]). Other contribution factors would arise from specific site binding mechanisms as the ligand exchange and/or surface complexation reaction between -OH groups on kaolinite and anionic groups of HA. With increasing HA concentration the percentage of HA uptake decreases due to saturation of binding sites of kaolinite.

Sorption of U(VI) onto kaolinite in the absence of HA:
a) Effect of CO_2:
In the presence of CO_2 U(VI) uptake onto kaolinite increases up to pH 8 above which it decreases. In the absence of CO_2, no decrease was observed at pH > 8. This behavior is a result of the uranium speciation in the solution in the presence and absence of CO_2. In the presence of CO_2 uranium forms strong negatively charged uranyl-carbonate complexes. The kaolinite surface is also negatively charged, which effects the electrostatic repulsions between uranyl-carbonate complexes and the kaolinite surface resulting in the low uranium adsorption in this pH range (Fig. 1).
b) Influence of U(VI) concentration:
The percentage of U(VI) adsorbed onto kaolininte decreases with increasing U(VI) concentration because of saturation of the binding sites on kaolinite.

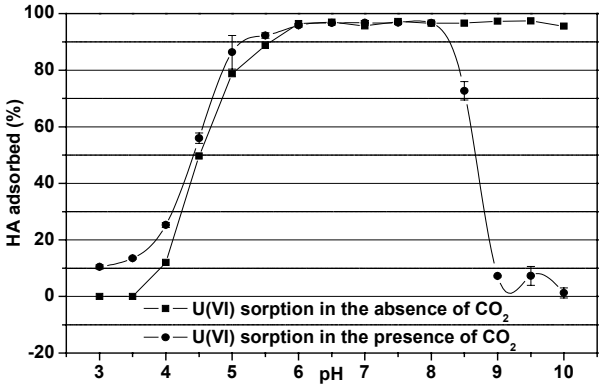

Fig. 1: Effect of CO_2 on U(VI) sorption onto kaolinite. [U] = $1 \cdot 10^{-6}$ M, I = 0.01M $NaClO_4$.

c) Effect of the ionic strength:
The ionic strength has no (pH > 6) or only small (pH 3 - 5.5) influence on the U(VI) sorption.

Sorption of U(VI) onto kaolinite in the presence of HA:
The sorption curve can be divided into three parts (Fig. 2). In the first pH region, at pH < 5, the presence of HA enhances the U(VI) uptake compared to the HA-free system because the adsorbed HA forms additional binding sites for U(VI). In the second pH region, between pH 5 and pH 8.5, the adsorption of U(VI) is higher in the absence of HA than in its presence due to the desorption of HA from the kaolinite surface resulting in the formation of dissolved U(VI)-HA complexes. In the third pH region, at the pH > 8.5 sorption of U(VI) again increases in the presence of HA. The reasons for that are unclear up to now. EXAFS studies are in progress in order to determine the surface complexes.

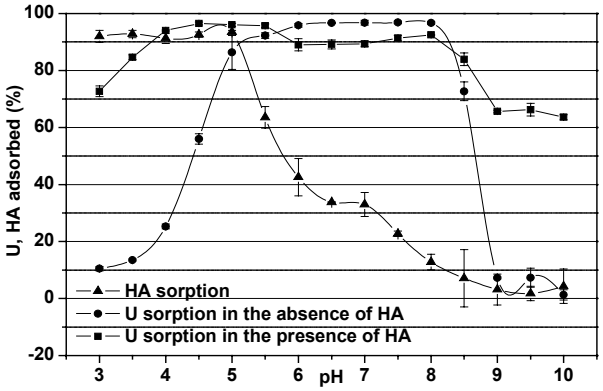

Fig. 2: Influence of HA on U(VI) sorption onto kaolinite. [HA] = 10 mg/L, [U] = $1 \cdot 10^{-6}$ M, I = 0.01 M $NaClO_4$.

ACKNOWLEDGEMENT. This work was financially supported by the Bundesministerium für Wirtschaft und Arbeit under contract No. 02E9673.

REFERENCES

[1] Sachs, S. *et al.* (2004) *Report FZR–399*.
[2] Pruet, R.J. *et al.* (1993) *Clays Clay Miner.* **41,** 514–519.
[3] Redden, G.D. *et al.* (1998) In: *Adsorption of Metals by Geomedia*, Academic Press, San Diego, p. 291–315.

Feasibility of EXAFS experiments at the Np L-edge to investigate neptunium sorption on kaolinite

T. Reich[1], S. Amayri[1], Ta. Reich[1], J. Drebert[1], A. Jermolajev[1], P. Thörle[1], N. Trautmann[1], C. Hennig, S. Sachs
[1]Institute of Nuclear Chemistry, Johannes Gutenberg-Universität Mainz, Mainz, Germany

ABSTRACT. We have investigated the feasibility of Np L-edge EXAFS measurements to study the sorption of neptunium onto the reference clay kaolinite KGa-1b.

Several collaborating groups selected the kaolinite KGa-1b from the Source Clays Repository as reference clay for a broad range of investigations dealing with the interaction of actinides in the system clay, humic substances, and aquifer. During recent EXAFS measurements of uranium(VI) sorption onto kaolinite KGa-1b, we found that this kaolinite contains traces of zirconium. The energy of the Zr K-edge equals 17998 eV. Therefore, we expected a distortion of the Np L_3-edge (17610 eV) EXAFS signal at this energy or at k approximately equal to 9.8 $Å^{-1}$. In our experiment we wanted to explore the possibilities for avoiding severe distortions in the Np EXAFS signal without limiting the useful k range to 9.8 $Å^{-1}$.

EXPERIMENTAL. Two samples, 1 and 2, with different amounts of neptunium(V) sorbed on KGa-1b were prepared from a 1.8 mM Np(V) stock solution of Np-237 under the following conditions: 4 g kaolinite/L, pH 9.0, $p(CO_2) = 10^{-3.5}$ atm, I = 0.1 M $NaClO_4$. The total neptunium concentration for samples 1 and 2 was $8 \cdot 10^{-6}$ and $2 \cdot 10^{-5}$ mol/L, respectively. The neptunium uptake of samples 1 and 2 as measured by γ-spectroscopy was 300 and 510 ppm, respectively. The solid residue was loaded without drying into the EXAFS sample holder. The neptunium EXAFS spectra were measured at ROBL (ESRF, BM20) [1] at room temperature in the fluorescence mode using a 13-element Ge solid-state detector.
The following measurements were performed on these samples:
1) The Np $L\alpha_1$-radiation at 13.9 keV was recorded as a function of photon energy across the Np L_3-edge EXAFS region using single-channel analyzers (SCA's). The signal was corrected for detector dead time.
2) The EXAFS spectrum was measured at the Np L_2-edge (21600 eV) by setting the SCA's to 17.8 keV to record the Np $L\beta_1$-radiation. Dead time correction was performed as described above.

RESULTS. Figure 1 shows the Np EXAFS spectra and the corresponding Fourier transforms of sample 1 (300 ppm Np) measured at the L_3- and L_2-edges. Seven sweeps at the Np L_2-edge and six sweeps at the L_3-edge were averaged. The useful k range at the L_3-edge was limited to k_{max} equal to 9.4 $Å^{-1}$ due to the Zr K-edge absorption. The Np L_2-edge EXAFS signal could be recorded with good statistics up to k_{max} equal to 11.4 $Å^{-1}$. To obtain a higher resolution in the Fourier transform, it is preferable to record the Np EXAFS signal of the kaolinite samples at the Np L_2-edge instead of the L_3-edge.
Table 1 summarizes the EXAFS structural parameters of sample 1 derived from the Np L_3- and L_2-edge k^3-weighted EXAFS spectra. The detected neptunium coordination shells and bond distances are consistent with the formation of a neptunium(V) carbonato species at the kaolinite surface. A similar result was obtained for sample 2 (510 ppm, not shown here).
In conclusion, these test experiments showed that it is possible to study the sorption of neptunium onto kaolinite KGa-1b successfully using Np L_2-edge EXAFS spectroscopy. In future EXAFS experiments, it will be possible to study sorption samples with less than 300 ppm neptunium by collecting more than seven sweeps per sample.

ACKNOWLEDGEMENTS. This work was supported by the BMWA grant No. 02 E 9653.

REFERENCES

[1] Matz, W. *et al.* (1999) *J. Synchrotron Rad.* **6**, 1076-1085.

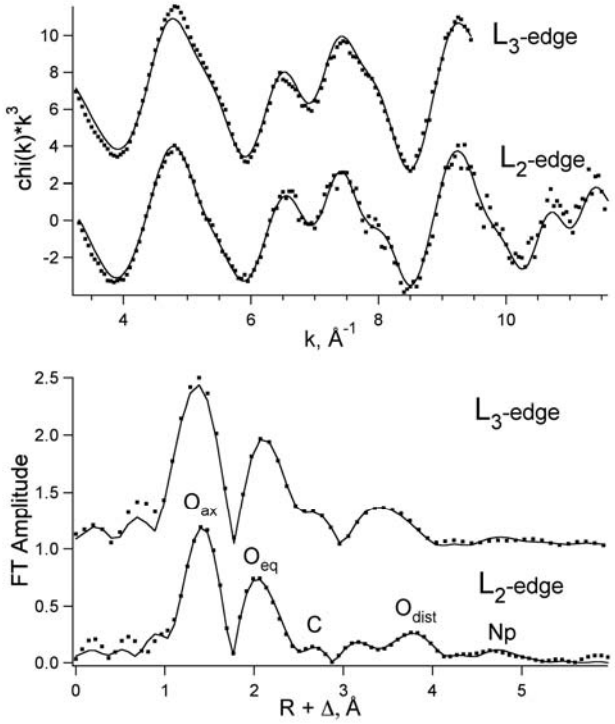

Fig. 1: Neptunium L-edge k^3-weighted EXAFS spectra (top) and corresponding Fourier transforms (bottom) of 300 ppm Np(V) sorbed onto kaolinite at pH 9.0 under ambient conditions. Dots – raw experimental data, solid line – best theoretical fit to the data.

Tab. 1: EXAFS structural parameters for 300 ppm Np(V) sorbed onto kaolinite at pH 9.0 under ambient conditions. Multiple-scattering paths are not listed. Coordination numbers were held constant during the final fit according to the result of previous fits.

Shell	Np L_2-edge		Np L_3-edge	
	R(Å)	σ^2(Å^2)	R(Å)	σ^2(Å^2)
2 x O_{ax}	1.85	0.0021	1.84	0.0010
4 x O_{eq}	2.55	0.0051	2.55	0.0054
2 x C	2.94	0.0060	2.95	0.0027
2 x O_{dist}	4.24	0.0040	4.25	0.0044
1 x Np	4.86	0.0023	4.89	0.0050

Uranium(VI) surface speciation on quartz

V. Brendler, N. Baumann, T. Arnold, G. Geipel

ABSTRACT. Characteristic fluorescence properties of uranium(VI) surface complexes on quartz suspensions have been determined, using time-resolved laser-induced fluorescence spectroscopy (TRLFS).

Quartz, together with Al-(hydr)oxides, serves as a model substance for more complex systems such as mica and clay minerals. The aim is to identify and quantify the various surface complexes probably forming on silanol surface sites, in competition with aluminol groups.

EXPERIMENTAL. The quartz used unaltered in all experiments was a commercial product (Merck SiO_2 p.a.). Its specific surface area was 0.11 and 0.66 m²/g for the two separated grain size fractions 20-63 µm and below 20 µm, respectively (five-point N_2-BET). All measurements were performed with 0.5 g quartz suspended in 40 mL of a 0.01 M $NaClO_4$ solution, the preconditioning time being 48 h (pH adjustment, overhead shaker). The pH was varied between 5.5 and 7.5, the uranium concentration (batch of $UO_2(ClO_4)_2$) was 1×10^{-5} M, 5×10^{-5} M, or 1×10^{-4} M. Usually the 20-63 µm particle size fraction was used, for the lowest uranium concentration also a series with the smaller grain size fraction was investigated. Before each TRLFS measurement the solid phase was centrifuges and then re-suspended in a solution identical to the previous one but without uranium. The Nd:YAG diode laser with subsequent 4th harmonic generation allows for an optimal excitation at 266 nm with 0.3 mJ pulse energy. Spectra were recorded by a diode array of 701 intensified diodes, with a spectral resolution of 0.325 nm. The exposure time was 2 µs, the delay times (after laser) covered 50 ns up to 37 µs. Fivefold measurements, cumulating 100 laser shots each, were averaged. For more details of both the experimental procedure and the TRLFS set-up refer to [1] and [2], respectively.

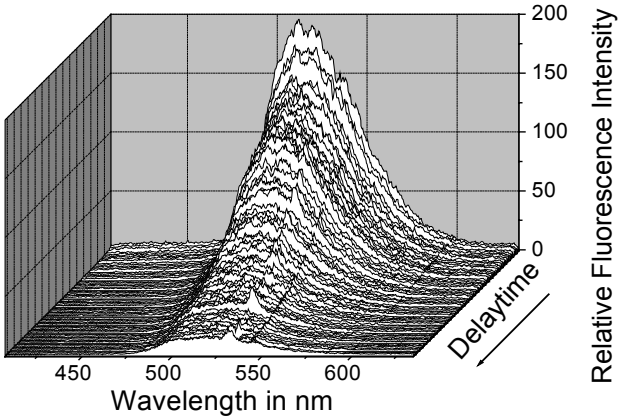

Fig. 1: TRLFS spectrum at pH 7 for $[U]_{total} = 1\times10^{-4}$ M

RESULTS. Fig. 1 shows a typical TRLFS spectrum, here with delay times ranging from 50 ns to 29 µs. Tab. 1 summarized the TRLFS results, grouped according to the different grain size fractions and total uranium concentrations in solution.

With the exception of spectra with a very low signal-to-noise ratio always two different fluorescence lifetimes could be detected, pointing to at least two distinct uranyl species on the quartz surface.

The TRLFS series with the smaller quartz particles gave fluorescence lifetimes being a function of pH. Whereas the shorter lifetime τ_1 decreases from about 1500 ns at pH 5.5 to about 570 ns at pH 7.5, the trend for the longer lifetime τ_2 is the opposite: shifting from 29 µs at pH 5.5 to 68 µs at pH 7.5.

At all concentration series with grain sizes larger than 20 µm the data scatter increases, for the highest uranium concentration level most probably due to a beginning formation of colloids as the saturation limit is exceeded. Whereas the decrease of the shorter lifetime τ_1 with increasing pH is again observable, no correlation of the longer fluorescence lifetime with pH could be detected.

Tab. 1: Fluorescence lifetimes τ_1 and τ_2 for the uranium(VI) sorption on quartz as function of pH, total uranium concentration and quartz grain size, errors equal one standard deviation

$[U]_{total}$ in M	Grain size in µm	pH	τ_1 in ns	τ_2 in µs
1×10^{5}	< 20	5.5	1540 ± 540	29.0 ± 4.1
		6.5	1020 ± 80	47.0 ± 4.9
		7.0	830 ± 60	49.8 ± 2.9
		7.5	570 ± 60	67.6 ± 3.9
1×10^{5}	20 - 63	5.5	1620 ± 160	35.5 ± 2.3
		6.5	860 ± 450	40.2 ± 4.7
		7.0	470 ± 40	36.0 ± 3.3
		7.5	370 ± 40	42.9 ± 2.7
5×10^{5}	20 - 63	5.5	1110 ± 450	32.7 ± 7.4
		7.0	420 ± 30	29.8 ± 1.6
		7.5	510 ± 100	28.6 ± 1.8
1×10^{4}	20 - 63	5.5	2340 ± 240	21.5 ± 2.5
		6.5	-	27.6 ± 5.7
		7.0	-	31.4 ± 4.3
		7.5	640 ± 50	25.6 ± 1.6

Possible explanations for this remarkable effect of the quartz grain size could be given at least for the species with the longer fluorescence lifetime. The high surface energy of these small particles will promote the formation of uranyl surface clusters slowly converting to surface precipitates. This would reduce the average number of water molecules in the uranyl coordination shell (*i.e.* the number of quenchers) and thus increase the fluorescence lifetime.

REFERENCES

[1] Baumann, N. *et al.* (2005) *J. Coll. Interface Sci.,* in press.
[2] Geipel, G. *et al.* (1996) *Radiochim. Acta.* **75**, 199-204.

Evidence of two uranyl(VI) surface species on gibbsite obtained by Time-Resolved Laser-Induced Fluorescence Spectroscopy (TRLFS)

T. Arnold, N. Baumann, V. Brendler, G. Geipel

ABSTRACT. TRLFS was combined with batch experiments to study the sorption of uranium(VI) onto gibbsite (γ-Al(OH)$_3$). Two uranyl surface species with fluorescence lifetimes of 330 ± 115 ns and 5600 ± 1640 ns, respectively, were identified. The first species was dominating the more acid pH region whereas the second one became gradually more prominent towards higher pH values. The fluorescence spectra of both adsorbed uranyl surface species were described with six characteristic fluorescence emission bands situated at 479.5 ± 1.1, 497.4 ± 0.8, 518.7 ± 1.0, 541.6 ± 0.7, 563.9 ± 1.2, and 585.8 ± 2.1 nm. The surface species with the short-lived fluorescence lifetime of 330 ns is attributed to a bidentate mononuclear inner-sphere surface complex and the second one is attributed to small sorbed clusters of polynuclear uranyl surface species.

EXPERIMENTAL. The gibbsite used for this work was a commercial product from Merck named hydrargillite [$AlH_3O_3 \cdot xH_2O$]. The average grain size x_{50} was 12.2 µm, with 95 % of the grains having a size between 0.9 µm and 50 µm. The specific surface area of the gibbsite was determined with a five-point N_2-BET, yielding 1.5 m^2/g. TRLFS spectra were recorded of gibbsite suspension, at permanent stirring. The complete description of the TRLFS measurement, including data evaluation as well as batch sorption experiments are described in [1].

RESULTS. Two different fluorescence lifetimes indicating uranyl surface species on gibbsite with a faster and a slower fluorescence decay were identified in the pH region 5 to 8.5, where also the maximum uranyl(VI) sorption on gibbsite is observed. There, $t_1 = 330 \pm 115$ ns and $t_2 = 5600 \pm 1640$ ns are the calculated average fluorescence lifetimes of the short and the long-lived species, respectively, with the errors representing two standard deviations (2 σ). The deconvoluted fluorescence spectra reveal six characteristic fluorescence emission bands that are almost identical for both uranyl surface species. The peak maxima are situated at 479.5 ± 1.1, 497.4 ± 0.8, 518.7 ± 1.0, 541.6 ± 0.7, 563.9 ± 1.2, and 585.8 ± 2.1 nm. The first four maxima are shifted relative to the values for the free uranyl ion in perchlorate medium [2] consistently by approximately 9-10 nm.

Due to the pronounced coincidence of all the fluorescence peaks, the two adsorbed uranium(VI) surface species, i.e. the short-lived and the long-lived species, are assumed to be similar in their coordination environment throughout the investigated pH range. They should thus have identical numbers of hydroxyl groups in their first coordination sphere, as different numbers of hydroxyl groups cause changes in the spectral features [3]. Considering the discriminative fluorescence lifetimes, the two distinguishable surface species should differ only in their respective water content [4].

Furthermore, a split into the contributions of the fluorescence intensities by the two distinguished surface species shows a gradual relative increased proportion of the species with the longer fluorescence lifetime towards higher pH values.

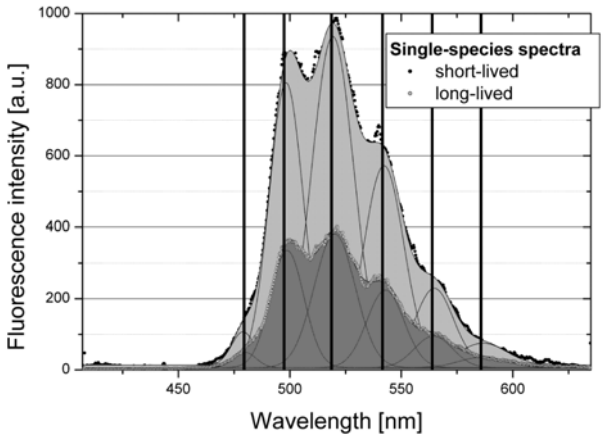

Fig. 1: Deconvoluted fluorescence spectra of two uranyl surface species on gibbsite at pH 6.5 with characteristic positions of the fluorescence emission bands.

Thus, the uranyl surface species with the short-lived fluorescence lifetime of 330 ns is attributed to a bidentate mononuclear inner-sphere surface complex in which the uranyl is bound to two OH^- groups. The second surface species with the significant longer fluorescence lifetime of 5600 ns and an increasing proportion of the fluorescence intensity towards higher pH values, is attributed to small clusters consisting of sorbed polynuclear surface species. The relative number of water molecules in the coordination environment of the sorbed uranyl atoms on gibbsite is smaller. Since H_2O in the coordination environment of uranyl quenches the fluorescence lifetime of the adsorbed uranyl surface species the fluorescence lifetime of this uranyl surface species is longer. In addition, the size of the polynuclear species will influence the fluorescence lifetime. The larger the polynuclear uranyl surface species become the larger will be its fluorescence lifetime. In this context the observed longer lifetime (7260 ns) of the long-lived uranyl surface species at pH 8.5 is in accordance with this explanation

ACKNOWLEDGEMENTS. The work was carried out within the EU project "Aquatic Chemistry and Thermodynamic of Actinides and Fission Products – ACTAF" with financial support by the European Commission under contract No. FIKW-CT-2000-00035 (ACTAF Project).

REFERENCES

[1] Baumann, N. *et al.* (2004) *J. Colloid Interface Sci.*, in press.
[2] Bell, J.T.; Biggers, R.E. (1968) *J. Mol. Spectrosc.* **25**, 312-328.
[3] Eliet, V. *et al.* (1995) *J. Chem. Soc., Faraday Trans.* **91**, 2275-2285.
[4] Kimura, T.; Choppin, G.R. (1994) *J. Alloys Comp.* **213/214**, 313-317.

Uranium(VI) sorption on ferrihydrite: I. ATR FT-IR investigations

H. Foerstendorf, K.-U. Ulrich, K. Muschter, S. Weiß

ABSTRACT. The sorption of uranium (VI) onto colloidal ferrihydrite (Fh) was investigated by attenuated total reflection (ATR) FT-IR spectroscopy in mildly acidic solution (pH 5.5). The presence of the actinide strongly effects the molecular interaction of atmospheric carbon dioxide with the mineral phase.

The iron hydroxide mineral phase ferrihydrite (Fh) is able to remove dissolved heavy metal species such as uranium *e.g.* from groundwater aquifers with a very high affinity. This infrared spectroscopic investigation focuses on the surface complexes of the uranyl cation on Fh at mildly acidic conditions (pH 5.5).

EXPERIMENTAL. Fh was prepared out of solutions of 1 mM $FeCl_3 \cdot 6H_2O$ and varied concentrations of UO_2Cl_2 (0, 12, 100 µM), by titration with NaOH up to pH 5.5 in presence and in absence of atmospheric CO_2, using 15 mM NaCl as background electrolyte. After stirring the batches for > 24 h at room temperature, the aggregated colloids were allowed to settle for ~65 h, centrifuged (285,000 g; 30 min), and put on the ATR crystal as a moist paste without further treatment. The FT-IR spectra were recorded by averaging 128 scans at a spectral resolution of 4 cm^{-1}. For adequate background correction reference spectra of the respective supernatants were recorded.

RESULTS. In the spectral range between 1800 and 700 cm^{-1} the spectrum of the pure Fh which was prepared in an inert gas atmosphere is characterized by a broad absorption band around 935 cm^{-1} (Fig. 1A). This band represents the δ(OH) bending vibration of the Fh phase. In the presence of the uranyl ion (UO_2^{2+}) an additional band around 903 cm^{-1} is observed in the spectra of UO_2^{2+}-containing samples. Its intensity is decreasing with the concentration of the actinide ions. This band can be assigned to the antisymmetric (ν_{as}) stretching vibration of the UO_2^{2+} cation sorbed to the iron hydroxide phase (Fig. 1E). For solutions of dissolved UO_2^{2+} this band is normally observed at significant higher wavenumbers (> 920 cm^{-1}).
In the spectra of the samples prepared under air additional bands appear around 1365 and 1500 cm^{-1} (Fig. 1B–D) which are assigned to the symmetric (ν_s) and antisymmetric (ν_{as}) stretching vibration of carbonate (CO_3^{2-}) anions bound to the mineral phase, respectively. With increasing concentration of uranium these bands undergo a shifting of their maximums. The $\nu_{as}(CO_3^{2-})$ is found to be shifted to higher wavenumbers from 1478 to 1515 cm^{-1} at a concentration of 100 µM UO_2^{2+}. This was also observed to a much smaller extent for the $\nu_s(CO_3^{2-})$ ($\Delta\nu \sim 4$ cm^{-1}; Fig. 1D).

DISCUSSION. Since in presence of uranium and CO_2 the frequency of the $\nu_{as}(UO_2^{2+})$ mode is unaltered compared to the spectra recorded in absence of CO_2, the molecular structure of the UO_2^{2+} sorption complexes on Fh remains unaffected. Thus the complexation of the carbonate anions can only take place equatorially to the actinide cation. A binding *via* the axial oxygen atoms would have induced a significant shifting of the $\nu_{as}(UO_2^{2+})$ band [1].

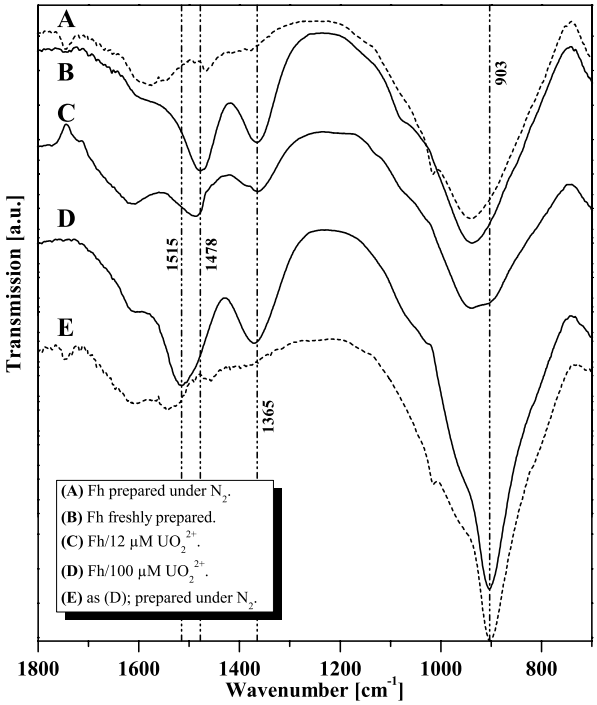

Fig. 1: ATR FT-IR spectra of ferrihydrite (Fh). Solid lines: Fh prepared in air equilibrium (B – D), dashed lines: Fh prepared under N_2 (A,E). Fh (A,B), Fh + 12 µM UO_2^{2+} (C). Fh + 100 µM UO_2^{2+} (D,E).

In contrast, the Fh-carbonate interactions are strongly affected by the presence of uranium. The degree of splitting of the ν_{as} and $\nu_s(CO_3^{2-})$ modes in the spectra can serve as a criterion for the distinction of mono- or bidentate binding of the carbonates to metal complexes [2]. In the spectra of pure Fh a splitting of ~110 cm^{-1} is observed (Fig. 1B). This can be interpreted as a monodentate binding of the CO_3^{2-} anions to the mineral phase. In the presence of uranium this splitting is found to be 150 cm^{-1} (Fig. 1D). Whether this increased value can be assigned to a bidentate binding of the carbonates to the UO_2^{2+} cation or to a distortion of the monodentate binding of the carbonates to Fh by uranium or to the formation of Fe-U-phases occurring during preparation cannot be unequivocally decided today. However, the infrared spectra of uranium carbonate minerals show a similar band splitting [3]. In consideration of the crystal structures it can be assumed that the carbonates may be bidentately coordinated to the uranyl cation. Since the positions of the carbonate bands are continuously shifted when the UO_2^{2+} concentration is varied we conclude that even at low UO_2^{2+} concentration uranyl complexes contribute to the sorption of uranium on ferrihydrite.

REFERENCES

[1] Čejka, J. (1999) In: *Uranium: Mineralogy, Geochemistry and the Environment*, The Mineralogical Society of America, Washington.
[2] Lefèvre, G. (2004) *Adv. Colloid Interface Sci.* **107**, 109-123.
[3] Amayri, S. *et al.* (2004) *Environ. Sci. Technol.* **38**, 6032-6036.

Uranium(VI) sorption on ferrihydrite: II. EXAFS investigations

K.-U. Ulrich, A. Rossberg, S. Weiß

ABSTRACT. The sorption complexes of U to colloidal ferrihydrite (Fh) were investigated by EXAFS spectroscopy in mildly acidic solution (pH 5.5). Since sulfate, silicate and carbonate are not involved as ligands bidentately bound with the adsorbed U, a new bond structure of U on hydrous ferric oxides is proposed.

Using EXAFS spectroscopy we investigated on molecular level the binding of uranium on colloids generated concomitantly with flooding of an abandoned U mine, simulated by mixing acid mine water with near-neutral ground water [1]. The prominent peaks of Fourier-transformed EXAFS (FT) suggest an inner-sphere, bidentate complex of UO_2^{2+} on Fh, the dominant mineral phase of the colloids. However, two minor peaks at R+Δ~2.4 Å and ~3.9 Å remained unexplained. Since EXAFS fitting could not discriminate the backscattering atoms S, Si, C, and O occurring in the colloidal matter, we conducted sorption experiments with Fh synthesized under varied conditions to clarify the complex structure by EXAFS spectroscopy.

EXPERIMENTAL. Fh was prepared out of solutions of 1 mM $Fe(NO_3)_3$ x 9 H_2O, 12 µM $UO_2(NO_3)_2$ and 10 mM $NaNO_3$ by titration with NaOH up to pH 5.5 in presence of sulfate (1.2 and 4.8 mM) or silicate (0.3 and 1.2 mM) or both at ambient atmosphere. In addition, we synthesized Fh from solution of 1 mM $FeCl_3$ x 6 H_2O, 12 µM or 100 µM UO_2Cl_2 and 15 mM NaCl, both at ambient and under inert gas atmosphere. Wet pastes were gained according to [2] and stored in liquid N_2 until measurement, performed in a He cryostat (~30 K) at the U-L_{III} edge in fluorescence mode. EXAFSPAK, FEFF and Monte-Carlo Target Transform Factor Analysis (MCTFA) [3] served for dead-time correction of the 13 element Ge fluorescence detector, ab initio calculation and data refinement.

RESULTS. The FT's of all samples prepared with 12 µM U included the shells of U-O_{ax} (N=2, R=1.78-1.80 Å, σ^2=0.002 Å^2), U-O_{eq1} (N=1.8-2.4, R=2.2-2.3 Å, σ^2=0.003-0.006 Å^2), U-O_{eq2} (N=2.8-4.1, R=2.39-2.41 Å, σ^2=0.003-0.008 Å^2), U-Fe (N=0.7-1.1, R=3.38-3.41 Å, σ^2=0.003-0.007 Å^2) and showed a peak at R+Δ~2.4 Å both in presence and in absence of sulfate and silicate (Fig. 1+2). Hence the responsible backscattering atom is not represented by S or Si. Therefore we tested role of carbonate on U sorption. Fig. 2 shows the EXAFS and FT's of Fh samples prepared with 12 µM and 100 µM U in presence and in absence of CO_2. The FT's of the calculated difference spectra reveal minor (in case of c(U)=12 µM) or even no backscattering contribution to the peak at R+Δ~2.4 Å, demonstrating that at c(U)=100 µM bidentately bound carbonate ligands are not involved. This conclusion conflicts with results gained from ATR FT-IR spectroscopy [2, 4]. A possible explanation could be that carbonate ligands are monodentately bound.
The samples B and D (Fig. 2) were prepared in absence of CO_2 thus the FT peak at R+Δ~2.4 Å cannot result from carbon. MCTFA provided a new structural model in which the bidentately bound UO_2^{2+} is oriented in a way that a distance of 2.88 Å results to the O atom of an adjacent, edge-shared FeO_6 octahedron (Fig. 3). This model predicts a second Fe shell at ~4.35 Å which tightly fits the experimental data.

REFERENCES

[1] Ulrich, K.-U. *et al.* (2004) *Report FZR-400*, p. 45.
[2] Foerstendorf, H. *et al.* this report, p. 54.
[3] Rossberg, A. *et al.* (2005) *Physica Scripta*, in press.
[4] Bargar, J.R. *et al.* (1999) *Environ. Sci. Technol.* **33**, 2481-2484.

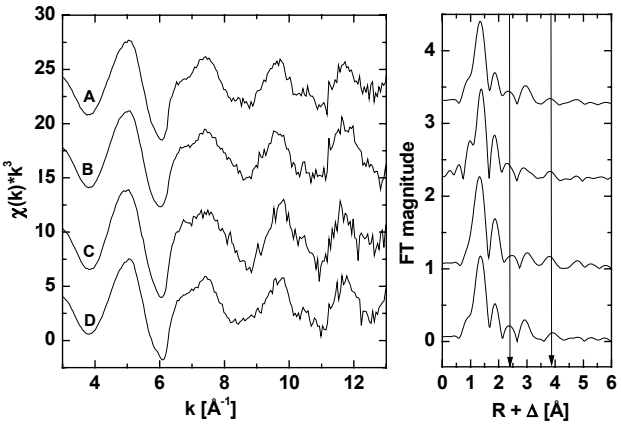

Fig. 1: U-L_{III} EXAFS spectra and FT's of Fh colloids on which 12 µM U adsorbed at pH 5.5 (ambient atmosphere) in presence of sulfate and silicate (A: 1.2 mM each, B: 4.8 mM and 0.3 mM), 4.8 mM sulfate (C) and 0.3 mM silicate (D).

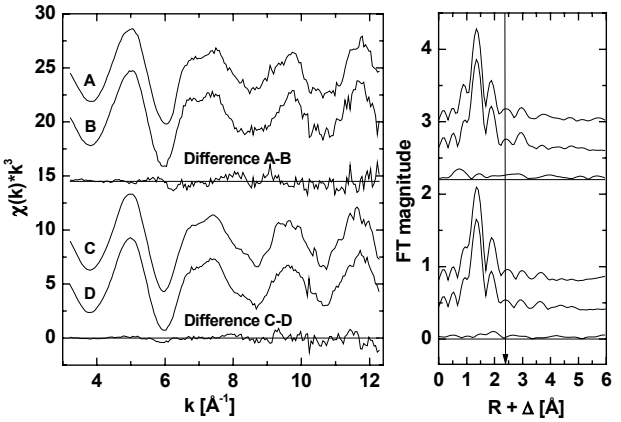

Fig. 2: U-L_{III} EXAFS spectra and FT's of Fh colloids on which 12 µM U (A+B) and 100 µM U (C+D) adsorbed at pH 5.5 at ambient (A+C) and under N_2 atmosphere (B+D) as well as calculated difference spectra (A-B) and (C-D).

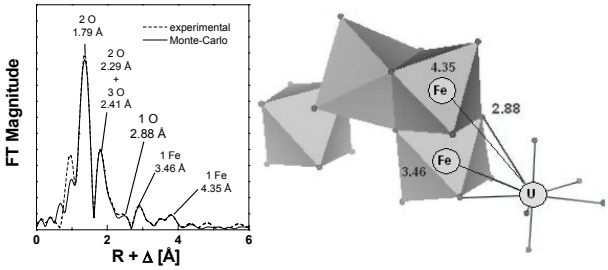

Fig. 3: U-L_{III} EXAFS-FT of Fh colloids formed at pH 5.5 concomitantly with simulated mine flooding: Experimental data and Monte-Carlo fit based on the depicted structural model.

Prediction of U(VI) species adsorbed on ferrihydrite colloids by surface complexation modeling

K.-U. Ulrich, V. Brendler, S. Weiß

ABSTRACT. A surface complexation model predicts sorption of U(VI) on ferrihydrite (Fh) at pH 5-7 to be dominated by the species =FeO-UO_2OH, but =$FeOH_2$-$(UO_2)_2CO_3(OH)_3$ participates at specific conditions.

Molecular speciation is a prerequisite for the proper assessment of radionuclide migration in the environment. We use both sophisticated techniques for preparation of colloids from solution (e.g. ultracentrifugation, ultrafiltration) in combination with spectroscopic techniques (ATR FT-IR [1], EXAFS [2], XRD, Mössbauer) and modeling of liquid phase and surface complexation reactions. This enables us to investigate the speciation of U(VI) in waters leaving abandoned uranium mines during the remediation process through flooding by groundwater [3]. Depending on pH, uranyl carbonato complexes are highly relevant in controlling the U sorption onto colloidal phases. This contribution presents the soluble and adsorbed U species predicted for our experiments by surface complexation modeling (SCM).

EXPERIMENTAL. The first experiment simulated mine flooding at oxidizing conditions in 100 L scale [3]. The EQ3/6 code with the most recent NEA data base yielded the speciation of U(VI) according to our water analysis data [4]. In order to simplify the natural matrix, we performed sorption experiments with synthetic Fh (1 mM Fe, 12 µM U_T, *I*=10 mM, solid/liquid ratio S/L=90 mg/L) and tested the interaction of sulfate, silicate, and carbonate with U sorption onto Fh [2]. FITEQL [5] modeling utilizing the RES^{3}T data base [6] probed whether ternary U(VI) carbonato complexes will adsorb under these conditions as suggested in [7].

RESULTS. In the final stage of simulated flooding a pH of 5.5 and c(U_T)=3.3 µM were reached. EQ3/6 predicts the following dissolved U species: 47 % $UO_2(OH)_2$(aq), 18 % UO_2OH^+, 13 % UO_2^{2+}, 11 % UO_2SO_4(aq), 5 % $UO_2OSi(OH)_3^+$, 2 % $(UO_2)_3(OH)_5^+$, 2 % $(UO_2)_2(OH)_2^{2+}$. As expected, the concentrations of HCO_3^- and all U(VI) carbonato species were negligible in solution due to the slightly acidic pH.
SCM requires more data: specific surface area (228 $m^2\,g^{-1}$, BET-N_2), normalized surface site density (12.05 nm^{-2}), surface hydrolysis and complexation constants for the Fh Diffuse-Double-Layer Model (Tab. 1). To test the effect of carbonate ($pCO_2=10^{-3.5}$ atm in air), pH was varied from pH 3 to 9; c(U_T)=12 (100) µM and S/L=90 (9) mg/L were fixed. In case of S/L=90 mg/L, up to 99 % of U_T were predicted to adsorb onto Fh in the pH range 5-8, dominated by the surface species =FeO-UO_2OH. At the tested pH 5.5, the complex =$FeOH_2$-$(UO_2)_2CO_3(OH)_3$ reached ~6 % and 30 % at c(U_T) of 12 and 100 µM, respectively, and yielded 29 % at c(U_T)=12 µM with S/L=9 mg/L. Thus at specific conditions such as very low S/L or higher uranyl concentrations, uranyl carbonato complexes are predicted to contribute to surface complexation. However, at pH 5.5 and c(U_T)=12 µM, such species are of minor relevance. Our results suggest that the affinity of carbonate and uranyl to form complexed surface species will be increased when sorption sites with high affinity, as provided by ferrihydrite, are present.

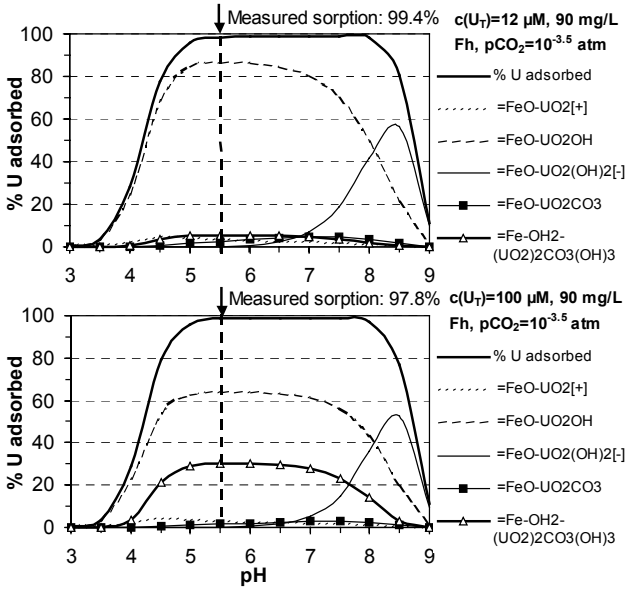

Fig. 1: U(VI) species predicted by FITEQL to explain U sorption on Fh at 12 µM and 100 µM UO_2^{2+} and *I*=10 mM.

ACKNOWLEDGEMENTS. This work is supported by DFG (ZA 238/2-1). We thank U. Schaefer, C. Eckardt and D. Birnstein for analytical work.

REFERENCES

[1] Foerstendorf, H. *et al.* this report, p. 54.
[2] Ulrich, K.-U. *et al.* this report, p. 55.
[3] Ulrich, K.-U. *et al.* (2004) *Report FZR-400*, p. 45.
[4] Ulrich, K.-U. *et al.* (2004) *Schriften des FZ Jülich, General & Interdisciplinary 3*, 645-647.
[5] Herbelin, A.L.; Westall, J.C. (1996) *FITEQL-Version 3.2., Report 96-01*, Oregon State Univ., Corvallis.
[6] Brendler, V. *et al.* (2003) *J. Cont. Hydrol.* **61**, 281-291.
[7] Wazne, M. *et al.* (2003) *Environ. Sci. Technol.* **37**, 3619-3624.

Tab. 1: Surface reactions (also on weak binding sites) and normalized constants (mean ± standard deviation) extracted from RES^{3}T [6].

Equation	log K_n ± SD	n	RES^{3}T reference code
»Fe-OH + UO_2^{2+} = »Fe-O-UO_2^+ + H^+	1.57 ± 0.44	5	MGM03, TS96, C96, PSDW92
»Fe-OH + UO_2^{2+} + H_2O = »Fe-O-$UO_2(OH)$ + 2 H^+	-4.90 ± 0.76	5	MGM03, TS96, DA96, PSDW92
»Fe-OH + UO_2^{2+} + 2 H_2O = »Fe-O-$UO_2(OH)_2^-$ + 3 H^+	-13.0 ± 0.60	2	TS96, VT98
»Fe-$(OH)_2$ + UO_2^{2+} + H_2CO_3 = »Fe-O_2-$UO_2CO_3^{2-}$ + 4 H^+	-17.19	1	DPW02
»Fe-OH + H_2CO_3 = »Fe-HCO_3 + H_2O	2.89 ± 0.35	4	WDPWX94, VRL94, AVTC02
»Fe-OH + H_2CO_3 = »Fe-CO_3^- + H_2O + H^+	-4.71 ± 0.37	4	WDPWX94, VRL94, AVTC02, S79

The effect of parameter uncertainty on blind prediction of Np(V) sorption onto hematite

A. Richter, V. Brendler, C. Nebelung

ABSTRACT. Surface Complexation Models (SCM) can be used for estimating distribution coefficients (K_D) for contaminants in well-defined mineral systems. The uncertainty analysis revealed that the large scatter of published surface protolysis constants does not result in significant uncertainties of predicted K_D values.

Still, the K_D concept of empirical distribution coefficients is the most often utilized model describing sorption phenomena. However, SCM is a better approach on a scientific, quasi-thermodynamic basis. The Np(V) sorption onto hematite was selected as an example to illustrate the effect of parameter uncertainty in sorption modeling.

MODEL SET UP. The Diffuse Double Layer Model (DDLM) was chosen as SCM submodel to keep the number of parameters at a minimum. The data collection is fully based on RES^{3}T [1]. The log K $\pm 2\sigma$ (95% level of significance) values of the relevant surface species formation are derived from the normalization to the reference surface site density 12.05 sites nm^{-2}, extrapolation to infinite dilution, and averaging.

Tab. 1: Selected surface reaction constants (DDLM)

Surface species	Log K ± 2σ
$\equiv FeOH_2^+$	6.69 ± 0.81
$\equiv FeO^-$	- 10.40 ± 0.76
$\equiv FeO\text{-}NpO_2$	- 3.38 ± 0.13
$\equiv FeO\text{-}NpO_2(HCO_3)_2^{2-}$	- 11.27
$\equiv FeO\text{-}HCO_2$	3.10 ± 0.57
$\equiv FeO\text{-}CO_2^-$	- 4.75 ± 0.59

BLIND PREDICTIVE MODELING. The modeling was performed with the FITEQL code [2]. Data published by Kohler *et al.* [3] are the basis for the predictions of the Np(V) sorption onto hematite (specific surface area 14.4 m^2 g^{-1}). Figure 1 shows the difference between predicted and experimental distribution coefficients log K_D. The simulation congruence for all data subsets is within one order of magnitude. Such a spreading is considered to be reasonable for performance assessment requirements.

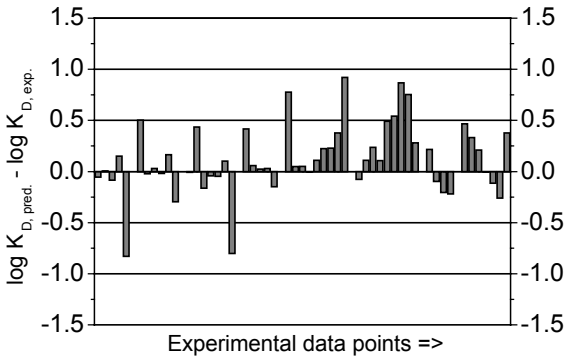

Fig. 1: Differences in log K_D between predicted and measured Np(V) sorption onto hematite.

UNCERTAINTY ANALYSIS. Because the protolysis constants $pK_1 = -6.69$ and $pK_2 = 10.40$ cannot be varied independently, the point of zero charge (PZC) and ΔpK was calculated according to the following equations:

$$PZC = \frac{-pK_1 + pK_2}{2} \pm 2\sqrt{\frac{\sigma_{pK_1}^2 + \sigma_{pK_2}^2}{4}} = 8.54 \pm 0.56 \quad (1)$$

$$\Delta pK = pK_1 + pK_2 \pm 2\sqrt{\sigma_{pK_1}^2 + \sigma_{pK_2}^2} = 3.71 \pm 1.11 \quad (2)$$

Thus we generated 20 pK data sets with the aid of 40 Gaussian-distributed random numbers (RN):

$$-pK_{1ij} = (PZC + 2\sigma_{PZC} \cdot RN_i) - \frac{1}{2}(\Delta pK + 2\sigma_{\Delta pK} \cdot RN_j) \quad (3)$$

$$pK_{2ij} = (PZC + 2\sigma_{PZC} \cdot RN_i) + \frac{1}{2}(\Delta pK + 2\sigma_{\Delta pK} \cdot RN_j) \quad (4)$$

Fig. 2 shows the varied pK values and the resulting mean difference between predicted (result of FITEQL modeling) and experimental distribution coefficients Σabs(Δlog K_D)/n (n=52 data points):

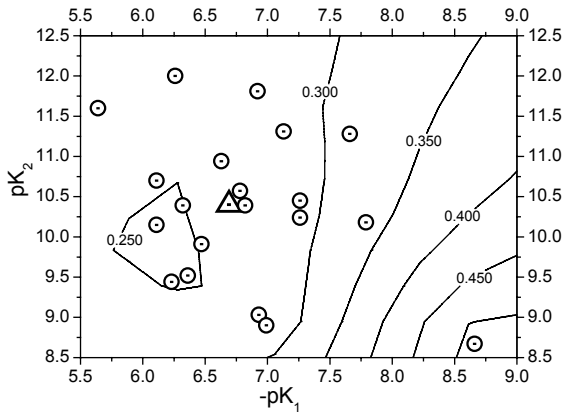

Fig. 2: Randomly distributed pK of hematite (○: varied pK, Δ: exp. mean pK) plotted in a surface of the resulting Σabs(Δlog K_D)/n (see numbers on the contour-lines).

Thus the formally large spreading of the pK values as extracted from literature is actually not critical. For well-defined mineral systems, provided a suitable database is accessible, the DDLM approach seems to be very promising. This will be confirmed by further studies extending the range of minerals and contaminants.

ACKNOWLEDGEMENTS. The development of the mineral-specific sorption database RES^{3}T was funded by the German Federal Ministry of Economics and Labour (BMWA) under contract No. PtWt+E 02E9471.

REFERENCES

[1] Brendler, V. *et al.* (2003) *J. Cont. Hydrol.* **61**, 281-291.
[2] Herbelin, A.L.; Westall, J.C. (1996) *FITEQL -Version 3.2.*, Report 96-01, Oregon State University, Corvallis.
[3] Kohler, M. *et al.* (1999) *Radiochim. Acta* **85**, 33-48.

Solubility of uranium oxide and radium sulfate in brines

C. Nebelung, L. Baraniak, U. Schaefer

ABSTRACT. The long-term solubility of U_3O_8 and $(Ba,Ra)SO_4$ in brines characteristic for the Morsleben radioactive waste disposal site were determined for purposes of near-field migration modeling.

EXPERIMENTAL. Special synthetic brines were prepared according to the surrounding materials of the radioactive waste in the Morsleben disposal site. First a saline concrete (SC) and a magnesia binder (MB) that are used as filling and sealing materials in the underground storage caves were preconditioned with two brines: (1) with 5.35 m NaCl and (2) with a solution of 3.8 m $MgCl_2$, 0.8 m KCl and 0.4 m Na_2SO_4. Then the preconditioned brines were equilibrated with the sediment "Grauer Salzton" (GS) which covers the disposal site.
The solubility of U_3O_8 was determined by shaking 5 mg U_3O_8 with 10 ml brine over one year. The dissolved uranium was determined in the brines after filtration (450 nm and 5 nm) by ICP-MS.
The determination of the $(Ba,Ra)SO_4$ solubility was carried out in two ways: (1) by equilibrating 8 ml brine samples with $2.0\cdot10^{-8}$ mol (4.8 µg) solid $(Ba,Ra)SO_4$ that contained 0.6 mol% ^{226}Ra and detecting the dissolved ^{226}Ra and (2) by measuring the remaining activity of 150 Bq ^{226}Ra in 6 ml brine samples after precipitation of $(Ba,Ra)SO_4$. ^{226}Ra in the ultra-filtrated brine samples was measured by liquid scintillation counting, barium by ICP-MS and sulfate by ion chromatography.

RESULTS. U_3O_8 dissolution takes less than 80 days (Fig. 1). In case of $MgCl_2$ brines a nearly constant value is observed for up to 350 days. Uranium concentration ranges from $2.6\cdot10^{-6}$ to $7.8\cdot10^{-6}$ M. In NaCl brines solubility decreases after the first rapid dissolution. In these brines a reducing environment is created during preequilibration with SC and GS (pH 10.4 and E_h -150 mV). Under these conditions the sparingly soluble $UO_2\cdot xH_2O$ is stable [1, 2]. Uranium concentration decreased below the detection limit. Colloidal particles were found in $MgCl_2$ brine, conditioned only with GS. The measured solubility is about one order of magnitude smaller than in [3].

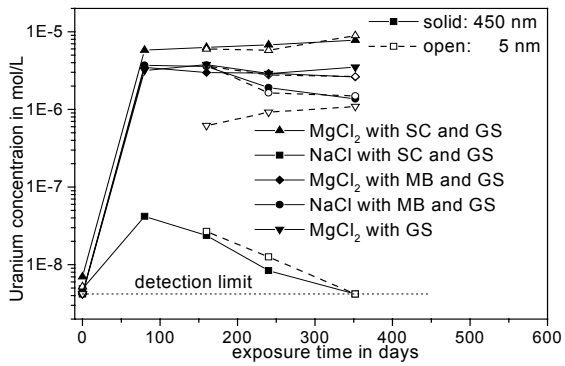

Fig. 1: Solubility of uranium in preconditioned brines.

The chemical behavior of $BaSO_4$ and $RaSO_4$ is nearly the same. The solubility products (log K_{sp}) in pure water are -10.0 and -10.3, respectively [4]. For the radium solubility, therefore, the concentration of Ba^{2+} and SO_4^{2-} in the brines has to be considered. In the case of dissolution of $(Ba,Ra)SO_4$ the concentrations of the ions and the solubility product according to $K_{sp}= ([Ba^{2+}]+[Ra^{2+}])\cdot[SO_4^{2-}]$ are listed in Tab. 1.

Tab. 1: Dissolution of $(Ba,Ra)SO_4$ in preconditioned brines: concentration and solubility product after 350 days.

Brine conditioned with	$[Ra^{2+}]$ mol/L	$[Ba^{2+}]$ mol/L	$[SO_4^{2-}]$ mol/L	K_{sp} mol^2/L^2
$MgCl_2$ SC/GS	$3.57\cdot10^{-8}$	$1.75\cdot10^{-6}$	0.058	$1.03\cdot10^{-7}$
NaCl SC/GS	$1.20\cdot10^{-8}$	$2.91\cdot10^{-6}$	0.048	$1.40\cdot10^{-7}$
$MgCl_2$ MB/GS	$2.56\cdot10^{-8}$	$4.85\cdot10^{-7}$	0.167	$8.47\cdot10^{-8}$
NaCl MB/GS	$1.23\cdot10^{-8}$	$1.32\cdot10^{-6}$	0.077	$1.04\cdot10^{-7}$
$MgCl_2$ GS	$4.67\cdot10^{-8}$	$1.21\cdot10^{-7}$	0.165	$3.40\cdot10^{-8}$

The corresponding values caused by precipitation of $(Ba,Ra)SO_4$ in brines, which are oversaturated with $(Ba,Ra)SO_4$ by $1.0\cdot10^{-3}$ mol/L Ba^{2+} are shown in Tab. 2.

Tab. 2: Precipitation of $(Ba,Ra)SO_4$ in preconditioned brines: concentration and solubility product after 350 days.

Brine conditioned with	$[Ra^{2+}]$ mol/L	$[Ba^{2+}]$ mol/L	$[SO_4^{2-}]$ mol/L	K_{sp} mol^2/L^2
$MgCl_2$ SC/GS	$8.47\cdot10^{-11}$	$7.10\cdot10^{-7}$	0.057	$4.03\cdot10^{-8}$
NaCl SC/GS	$7.46\cdot10^{-11}$	$1.28\cdot10^{-6}$	0.047	$6.05\cdot10^{-8}$
$MgCl_2$ MB/GS	$8.07\cdot10^{-11}$	$2.59\cdot10^{-7}$	0.172	$4.44\cdot10^{-8}$
NaCl MB/GS	$7.75\cdot10^{-11}$	$7.81\cdot10^{-7}$	0.076	$5.93\cdot10^{-8}$
$MgCl_2$ GS	$7.10\cdot10^{-11}$	$1.13\cdot10^{-7}$	0.163	$1.84\cdot10^{-8}$

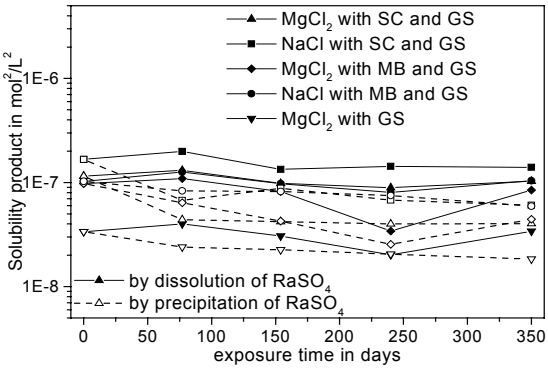

Fig. 2: Solubility of radium in preconditioned brines.

The solubility product of $(Ba,Ra)SO_4$ for the $MgCl_2$ brines is somewhat higher than that for the NaCl brines (the mean value of log K_{sp} is -7.34±0.2 in comparison to -7.07±0.06). These solubility products of $(Ba,Ra)SO_4$ are three orders of magnitude higher than that for pure water, which has great consequences for radionuclide migration assessment.

ACKNOWLEDGEMENT. The project was supported by the BfS under the contract No.: 9M 212 230-62.

REFERENCES

[1] Neck, V. *et al.* (2001) *Radiochim. Acta* **89,** 1-16.
[2] Wanner, H. *et al.* (eds.) (1992) *Chemical Thermodynamics of Uranium,* Elsevier Sci. Publ., Amsterdam.
[3] Vejmelka, P. (1999*) Nuklidmigration im Deckgebirge des Endlagers für radioaktive Abfälle Morsleben (Final report)*, FZK-INE 20/98, Karlsruhe.
[4] Langmuir, D. *et al.* (1985) *Geochim. Cosmochim. Acta* **49,** 1593-1601.

Spectroscopic characterization of the uranium carbonate andersonite $Na_2Ca[UO_2(CO_3)_3]\cdot 6H_2O$

T. Arnold, S. Amayri[1], H. Foerstendorf, G. Geipel
[1]Institute of Nuclear Chemistry, Johannes Gutenberg-Universität Mainz, Mainz, Germany

ABSTRACT. Synthetically prepared andersonite was characterized with TRLFS by six fluorescence emission bands at 470.6, 486.1, 505.4, 526.7, 549.6, and 573.9 nm. In addition, andersonite was characterized by FT-IR measurements by the appearance of the asymmetric stretching vibration of the uranyl cation (ν_3 UO_2^{2+}) at 902 cm^{-1} with a shoulder at 913 cm^{-1}.

EXPERIMENTAL. The synthesis of andersonite is described in detail in [1]. A Nd-YAG laser system (model GCR 190, Spectra Physics, Mountain View, USA) was used to study the solid samples of andersonite by Time-Resolved Laser-induced Fluorescence Spectroscopy (TRLFS). A detailed description of the experimental setup can be found in [1, 2]. Diffuse reflectance infrared Fourier transform (DRIFT) measurements have been carried out with a spectral resolution of 4 cm^{-1} (Perkin Elmer GX-2000). The synthetic mineral phase powder (0.7 mg) was mixed with solid KBr (300 mg).

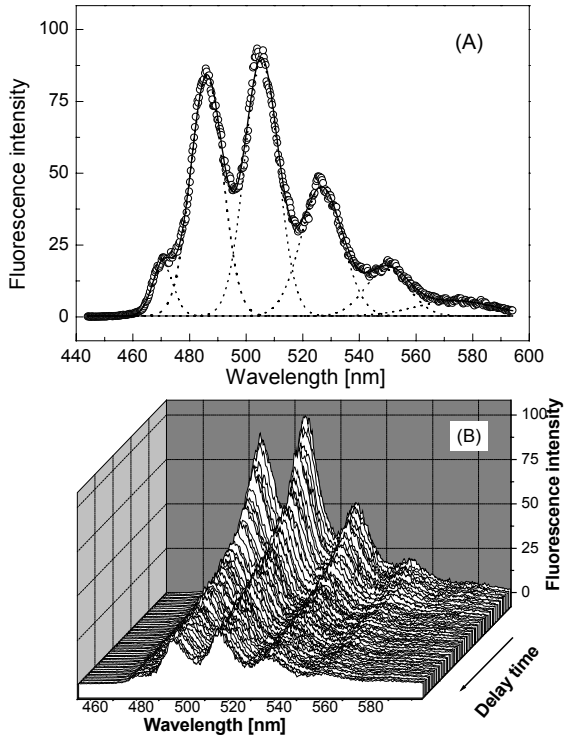

Fig 1: Fluorescence emission bands of andersonite (A). (The dotted lines show the curve fit of the spectra Gaussian shapes).) Fluorescence spectra of synthetic andersonite as a function of delay time (B).

RESULTS. The detected fluorescence emissions bands are represented by a set of evenly spaced peaks shown in Fig. 1a. The deconvoluted fluorescence spectrum reveals six characteristic intensive fluorescence emission bands at 470.6, 486.1, 505.4, 526.7, 549.6, and 573.9 nm. These bands were determined with an analytical error of 1 nm.

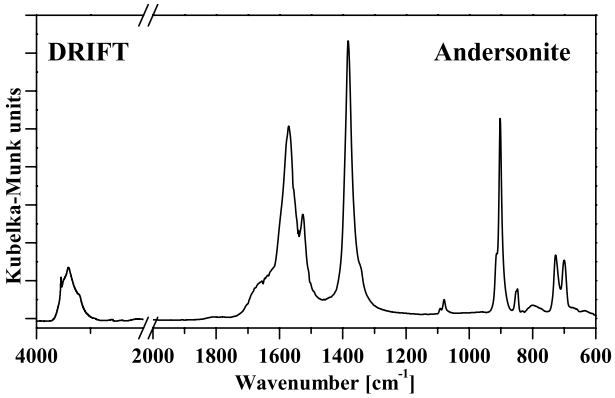

Fig. 2: FT-IR DRIFT spectrum of synthetic andersonite.

The TRLFS spectra displayed in Fig. 1 show that the fluorescence signals of the above listed emission bands decrease with time with a characteristic lifetime of 65.2 ± 0.6 µs.

The diffusion reflectance infrared (DRIFT) spectrum of andersonite is shown in Fig. 2. The bands at 3408 and 3547 cm^{-1} represent OH stretching vibrations which can be mainly assigned to crystal water molecules of the mineral phase. The sharp band at 3547 cm^{-1} possibly indicates the presence of a weakly bound species of water molecules in the crystal structure. The asymmetric stretching vibration of the uranyl cation (ν_3 UO_2^{2+}) appears at 902 cm^{-1} showing a shoulder at 913 cm^{-1}. This is in accordance to spectra of other $[UO_2(CO_3)_3]^{4-}$ minerals containing bivalent metal cations and crystal water. The most significant bands of the spectrum represent the carbonate anions bidentately bound to the uranyl cation. The bands at 1571 and 1383 cm^{-1} can be assigned to the doubly degenerated ν_3 mode of the CO_3^{2-} anion showing C_{2v} symmetry. The strong splitting of this mode ($\Delta\nu \approx 190$ cm^{-1}) is characteristic for the bidentate binding of the anion to the UO_2^{2+} ion. For symmetry reasons a splitting of the ν_4 mode is also expected and the bands at 727 and 700 cm^{-1} have to be assigned to this mode. The other vibrational modes (ν_1 and ν_2) of the carbonates are showing up at 1080 and 847 cm^{-1}, respectively. The refinement of the crystal structure shows two different species of CO_3^{2-} present in andersonite. In the infrared spectrum these structurally nonequivalent functional groups are obviously reflected by the appearance of additional bands and shoulders for the vibrational modes ($\nu_1 - \nu_3$) of the CO_3^{2-} anion as they are given in [1].

ACKNOWLEDGEMENTS. The authors thank K. Muschter for conducting FT-IR measurements.

REFERENCES

[1] Amayri, S. *et al.* (2004) *Environ. Sci. Technol.* **38**, 6032-6036.
[2] Geipel, G. *et al.* (1996) *Radiochim. Acta* **75**, 199-204.

Detection of U(VI) on the surface of altered depleted uranium by TRLFS

N. Baumann, T. Arnold, G. Geipel, E. Trueman[1], S. Black[1], D. Read [1,2]
[1] University of Reading, [2] Enterpris, University of Reading & University of Aberdeen; Great Britain

ABSTRACT. Time-resolved Laser-induced Fluorescence Spectroscopy (TRLFS) was applied to study the surface of an artificially weathered depleted uranium (DU) disc. The weathering solution contained calcium and phosphate. The TRLFS results clearly show that a U(VI) phase, most probably metaautunite, has formed on the DU disc. It is characterized by six fluorescence emission bands at 486, 501, 522, 546, 573, and 601 nm, and two fluorescence lifetimes of 50 ± 5 ns and 700 ± 25 ns.

Depleted uranium (DU) is a waste product in the extraction of nuclear fuel. Approximately 500,000 t of it are stored to date in the US alone. Because of its high density and ready availability at low cost this material is used to make projectiles for the armed forces and is also used as counterweights in airplanes. DU got public attention after the Gulf and Balkan wars in which it was used as ammunition to destroy heavy armored vehicles. Fine dispersed powder from that ammunition is now widespread in various areas and may cause severe environmental problems.

EXPERIMENTAL. The discs (25 mm in diameter, 0.5 mm in thickness) were obtained from a pristine British military tank shell [1]. After degreasing, one sample was placed in a solution containing $2.49 \cdot 10^{-3}$ M calcium and $1.05 \cdot 10^{-3}$ M phosphate representing agricultural soils. TRLFS measurements were made on the surface of this sample and the results were compared with measurements on a DU disc which had not been in contact with the solution.
The TRLFS system consists of a Nd:YAG diode laser with an excitation wavelength of 266 nm. For further details concerning the set-up of the TRLFS equipment and operation modes see [2]. TRLFS spectra of 15 different spots (3 mm in diameter) on the DU disc were recorded, see Fig. 1 for a typical spectrum. Whereas elementary U does not emit any fluorescence, potentially formed secondary U(VI) phases should be detectable.

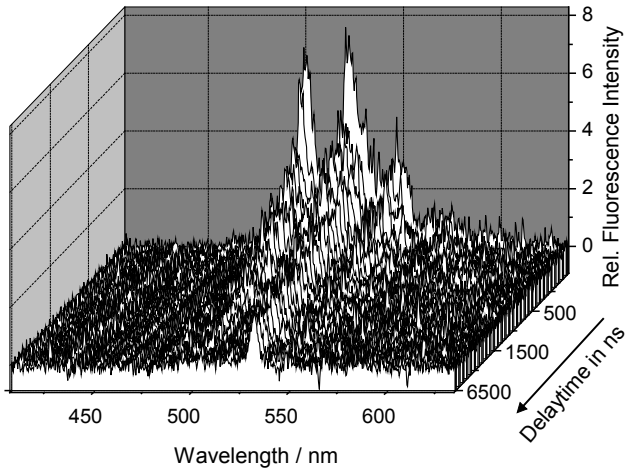

Fig. 1: Fluorescence spectra of altered DU as a function of delay time.

RESULTS. TRLFS clearly gave evidence for the formation of secondary U(VI) phases. The intensity of the 15 measured fluorescence spectra was different, which indicates that the secondary phase is not homogeneously distributed on the DU disc. The TRLFS spectra show six emission bands at 486, 501, 522, 546, 573, and 601 nm (Fig. 2), a pattern typical for U(VI) minerals. The time-resolved spectrum is best described with two distinguishable life times of 50 ± 5 and 700 ± 25 ns.
Possible secondary uranium phases on the DU disc are U-oxides, U-hydroxides, U-carbonates, and U-phosphates.

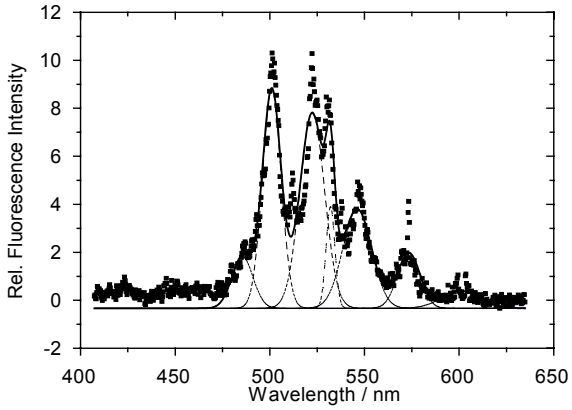

Fig. 2: Deconvoluted fluorescence spectra of uranyl(VI) detected on the surface of altered DU with laser dispersion peak at 532 nm.

The observed redshift of the spectra compared to the UO_2^{2+}-cation in solution is indicative of U-phosphates.
We have compared this spectrum with data available in our mineral database (autunite, chernikovite, metaautunite etc.). The best match with our weathered DU sample was found for metaautunite - $Ca(UO_2)_2(PO_4)_2 \cdot 6\ H_2O$.
Fig. 3 shows the fluorescence spectrum of metaautunite from the mineral database with emission maxima at 487, 501, 522, 546 and 569 nm. Typical fluorescence lifetimes of metaautunite are 740 ± 100 ns [3] and 43 ± 4 ns.
Therefore, the uranium phase on the surface of the disc is supposed to be (disordered) metaautunite. The existence of traces of further U(VI) minerals can not be excluded, however.

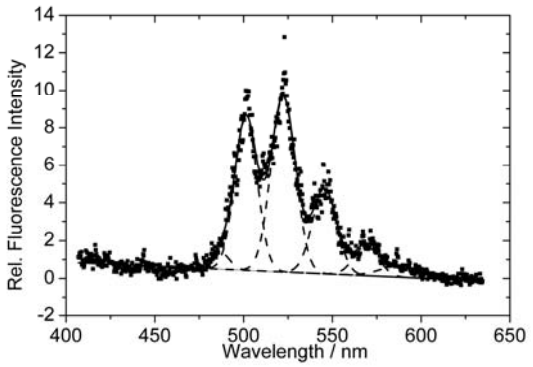

Fig. 3: Deconvoluted fluorescence spectrum of metaautunite.

REFERENCES

[1] Trueman, E. *et al.* (2004) *Sci. Total Environ*. **327**, 337-340.
[2] Geipel, G. *et al.* (1996) *Radiochim. Acta* **75**, 199-204.
[3] Geipel, G. *et al.* (2000) *Radiochim. Acta* **88**, 757-762.

Temperature dependency of the EXAFS Debye-Waller factors of $H[UO_2AsO_4]\cdot 4H_2O$

C. Hennig, H. Funke, A.C. Scheinost

ABSTRACT. The temperature dependence of Debye-Waller factors were studied using $H[UO_2AsO_4]\cdot 4H_2O$ from 20 to 273 K. The U-O_{ax} bond is not influenced by thermal vibrations, whereas U-As and U-O_{eq} are significantly influenced.

The Debye-Waller factor determined by EXAFS differs from that obtained by XRD. The EXAFS Debye-Waller factor is the mean squared *relative* displacement (MSRD) between absorbing and backscattering atom, whereas XRD experiments provide the mean squared *absolute* displacements (MSD). The EXAFS Debye-Waller factor σ comprises two components σ_{stat} and σ_{vib} due to static structural disorder and thermal vibrations, respectively. Assuming disorder effects with symmetric pair distribution function for static disorder and harmonic vibrations for thermal disorder, the Debye-Waller factor is given by $\sigma^2 = \sigma_{stat}^2 + \sigma_{vibv}^2$. The two factors can be separated by temperature dependent measurements of $\sigma(T)$. For small disorder effects with $\Delta r < 0.1$ Å the terms can be combined to one single term corresponding to the average distance whereas for $\Delta r > 0.1$ Å the EXAFS equation must be averaged over a pair distribution function g(r) including asymmetric correlation functions or/and anharmonic vibrations as described e.g. by the cumulant approach. EXAFS is sensitive only to a relative motion along the bond direction. At T = 297 K the U-O_{eq} distances in $H[UO_2AsO_4]\cdot 4H_2O$ are equal due to the space group symmetry P4/nnc. After the low-temperature phase transition P4/nnc $\rightarrow$ P $\bar{1}$ the atomic positions O_{eq} will become symmetry independent [1,2]. Hence, U-O_{eq} splits up into several distances, and σ_{stat} should increase affecting $\sigma(T)$ [3].

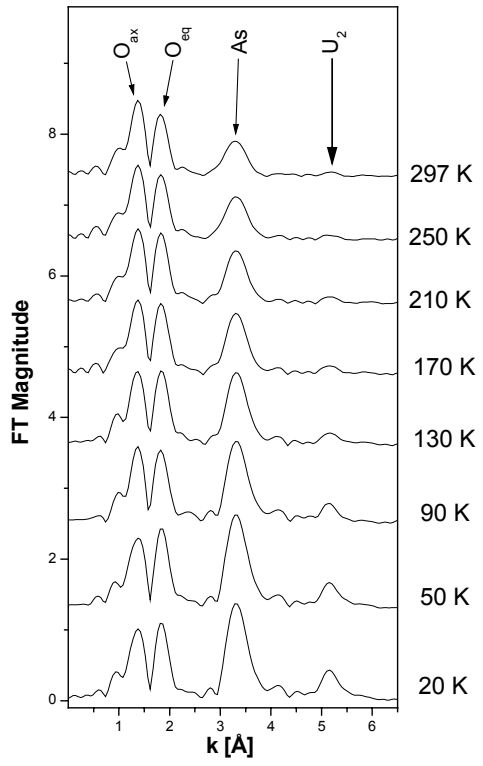

Fig. 1: Fourier transform of the U L_{III}-edge k^3-weighted EXAFS data ($3.2 \le k \le 15.7$ Å^{-1}).

EXAFS measurements were performed in transmission mode at the U-L_{III} and the As-K edges at temperatures from 20 K to 297 K using a closed-cycle He cryostate. The solid powder samples were prepared as pellets and mounted in a teflon sample holder. EXAFS signals were extracted and Fourier transformed in the *k*-range of 3.2 - 15.7 Å^{-1} (Fig. 1). Backscattering shells were separated by Fourier filtering. Subsequent data analysis was performed by fixing the coordination number to the crystallographic values. Distances R, Debye-Waller-Factors σ^2, and energy shifts ΔE were used as free fit parameters.

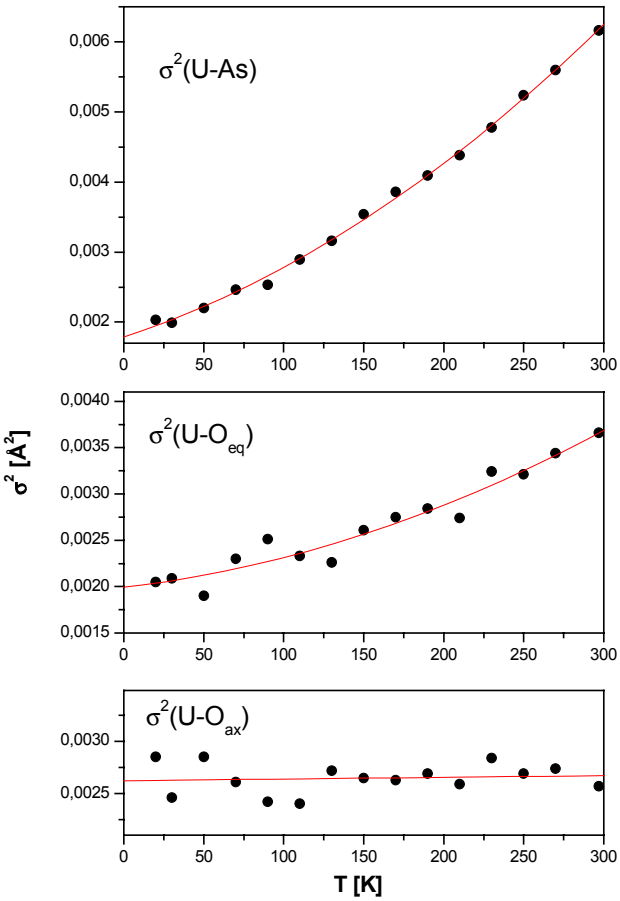

Fig. 2: Temperature dependence of EXAFS Debye-Waller factor for the first three backscattering shells.

We observed a strong temperature dependence of the U-As scattering pair $R_{(U\text{-}As)} = 3.69$ Å (Fig. 2). The temperature dependence of the scattering pair U-O_{eq} is less pronounced. However, we observed no P4/nnc $\rightarrow$ P $\bar{1}$ phase transition. In principle, the metal-oxygen bond is sensitive for phase transitions: Sani *et al.* [4] observed a phase transition in $La_{1.48}Nd_{0.4}Sr_{0.12}CuO_4$ using the σ^2 of the Cu-O scattering pair. In contrast to σ^2(U-O_{eq}), σ^2(U-O_{ax}) is almost constant over the whole temperature range. This indicates that this covalent bonding is not influenced by thermal vibrations.

REFERENCES

[1] Fitch, A.N. *et al.* (1983) *Acta Cryst.* **C 39**, 159-162.
[2] Fitch, A.N. *et al.* (1982) *Acta Cryst.* **B 38**, 2546-2554.
[3] Hennig, C. *et al.* (2001) *J. Synchr. Rad.* **8**, 695-697.
[4] Saini, N.L. *et al.* (2001) *Phys. Rev.* **B 64**, 132510(1)-132510(4).

Enhancement of the spatial resolution of the photothermal beam deflection technique towards the low micrometer range

H. Foerstendorf, W. Seidel[1], F. Glotin[2], R. Prazeres[2], J.M. Ortega[2]
[1]Institute of Nuclear and Hadron Physics, FZR, Dresden, Germany; [2]LURE, Université de Paris-Sud, Orsay, France

ABSTRACT. Photothermal beam deflection (PTBD) spectroscopy provides spatial information about surfaces of samples. Recent results of PTBD experiments using a free electron laser (FEL at CLIO) as an infrared pump source are presented. A high spatial resolution (< 30 µm) was obtained which is near the diffraction limit of the pump beam.

The PTBD technique is based on the theory of photothermal spectroscopy which describes the conversion of absorbed energy of a light beam incident on a sample into heat by nonradiative de-excitation processes [1]. In typical PTBD experiments a solid sample is irradiated by a modulated beam of monochromatic light produced by a tunable infrared laser and a probe beam (*e.g.* a HeNe laser) which is reflected from the sample. Depending on the modulated intensity of the pump beam the probe beam is deflected due to the photoinduced displacement which can be observed by a position detector. In PTBD generation and detection of the thermal waves occur generally in the sub-millimeter length scale. With a sufficiently small laser probe it should therefore be possible to obtain a spatial resolution of a few micrometers.

EXPERIMENTAL. We investigated a distinct pattern of O^+-implanted and untreated regions of germanium (Ge) substrates serving as complex model surface. The pattern was created by a special stainless steal mask in front of the substrate during the implantation process. The areas of the O^+-doped regions can be distinguished from areas of pure germanium by increased optical absorption (*i.e.* the amplitude of the deflection signal, see Fig. 1) at λ_{FEL} = 11.6 µm. The dimensions of the mask are given in Fig. 2A and as grey stripes throughout Figs. 2B–D. The diameter of the probe beam at the sample surface was ~15 µm as verified by pinholes.

RESULTS. The acquisition of deflection signals at distinct positions of the sample permits the calculation of absorption profiles as shown in Fig. 2B–D. The profile presented in Fig. 2B clearly reproduces the structure of the implanted regions generated by the mask.
In Fig. 2C an enlarged range of five thin implanted regions was detected at high resolution of positioning (step width: 2 µm). Again, the recovery of the pattern of implantation (dimensions of 30 µm) is of excellent quality. For demonstration that the deflection signal is solely caused by optical absorption the same sample area was scanned at a wavelength of 7.7 µm where no absorption occurs (Fig. 2D). It is noteworthy, that all profiles shown in this work were obtained with only one FEL macropulse for each sample position. In future a better focusing of the probe beam by using an objective lens and averaging of several FEL pulses are expected to enhance the quality of the microspectrometric PTBD measurements.

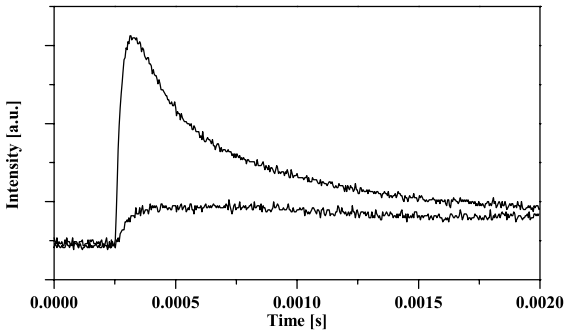

Fig. 1: Time-resolved beam deflection signals of a strong absorbing (upper trace) and a nearly transparent sample (lower trace).

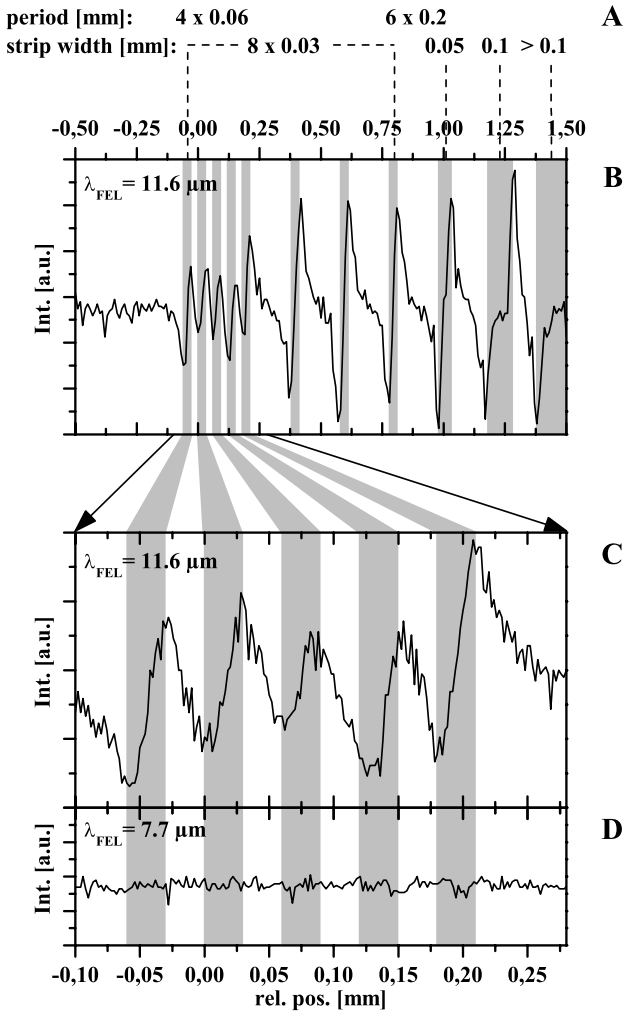

Fig. 2: Dimensions of the implantation pattern for the preparation of the Ge-substrate with O^+-ions (A). Extracted absorption profiles from the maximum of the deflection curves (B–D): Profile (step width: 10 µm) of the whole implanted structure (B). Profiles (step width: 2 µm) of five thin lines at different FEL wavelengths (C–D) with max. absorption (C) and no absorption (D).

REFERENCES

[1] Rosencwaig, A. *et al.* (1976) *J. Appl. Phys*. **47**, 64-69.

Theoretical EXAFS functions as mother wavelets for EXAFS analysis

H. Funke, M. Chukalina[1], A.C. Scheinost
[1]Institute of Microelectronics Technology RAS, Chernogolovka, Russia

ABSTRACT. A model EXAFS function, calculated from the FEFF8.2 program is chosen as mother wavelet function for EXAFS data analysis. The goal is to increase the resolution at a specific distance of one or several backscatterers. Some necessary new computational tools are shortly described.

The result of an integral transformation of a signal is a curve, which has maxima if the test function (the kernel) of the transformation coincides with the signal itself. Vice versa the result is zero if there is no coincidence between the signal and the transformation kernel. For example, the modulus of the Fourier transform (FT) shows maxima for such frequencys of the sine function, which are also contained in the signal.
To test the new model function, we re-examine the EXAFS spectrum of a Zn-Al Layered Double hydroxide (Zn-Al LDH) mineral previously published [1]. If 1/3 of the cationic positions of such an LDH layer are filled with Al, and the remaining 2/3 of the positions are filled with Zn, one would expect formation of a regular pattern as shown below to achieve an even charge distribution:

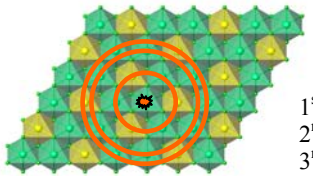

1st shell (~3.0 Å): 3 Al^{3+}, 3 Zn^{2+}
2nd shell (~5.2 Å): 6 Zn^{2+}
3rd shell (~6.0 Å): 3 Al^{3+}, 3 Zn^{2+}

Fig. 1: Model of the octahedral layer of Zn/Al LDH. $Zn(OH)_6$-octahedra are shown in green, those of Al are shown in yellow.

The EXAFS spectrum of this LDH sample has been investigated using the wavelet transform (WT):

$$W_\chi^\psi(k,R) = \sqrt{2R}\int \chi(k')k'^3\psi(2R(k'-k))dk',$$

where the EXAFS signal $\chi(k)$ is decomposed into a set of basic functions ψ, called the wavelets, see *e.g.* [2, 3].
With the previously used Morlet wavelet, it was possible to distinguish Zn and Al in the first shell (~3 Å). However, it was not possible to resolve the two more distant shells at 5.2 and 6 Å *simultaneously* with respect to wavenumber k (element identity) and the distance r.
Hence to further improve the k-r resolution in the wavelet space we used simulation results, calculated with FEFF8.2, as mother wavelet function. Four spectra were modeled: Zn-Zn @ 6 Å (see Fig. 2), Zn-Al @ 6 Å, Zn-Zn @ 5.2 Å, and Zn-Al @ 5.2 Å (although not meaningful according to our model).

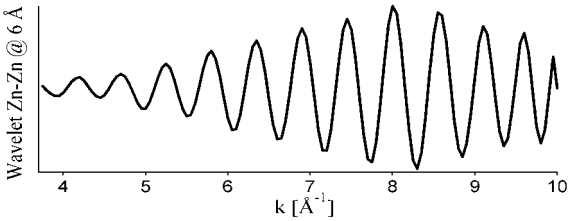

Fig. 2: Wavelet function obtained from the Zn-Zn EXAFS signal @ 6 Å, calculated with FEFF8.2.

These calculated EXAFS functions (l^2) were then numerically transformed into a wavelet. The condition $\int\psi(k)dk = 0$ must be fulfilled, *i.e.* the "center of gravity" of the curve must be set to zero.
(Remark: These constructed wavelets are real functions, and the resulting WT plots differ from the usual modulus of the WT performed with complex Morlet wavelets.)
In the next step a new subroutine, which calculates the wavelet transform (performing translation and scaling of the new non-analytic wavelet function) was developed. Thereby the scaling parameter, *i.e.* the distance r, was replaced by a scale parameter s. Its definition is: $s = 1$ if the wavelet is not dilated. Hence, the signal should have a maximum for $s = 1$, if the selected model function for a given distance is correct. As example we show in Fig. 3 the WT of the LDH spectrum around ~6.0 Å, based on the wavelet shown in Fig. 2.

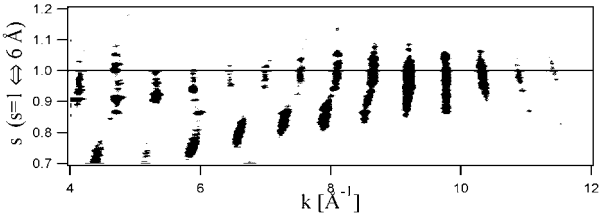

Fig. 3: WT of LDH built with the wavelet from the model Zn-Zn @ 6.0 Å.

The maximum of the WT is correctly located at $s = 1$, and at a higher k, *i.e.* indicative of the heavier Zn. Similar results were achieved for the other distances.
In order to simplify this complicated analysis, we introduced the power density function (PDF) depending on either k or s:

$$\Phi(k) = \int\left[W_\chi^\psi(k,s)\right]^2 ds, \qquad \Phi(s) = \int\left[W_\chi^\psi(k,s)\right]^2 dk.$$

Example:

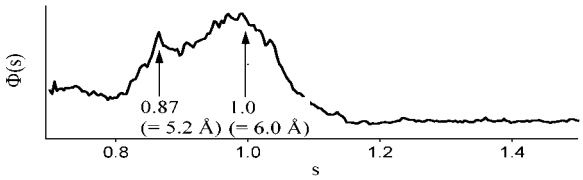

Fig. 4: PDF $\Phi(s)$ for the WT of figure 3.

The relation between the radii and the scale parameter is:

$$r = r_{opt} \cdot s, \ (r_{opt} = 6 \text{ Å}).$$

Thus the peak at $s = 0.87$ corresponds to the expected backscatterer distance 5.2 Å.

CONCLUSIONS. The examined method opens new possibilities, but is too complex to be routinely used. Therefore, we recommend the analysis based on the flexible Morlet wavelet [1,2,3].

REFERENCES

[1] Funke, H. *et al.* (2003) *Report FZR–400*, p. 56.
[2] Funke, H. *et al.*, (2002) *Report FZR–373*, p. 43.
[3] Mallat, S. (1999) *A wavelet tour of signal processing*, Academic Press.

Part 4:

Reactive transport of actinides

Diffusion of humic colloids in compacted kaolinite

J. Mibus, S. Sachs

ABSTRACT. The migration of humic acid in compacted clay is governed by diffusion. Size exclusion of the organic colloids clearly affects the diffusion parameters. Also a strong size fractionation is observed.

Clay minerals as well as organic substances are widespread components of many soils and sediments. However, little is known on the migration of humic substances in clay systems. Since humic acids (HA) are efficient complexing agents for metal ions they can also influence the migration behavior of actinides. Here, the diffusion of HA in compacted clay is investigated.

EXPERIMENTAL. Georgia kaolinite KGa-1B was compacted to a dry bulk density $\rho = 1.66$ g/cm^3 and fixed between two filter plates in a diffusion cell [1] with a layer thickness L = 0.82 cm and a cross sectional area S = 5.19 cm^2. The clay plug was conditioned with a 0.01 M $NaClO_4$ solution at pH 5.2 for four weeks. The effective porosity ε and the effective diffusion coefficient D_e were determined using tritiated water (HTO). A synthetic ^{14}C-labeled HA type M42 [2] with a concentration of 11.0 mg/L and a specific activity of (17.0 ± 0.5) MBq/g was used as tracer. We applied a steady-state through-diffusion technique with constant gradient [1]. The tracer concentrations at both boundary conditions were kept constant ($C(0,t) = C_0 = (185 \pm 9$ Bq/mL); $C(L,t) = 0$). The activity in both reservoirs was measured periodically by liquid scintillation counting. The particle size distribution of the HA was determined by filtration using filters (Microsep Centrifugal Devices, Pall) of pore width between 1 and 1000 kD.

MODELING. Data evaluation is based on Fick's second law (cf. [1]). Once steady state is reached, the accumulated activity A [Bq] becomes a linear function of time t:

$$A(t) = \frac{-SLC_0\alpha}{6} + \frac{SC_0D_e}{L}t \qquad (1)$$

where α is the rock capacity factor which is related to the empirical distribution coefficient K_d by $\alpha = \varepsilon + \rho \cdot K_d$.

RESULTS. Fig. 1 depicts the activity A diffused through the clay plug and the diffusive flux J versus time. After a transient period of about 14 days the flux significantly rises. However, no steady-state is reached but J subsequently decreases to about 0.4 Bq/(cm^2·d). Consequently, the activity in the low concentration reservoir increases with time exhibiting two phases of different incline. So far, the reason for these two steps remains unclear.
The parameters in Tab. 1 are derived considering these two phases as distinct linear intervals. The D_e values found for HA in both phases are about three orders of magnitude lower than that of HTO. Likewise α(HA) amounts to only 10 % of ε which equals α(HTO). The

Tab. 1: D_e and α for diffusion of HTO and HA (phase 1 and 2)

	D_e [m^2/s]	α [-]
HTO	$(2.4 \pm 0.1) \cdot 10^{-10}$	0.42 ± 0.02
HA(1)	$(5.9 \pm 1.3) \cdot 10^{-13}$	0.04 ± 0.02
HA(2)	$(1.9 \pm 0.3) \cdot 10^{-13}$	n/a

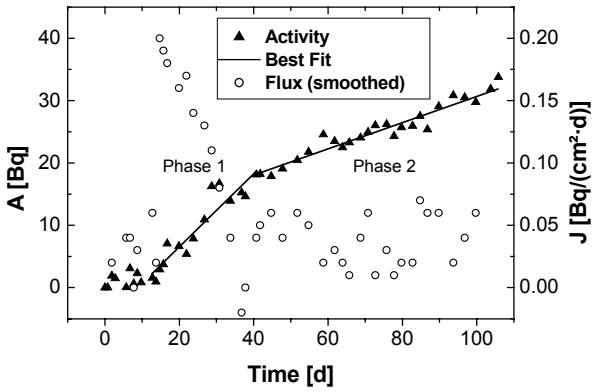

Fig. 1: Diffused activity A and diffusive flux J of HA vs. time.

spatial extension of the humic colloids constricts their mobility in the narrow pore space thus increasing the tortuosity of the diffusion path and decreasing the pore volume accessible for HA. This phenomenon is referred to as size exclusion effect. In [3] a significant adsorption of HA on KGa-1B was found ($K_d = 680$ ml/g) which would result in a large value for α. Obviously, the size exclusion dominates the HA migration.

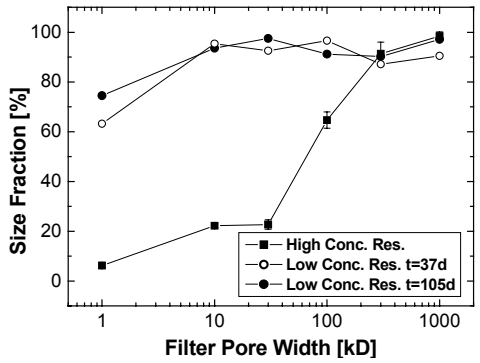

Fig. 2: Particle size distribution of humic colloids in the high and low concentration reservoir at different times.

The particle size distribution of both reservoirs is shown in Fig. 2. The mean particle size shifts from about 50 kD in the high to less than 1 kD in the low concentration reservoir. Only small particles are able to pass the pore system. This size fractionation is in agreement with the size exclusion deduced from the rock capacity factors.

CONCLUSIONS. The diffusion of HA in compacted clay is influenced by its colloidal behavior. Particle size exclusion clearly affects the diffusion parameters. Size fractionation restricts the flux. Future work focuses on the impact of HA on actinide migration in clay systems.

ACKNOWLEDGEMENT. The German Federal Ministry of Economics and Labor funded this study (02E9673).

REFERENCES

[1] Van Loon, L.R. *et al.* (2003). *J. Contam. Hydrol.* **61**, 73-83.
[2] Sachs, S. *et al.* (2004) *Report FZR–399*.
[3] Křepelová, A. *et al.* this report, p. 50.

Determination of the minimal sample thickness in diffusion experiments

P. Trepte, J. Mibus, V. Brendler

ABSTRACT. A reduction of the sample thickness in diffusion experiments to the dimension of the filter plates led to a distortion of the derived parameters.

The long-term risk assessment of underground repositories for radioactive waste requires diffusion coefficients of actinides in bentonite. The time-consuming determination of effective diffusion coefficients of actinides necessitates a minimization of the sample thickness. However, falling below a critical distance can lead to a misinterpretation of the data. We studied the dependence of the diffusion parameters of tritiated water (HTO) in bentonite on the sample thickness.

EXPERIMENTAL. MX-80 bentonite samples were compacted in pressure cells of 50 mm inner diameter to a dry bulk density of 1.6 g cm^{-3} and final sample thicknesses of L = 2.5, 5.0, 7.5, or 10.0 mm. Titanium filter plates of 5 mm thickness and 10 µm pore size were used. The samples were saturated with synthetic Opalinus Clay pore water [1] applying a hydraulic pressure of maximal 10 MPa to verify the sealing function. After dropping the hydraulic pressure and conditioning for three weeks the through-diffusion of HTO was investigated using a stationary technique (Fig. 1) with a tracer activity of C_0 = (97.9 ± 0.7) Bq/mL in the high concentration reservoir. After maintenance of the through-diffusion over an appropriate time the out-diffusion of HTO was measured.

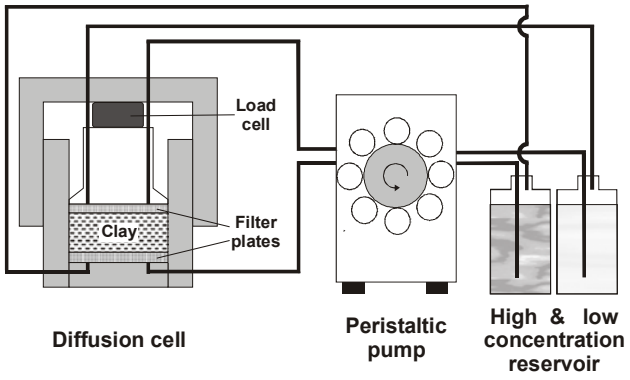

Fig. 1: Schematic set-up of the diffusion experiment.

MODELING. Data evaluation is based on Fick's second law where C is the concentration (or activity), D is the apparent diffusion coefficient, t is time and x is distance.

$$\frac{\partial C}{\partial t} = D\frac{\partial^2 C}{\partial x^2} \quad (1)$$

D is related to the effective diffusion coefficient of the porous medium D_e by

$$D = D_e / \alpha \quad (2)$$

where α is the rock capacity factor, for a conservative tracer equaling the effective porosity ε. Parameter estimation uses analytical solutions [2]. We applied linear regression analysis in the case of through-diffusion and a nonlinear fitting routine in the case of out-diffusion. Parameter uncertainty was estimated from the squared residuals between measured and fitted concentrations.

RESULTS. The experimental data show that the clay plugs are representative concerning their sealing behavior. The swelling pressure was nearly constant over the duration of the diffusion experiments. No formation of cracks or channels was observed.

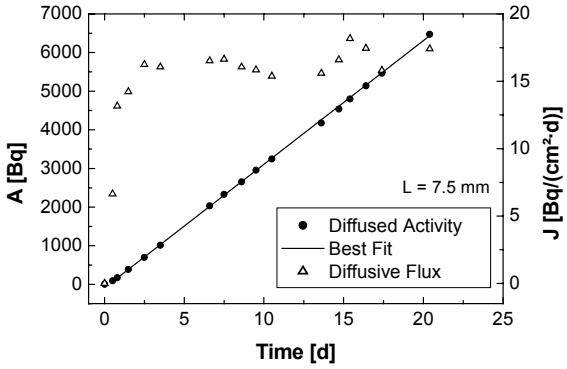

Fig. 2: Diffused activity A and diffusive flux J vs. time.

The diffused activity and the flux of a through-diffusion experiment is illustrated in Fig. 2. The D_e and α values for all through-diffusion experiments are shown in Tab. 1.

Tab. 1: D_e and α for the diffusion of HTO in MX-80.

L [mm]	D_e [10^{-10} m^2/s]	α [-]
2.5	0.74±0.04	1.1±0.86
5.0	0.89±0.03	-*
7.5	1.04±0.02	0.41±0.13
10.0	1.05±0.03	-*

* not determined due to disturbances in the transient phase.

The D_e values at 7.5 and 10.0 mm are in a good agreement. A slight decrease was found at 5.0 mm, whereas D_e considerably dropped at 2.5 mm. The α at 2.5 mm is affected by the filter plates as well, exhibiting a porosity above unity. At 7.5 mm a plausible α was found which meets the porosity expected from the bulk dry density. In the case of out-diffusion a stronger scattering of the parameters was observed, probably due to low ^3H activities.

CONCLUSIONS. The clay plugs are mechanically stable and fulfill the hydraulic sealing function. From the relationship between sample thickness and D_e we see that the filter plates exert a significant influence on the boundary condition as soon as sample and filter plate are of the same thickness. Filter plates should be of about 1 to 2 mm thickness to resist the swelling pressure. Thus, a sample thickness above this dimension enables the work with strong sorbing tracers minimizing the duration of the diffusion experiment and providing representative results.

ACKNOWLEDGEMENT. Funding by the European Commission (NF-PRO C2-ST-C-01) is gratefully acknowledged.

REFERENCES

[1] Pearson, F.J. (1998) *Report PSI TM-44-98-07*.
[2] Van Loon, L.R. *et al.* (2004) *Report PSI 04-03*.

- *Articles (peer-reviewed)*
- *Proceedings, reports*
- *Lectures, oral presentations*
- *Posters*
- *Theses*
- *Patents*
- *Awards*

▸ *Articles (peer-reviewed)*

Abraham, A.; Baraniak, L.; Bernhard, G.
Bog ground aquifer system as a natural analogue for future redox conditions in flooded underground mines
Journal of Radioanalytical and Nuclear Chemistry, 261, 597-604 (2004).

Amayri, S.; Arnold, Th.; Foerstendorf, H.; Geipel, G.; Bernhard, G.
Spectroscopic characterization of synthetic becquerelite, $Ca[(UO_2)_6O_4(OH)_6]\cdot 8H_2O$, and swartzite, $CaMg[UO_2(CO_3)_3]\cdot 12H_2O$
The Canadian Mineralogist, 42, 953-962 (2004).

Amayri, S.; Arnold, Th.; Reich, T.; Foerstendorf, H.; Geipel, G.; Bernhard, G.; Massanek, A.
Spectroscopic characterization of the uranium carbonate andersonite $Na_2Ca[UO_2(CO_3)_3]\cdot 6H_2O$
Environmental Science & Technology, 38, 6032-6036 (2004).

Baumann, N.; Brendler, V.; Arnold, T.; Geipel, G.
Investigations of uranyl sorption onto gibbsite
Geochimica et Cosmochimica Acta, 68, A509 (2004).

Chukalina, M.; Funke, H.
An approach to the analysis of EXAFS spectra based on the wavelet transformation
Izvestia Akademii Nauk. Seria Fizicheskaja, 60, 235-238 (2004).

Chukalina, M.; Funke, H.; Dubrovskii, Yu.
Wavelet analysis and its application to the tunneling and X-ray spectroscopy
Low Temperature Physics, 30, 930-936 (2004).

Chukalina, M.; Golosio, B.; Simionovici, A.; Funke, H.
X-ray tomography: How to evaluate the reconstruction quality?
Spectrochimica Acta Part B, 59, 1755-1758 (2004).

Gäggeler, H.W.; Brüchle, W.; Düllmann, C.E.; Dressler, R.; Eberhardt, K.; Eichler, B.; Eichler, R.; Folden, C.M.; Ginter, T.N.; Glaus, F.; Gregorich, K.E.; Haenssler, F.; Hoffman, D.C.; Jäger, E.; Jost, D.T.; Kirbach, U.W.; Kratz, J.V.; Nitsche, H.; Patin, J.B.; Pershina, V.; Piguet, D.; Qin, Z.; Rieth, U.; Schädel, M.; Schimpf, E.; Schausten, B.; Soverna, S.; Sudowe, R.; Thörle, P.; Trautmann, N.; Türler, A.; Vahle, A.; Wilk, P.A.; Wirth, G.; Yakushev, A.B.; von Zweidorf, A.
Chemical and nuclear studies of hassium and element 112
Nuclear Physics A 734, 208-212 (2004).

Geipel, G.; Acker, M.; Vulpius, D.; Bernhard, G.; Nitsche, H.; Fanghänel, T.
An ultrafast time-resolved fluorescence spectroscopy system for metal ion complexation studies with organic ligands
Spectrochimica Acta Part A - Molecular and Biomolecular Spectroscopy, 60, 417-424 (2004).

Koban, A.; Bernhard, G.
Complexation of uranium(VI) with glycerol 1-phosphate
Polyhedron, 23, 1793-1797 (2004).

Koban, A.; Geipel, G.; Roßberg, A.; Bernhard, G.
Uran(VI) complexes with sugar phosphates in aqueous solution
Radiochimica Acta, 92, 903-908 (2004).

Krawczyk-Bärsch, E.; Arnold, T.; Reuther, H.; Brandt, F.; Bosbach, D.; Bernhard, G.
Formation of secondary Fe-oxyhydroxide phases during the dissolution of chlorite effect on uranium sorption
Applied Geochemistry, 19, 1403-1412 (2004).

Kretzschmar, R.; Pfister, S.; Voegelin, A.; Scheinost, A.C.
Zinc speciation in an artificially contaminated soil: Formation of a new mineral phase within 3 years
Geochimica et Cosmochimica Acta, 68, A361 (2004).

Livens, F.; Jones, M.; Hynes, A.; Charnock, J.; Mosselmans, J.; Hennig, C.; Steele, H.; Collins, D.; Vaughan, D.; et, al.
X-ray absorption spectroscopy studies of reactions of technetium, uranium and neptunium with mackinawite
Journal of Environmental Radioactivity, 74, 211-219 (2004).

Maes, A.; Geraedts, K.; Bruggeman, C.; Vancluysen, J.; Rossberg, A.; Hennig, C.
Evidence for the interaction of technetium colloids with humic substances by X-ray absorption spectroscopy
Environmental Science & Technology, 38, 2044-2051 (2004).

Matys, S.; Raff, J.; Soltmann, U.; Selenska-Pobell, S.; Böttcher, H.; Pompe, W.
Calcium dipicolinate induced germination of *Bacillus* spores embedded in thin silica layers: novel perspectives for the usage of biocers
Chemistry of Materials, 16, 5549-5551 (2004).

Merroun, M.L.; Raff, J.; Rossberg, A.; Hennig, C.; Reich, T.; Selenska-Pobell, S.
Interaction of U(VI) with bacterial strains isolated form uranium mining piles: spectroscopic and microscopic studies
Geochimica et Cosmochimica Acta, 68, A499 (2004).

Mibus, J.; Lambarki, M.; Küchler, R.
Determination of effective diffusion parameters in compacted kaolinite
Geochimica et Cosmochimica Acta, 68, A165 (2004).

Moll, H.; Stumpf, T.; Merroun, M.; Rossberg, A.; Selenska-Pobell, S.; Bernhard, G.
Time-Resolved Laser Fluorescence Spectroscopy study on the interaction of Cm(III) with *Desulfovibrio äspöensis* DSM 10631^{T}
Environmental Science & Technology, 38, 1455-1459 (2004).

Radeva, G.; Selenska-Pobell, S.
Molecular analysis of bacterial populations in water samples from two uranium mill tailings by using a RISA retrieval
Comptes Rendues de l´Académie Bulgare des Sciences 57, 111-115 (2004).

Reuther, H.; Arnold, T.; Krawczyk-Bärsch, E.
Quantification of secondary Fe-phases formed during sorption experiments on chlorites
Hyperfine Interactions, 156/157, 439-443 (2004).

Satchanska, G.; Golovinski, E.; Selenska-Pobell, S.
Bacterial diversity in a soil sample from a uranium mining waste pile as estimated via a culture-independent 16S rDNA approach
Comptes Rendues de l'Académie bulgare des Sciences 57, 75-82 (2004).

Scheinost, A.C.
Metal oxides in soils
Encyclopedia of Soils in the Environment (D. Hiller, ed.), Academic Press, Amsterdam, 428-438 (2004).

Scheinost, A.C.; Bernhard, G.; Selenska-Pobell, S.
Fate of uranium in the environment
Geochimica et Cosmochimica Acta, 68, A526 (2004).

Scheinost, A.C.; Rossberg, A.; Hennig, C.; Vantelon, D.; Kretzschmar, R.; Johnson, C.
Quantitative antimony speciation in Swiss shooting range soils
Geochimica et Cosmochimica Acta, 68, A521 (2004).

Schmeide, K.; Heise, K.-H.; Bernhard, G.; Keil, D.; Jansen, K.; Praschak, D.
Uranium(VI) separation from aqueous solution by calix[6]arene modified textiles
Journal of Radioanalytical and Nuclear Chemistry, 261, 61-67 (2004).

Schumacher, M.; Scheinost, A.C.; Christl, I.; Jacobsen, C.; Kretzschmar, R.
Chemical heterogeneity of humic substances and mobile soil colloids studied by X-ray microscopy and microspectroscopy
Geochimica et Cosmochimica Acta, 68, A225 (2004).

Seidel, W.; Foerstendorf, H.; Heise, K. H.; Nicolai, R.; Schamlott, A.; Ortega, J. M.; Glotin, F.; Prazeres, R.
Infrared characterization of environmental samples by pulsed photothermal spectroscopy
The European Physical Journal – Applied Physics, 25, 39-43 (2004).

Selenska-Pobell, S.; Radeva, G.
Bacterial diversity in water samples from two uranium mill tailings as revealed by 16S rDNA retrieval
Comptes Rendues de l'Académie bulgare des Sciences, 57, 85-90 (2004).

Stumpf, Th.; Hennig, C.; Bauer, A.; Denecke, M. A.; Fanghänel, Th.
An EXAFS and TRLFS study of the sorption of trivalent actinides onto smectite and kaolinite
Radiochimica Acta, 92, 133-138 (2004).

Tositti, L.; Hübener, S.; Kanter, H.-J.; Ringer, W.; Sandrini, S.; Tobler, L.
Intercomparison of sampling and measurement of Be-7 in air at four high-altitude locations in Europe
Applied Radiation and Isotopes, 61, 1497-1502 (2004).

Yakushev, A.B.; Zvara, I.; Oganessian ,Y.T.; Belozerov, A.V.; Dmitriev, S.N.; Eichler, B.; Hübener, S.; Sokol, E.A.; Türler, A.; Yeremin, A.V.; Buklanov, G.V.; Chelnokov, M.L.; Chepigin, V.I.; Gorshkov, V.A.; Gulyaev, A.V.; Lebedev, V.Y.; Malyshev, O.N.; Popeko, A.G.; Soverna, S.; Szeglowski, Z.; Timokhin, S.N.; Tretyakova, S.P.; Vasko, V.M.; Itkis, M.G.
Chemical identification and properties of element 112
Nuclear Physics A, 734, 204-207 (2004).

▶ *Proceedings, reports*

Altmaier, M.; Brendler, V.; Bosbach, D.; Kienzler, B.; Marquardt, C.; Neck, V.; Richter, A.
Geochemische Prozesse bei der Ausbreitung von Schadstoffen aus einem Endlager für radioaktive Abfälle
Final report, FZK-INE 002/04, Forschungszentrum Karlsruhe, Germany (2004).

Arnold, T.; Baumann, N.; Brendler, V.; Geipel, G.
Detection of adsorbed U(VI) surface species on muscovite by TRLFS
SOPRO 2004, International Workshop on Sorption Processes at Oxide and Carbonate Mineral Water Interfaces, March 25-26, 2004, Karlsruhe, Germany (J. Lützenkirchen, T. Stumpf, V. Brendler, B. Bayens, and D. Grolimund, eds.), Forschungszentrum Karlsruhe, Wissenschaftliche Berichte FZKA 6986, Karlsruhe, 3-6 (2004).

Baumann, N.; Brendler, V.; Arnold, T.; Geipel, G.
Investigations of uranyl sorption onto gibbsite
Tagung der Deutschen Mineralogischen Gesellschaft, Karlsruhe, Germany, September 19-22, 2004, Beiheft zum European Journal of Mineralogy, 16 (2004).

Bernhard, G.
Transfer of uranium to plants – Aspects of chemical speciation
Proceedings of the 227th ACS National Meeting, March 28–April 1, 2004, Anaheim, CA, USA (2004).

Brendler, V.; Richter, A.; Nebelung, C.; Vahle, A.
Development of a mineral-specific sorption database for surface complexation modeling (Final report and manual)
Wissenschaftlich-Technische Berichte FZR-409 (2004).

Brendler, V.; Richter, A.; Bernhard, G.
Verlässlichere Prognosen zur Schadstoffausbreitung mit Hilfe einer mineral-spezifischen Sorptionsdatenbank des Forschungszentrums Rossendorf (FZR)
Umwelt-Report, 10-11 (Dresden), 56-57 (Chemnitz) (2004).

Chukalina, M.; Funke, H.
An approach to the analysis of EXAFS spectra based on the wavelet transformation
X-ray optics, Institute of Microstructures Physics, May 2-6, 2004, Nizhnii Novgorod, Russia, 106-111 (2004).

Chukalina, M.; Funke, H.
Sage of wavelet transform for extraction of the information needed to describe an object
Intelligent systems AIS-04 IEEE Conference, PhysMathLit (2004), September 3-10, 2004, Divnomorskoe, Russia, 194-198 (2004).

Chukalina, M.; Funke, H.; Dubrovskii, Y.; Golossio, B.; Shapoval, S.; Ivanov, D.; Volkov, V.; Simionovici, A.; Somogyi, A.
Wavelet transformation for image analysis and signal processing: some estimations and real applications
6th Open Russian-German Workshop on Pattern Recognition and Image Understanding, August 25-30, 2004, Village Katun of Altai Region, Russia, 153-156 (2004).

Geipel, G.
Femto-second spectroscopy in actinide research
Proceedings of the 227th ACS National Meeting, March 28 – April 1, 2004, Anaheim, CA, USA (2004).

Günther, A.; Geipel, G.; Roßberg, A.; Bernhard, G.
Complex formation of U(VI) with amino acids studied by UV-vis spectroscopy, TRLFS and EXAFS
Advances in Nuclear and Radiochemistry, 6th International Conference on Nuclear and Radiochemistry (NRC-6), August 29 – September 3, 2004, Aachen, Germany (S.M. Qaim and H.H. Coenen, eds.), Schriften des Forschungszentrums Jülich, Reihe Allgemeines und Interdisziplinäres Band 3, Jülich, 43-45 (2004).

Hüttig, G.; Zänker, H.
Kolloidgetragene Schwermetalle im Entwässerungsstollen einer stillgelegten Zn-Pb-Ag-Grube
Wissenschaftlich-Technische Berichte FZR-403 (2004).

Křepelová, A.; Mibus, J.; Sachs, S.; Nebelung, C.; Bernhard, G.
Interaction processes of tetravalent actinides in the system humic acid / quartz sand / solution
SOPRO 2004, International Workshop on Sorption Processes at Oxide and Carbonate Mineral Water Interfaces, March 25-26, 2004, Karlsruhe, Germany (J. Lützenkirchen, T. Stumpf, V. Brendler, B. Bayens, and D. Grolimund, eds.), Forschungszentrum Karlsruhe, Wissenschaftliche Berichte FZKA 6986, Karlsruhe, 75-79 (2004).

Mibus, J.; Sachs, S.; Nebelung, C.; Bernhard, G.
Influence of humic acids on the migration of uranium (IV)/(VI) in quartz sand
Proceedings of the 11th International Symposium on Water-Rock Interaction WRI-11, June 27 -July 2, 2004, Saratoga Springs, New York, USA (R.B. Wanty and R.R. Seal II, eds.), Balkema Publ., Leiden, 691-695 (2004).

Moll, H.; Geipel, G.; Bernhard, G.
Complex formation of curium with adenosine 5'-triphosphate (ATP) studied by TRLFS
Advances in Nuclear and Radiochemistry, 6th International Conference on Nuclear and Radiochemistry (NRC-6), August, 29 – September, 3, 2004, Aachen, Germany (S.M. Qaim and H.H. Coenen, eds.), Schriften des Forschungszentrums Jülich, Reihe Allgemeines und Interdisziplinäres Band 3, Jülich, 72-74 (2004).

Opel, K.; Hüttig, G.; Zänker, H.
Anorganische Kolloide im Wasser der Elbe
Wissenschaftlich-Technische Berichte FZR-395 (2004).

Raff, J.; Merroun, M.; Rossberg, A.; Soltmann, U.; Böttcher, H.; Selenska-Pobell, S.
Interactions of the U mining waste pile isolate *Bacillus sphaericus* JG-A12 with U
Proceedings of the 11th International Symposium on Water-Rock Interaction WRI-11, June 27 -July 2, 2004, Saratoga Springs New York, USA (R.B. Want and R.R. Seal II, eds.), Balkema Publ., Leiden, 697-701 (2004).

Raff, J.; Selenska-Pobell, S.
Bacteria from extreme environments: basis for new technical applications
BioMeT-Magazin, 18 (2004).

Raff, J.; Selenska-Pobell, S.
Use of bacteria for cleaning radioactive wastewaters
Genomics/Proteomics Technology, 22, 32L-32N (2004).

Richter, A.; Brendler, V.
Capability of SCM and RES^{3}T database for blind predictions
SOPRO 2004, International Workshop on Sorption Processes at Oxide and Carbonate Mineral Water Interfaces, March 25-26, 2004, Karlsruhe, Germany (J. Lützenkirchen, T. Stumpf, V. Brendler, B. Bayens, and D. Grolimund, eds.), Forschungszentrum Karlsruhe, Wissenschaftliche Berichte FZKA 6986, Karlsruhe, 127-131 (2004).

Richter, A.; Brendler, V.; Nebelung, C.
The effect of parameter uncertainty on blind prediction of Np(V) sorption onto haematite using surface complexation modelling
Advances in Nuclear and Radiochemistry, 6th International Conference on Nuclear and Radiochemistry (NRC-6), August 29 – September 3, 2004, Aachen, Germany (S.M. Qaim and H.H. Coenen, eds.), Schriften des Forschungszentrums Jülich, Reihe Allgemeines und Interdisziplinäres Band 3, Jülich, 493-495 (2004).

Sachs, S.; Benes, P.; Vopalka, D.; Stamberg, K.; Mibus, J.; Bernhard, G.; Bauer, A.
Sampling and characterization of rock material from uranium mining waste rocks for study and modeling of release and migration of uranium
Humic Substances in Performance Assessment of Nuclear Waste Disposal: Actinide and Iodine Migration in the Far-Field. Second Technical Progress Report (G. Buckau, ed.), Forschungszentrum Karlsruhe, Wissenschaftliche Berichte FZKA 6969, Karlsruhe, 73-84 (2004).

Sachs, S.; Bernhard, G.
NIR spectroscopic study on the influence of phenolic OH groups on the neptunium(V) humate complex formation
Humic Substances in Performance Assessment of Nuclear Waste Disposal: Actinide and Iodine Migration in the Far-Field. Second Technical Progress Report (G. Buckau, ed.), Forschungszentrum Karlsruhe, Wissenschaftliche Berichte FZKA 6969, Karlsruhe, 61-71 (2004).

Sachs, S.; Geipel, G.; Bernhard, G.
Redox stability of uranium(VI) in presence of synthetic and natural humic acids
Humic Substances and Soil and Water Environment. Proceedings of the 12th International Meeting of the International Humic Substances Society, July 25-30, 2004, Sao Pedro, Sao Paulo, Brazil (L. Martin-Neto, D.M.B.P. Milori, and W.T.L. da Silva, eds.), Embrapa Instrumentacao Agropecuária, 172-174 (2004).

Sachs, S.; Schmeide, K.; Brendler, V.; Křepelová, A.; Mibus, J.; Geipel, G.; Heise, K.-H.; Bernhard, G.
Investigation of the complexation and the migration behavior of actinides and non-radioactive substances with humic acids under geogenic conditions - Complexation of humic acids with actinides in the oxidation state IV Th, U, Np
Wissenschaftlich-Technische Berichte FZR-399 (2004).

Sachs, S.; Schmeide, K.; Brendler, V.; Křepelová, A.; Mibus, J.; Geipel, G.; Reich, T; Heise, K.-H.; Bernhard, G.
Investigation of the complexation and the migration behavior of actinides and non-radioactive substances with humic acids under geogenic conditions - Complexation of humic acids with actinides in the oxidation state IV Th, U, Np
Investigations on the Complexation Behaviour of Humic Acids and their Influence on the Migration of Radioactive and Non-radioactive Substances under Conditions Close to Nature. Final Report (C.M. Marquardt, ed.), Forschungszentrum Karlsruhe, Wissenschaftliche Berichte FZKA 6999, Karlsruhe, 19-94 (2004).

Schmeide, K.; Bernhard, G.
Influence of humic acid on the neptunium(V) sorption onto granite and its mineral constituents
SOPRO 2004, International Workshop on Sorption Processes at Oxide and Carbonate Mineral Water Interfaces, March 25-26, 2004, Karlsruhe, Germany (J. Lützenkirchen, T. Stumpf, V. Brendler, B. Bayens, and D. Grolimund, eds.), Forschungszentrum Karlsruhe, Wissenschaftliche Berichte FZKA 6986, Karlsruhe, 132-136 (2004).

Schmeide, K.; Bernhard, G.
Neptunium(V) sorption onto granite and its mineral constituents in the absence and presence of humic acid
Humic Substances in Performance Assessment of Nuclear Waste Disposal: Actinide and Iodine Migration in the Far-Field. Second Technical Progress Report (G. Buckau, ed.), Forschungszentrum Karlsruhe, Wissenschaftliche Berichte FZKA 6969, Karlsruhe, 85-94 (2004).

Schmeide, K.; Bernhard, G.; Keil, D.; Buschmann, H.-J.; Praschak, D.
Separation of uranium(VI) from aqueous solution by textile bound calix[6]arenes
Wissenschaftliche Mitteilungen 25, GIS – Geoscience Applications and Developments / Treatment Technologies for Mining Impacted Water (B. Merkel et al., eds.). Technische Universität Bergakademie Freiberg, Freiberg, 133-139 (2004).

Schmeide, K.; Geipel, G.; Bernhard, G.
Abtrennung von Uran aus wässriger Lösung durch Calix[6]arene mittels Flüssig-Flüssig-Extraktion sowie Festphasen-Extraktion
Wissenschaftlich-Technische Berichte FZR-414 (2004).

Schollmeyer, E.; Jansen, K.; Buschmann, H.-J.; Schmeide, K.
Functionalization of synthetic polymers by supramolecular compounds: immobilization of calix[n]arenes on polyester
Polymer Surface Modification: Relevance to Adhesion 3 (K.L. Mittal, ed.). VSP, Zeist, 353-366 (2004).

Seidel, W.; Foerstendorf, H.; Glotin, F.; Ortega, J.-M.; Prazeres, R.
Exploring the spatial resolution of the photothermal beam deflection technique in the infrared region
Proceedings of the 2004 FEL Conference, ELETTRA, August 29 – September 3, 2004, Trieste, Italy, 679-680 (2004).

Ulrich, K.-U.; Zänker, H.; Jenk, U.
Colloid-borne uranium in an abandoned uranium mine in the stage of flooding
Advances in Nuclear and Radiochemistry, 6th International Conference on Nuclear and Radiochemistry (NRC-6), August 29 – September 3, 2004, Aachen, Germany (S.M. Qaim and H.H. Coenen, eds.), Schriften des Forschungszentrums Jülich, Reihe Allgemeines und Interdisziplinäres Band 3, Jülich, 645-647 (2004).

Vejmelka, P.; Lützenkirchen, J.; Kelm, M.; Bohnert, E.; Gompper, K.; Nebelung, C.; Baraniak, L.
Nuklidmigration im Deckgebirge des ERAM (DGL)
Final report, FZK-INE 14/03, Forschungszentrum Karlsruhe, Germany (2004).

Zänker, H.; Richter, W.; Hüttig, G.; Moll, H.; Brendler, V.; Hübener, S.; Opel, K.
Die Welt der vernachlässigten Dimensionen
Wissenschaftlich-Technische Berichte FZR-398 (2004).

Zänker, H.; Ulrich, K.-U.; Jenk, U.; Moll, H.; Richter, W.
Kolloidgetragene Schadstoffe in oxischen Bergwerkswässern
Jahrestagung 2004 der Wasserchemischen Gesellschaft, May 17 – 19, 2004, Bad Saarow, Germany, 181 (2004).

▶ *Lectures, oral presentations*

Arnold, T.; Baumann, N.; Brendler, V.; Geipel, G.
Detection of adsorbed U(VI) surface species on muscovite by TRLFS
SOPRO 2004, International Workshop on Sorption Processes at Oxide and Carbonate Mineral Water Interfaces, March 25-26, 2004, Karlsruhe, Germany.

Bernhard, G.
Aspekte der biogeochemischen Forschung im Institut für Radiochemie des Forschungszentrums Rossendorf
5. Leipziger Kolloquium "Radionuklidanwendung zur Gesunderhaltung des Menschen", October 27, 2004, IIF Leipzig, Germany (Invited lecture).

Bernhard, G.
Institute of Radiochemistry - Profile, goals and scientific results
Group Meeting, UC at Berkeley, LBNL, April 5, 2004, Berkeley, CA, USA (Invited lecture).

Bernhard, G.
Natürliche Hintergrundwerte des Uran
1. Statusseminar zum Thema Uran, Uran-Umwelt-Unbehagen, Bundesforschungsanstalt für Landwirtschaft, October 14, 2004, Braunschweig, Germany (Invited lecture).

Bernhard, G.
Radioecological research at the Institute of Radiochemistry, FZR
Shanghai Institute of Applied Physics, April 26, 2004.

Bernhard, G.
Transfer of uranium to plants - Aspects of chemical speciation
227th ACS National Meeting, March 28 – April 1, 2004, Anaheim, CA, USA (Invited Lecture).

Bernhard, G.
Uranium speciation in biogeochemistry
3. Jenaer Sanierungskolloquium "Geomicrobiology in remediation of mine waste", October 3-6, 2004, Jena, Germany (Invited Lecture).

Bernhard, G.
Wechselwirkung von Uran mit Biosystemen - Aspekte der chemischen Speziation
Freie Universität Berlin, June 21, 2004, Berlin, Germany.

Bhatt, A.; Kinoshita, H.; Koster, A. L.; May, I.; Sharrad, C. A.; Volkovich, V. A.; Vox, O. D.; Jones, C. J.; Lewin, B. G.; Charnock, J. M.; Hennig, C.
Actinide, lanthanide, fission product speciation and electrochemistry
227th ACS National Meeting, March 28 – April 1, 2004, Anaheim, CA, USA.

Brendler, V.; Richter, A.; Arnold, T.; Bernhard, G.
Thermodynamic sorption models: Derivation of recommended data sets and application to performance assessment
Waste Management Conference 2004, February 29 – March 4, 2004, Tucson, Arizona, USA.

Geipel, G.
Laserspektroskopie zur Aufklärung des Umweltverhaltens von Metallen
Lehrerfortbildungstag Rossendorf 2003/2004, February 9, 2004, Dresden, Germany.

Geipel, G.
Femto-second spectroscopy in actinide research
227th ACS National Meeting, March 28 – April 1, 2004, Anaheim, CA, USA.

Geipel, G.
Laser-induced spectroscopic methods used for determination of complex stability constants and speciation
Group Meeting, UC at Berkeley, LBNL, April 5, 2004, Berkeley, CA, USA (Invited lecture).

Geipel, G.
Copper(II)-complexes of phenanthrolic dendrimers studied by Time-Resolved Laser-Induced Fluorescence Spectroscopy
Supraphone Meeting, May 7-8, 2004, Xanten, Germany.

Geipel, G.
Mit Lasern auf Spurensuche – Aufklärung des Umweltverhaltens von Schwermetallen
Open House FZR 2004, September 18, Dresden, Germany.

Geipel, G.
Aktuelle Ergebnisse Fluoreszenzspektroskopischer Untersuchungen an Actiniden und organischen Liganden
BAM Berlin, Bundesanstalt für Materialforschung und -prüfung, December 21, 2004, Berlin, Germany.

Geipel, G.
Laser-induced spectroscopy: Tools to study actinide speciation in environmental concentration ranges
Faculty of Physics, Charles University Prague, December, 2004, Prague, Czech Republic (Invited lecture).

Günther, A.
Uran-Aufnahme in Pflanzen - Transferfaktoren und chemische Speziation
Friedrich-Schiller-Universität Jena, Biologisch-Pharmazeutische Fakultät, May 18, 2004, Jena, Germany.

Günther, A.; Geipel, G.; Rossberg, A.; Bernhard, G.
Complex formation of U(VI) with amino acids studied by UV-vis spectroscopy, TRLFS and EXAFS
NRC-6, *6th International Conference on Nuclear and Radiochemistry, August 29 – September 3, 2004, Aachen, Germany.*

Hennig, C.
Speciation of U^{4+} in high concentrated [Cl^-] solutions with a spectro-electrochemical cell
ACTINET Coordination Meeting "Electrochemistry of Ionic Liquids", November 8, 2004, Strasbourg, France.

Hennig, C.
Structure analysis and speciation of actinide systems using XAFS
CEA Marcoule, February 16, 2004, Bagnols, France.

Hennig, C.; Tutschku, J.; Rossberg, A.; Scheinost, A.C.; Bernhard, G.
In situ speciation of U(IV) and U(VI) aqueous complexes with a newly developed spectro-electrochemical cell
Actinide-XAS-2004, 3rd Workshop on Speciation, Techniques, and Facilities for Radioactive Materials at Synchrotron Light Sources, September 14-16, 2004, Berkeley, CA, USA.

Klenze, R; Fanghänel, Th.; Kim, J. I.; Brendler, V.; Hadermann, J.; Grenthe, I.; Bruno, J.; Stipp, S.L.S.; Read, D.; Missana, T.
Aquatic chemistry and thermodynamics of actinides and fission products relevant to nuclear waste disposal (ACTAF)"
EURADWASTE Conference, March 29-31, 2004, Luxemburg.

Křepelová, A.
First results of kaolinite characterization and of sorption experiments in the system U(VI)/humic acid/kaolinite
Workshop on research project "Migration von Actiniden im System Ton, Huminstoff, Aquifer", May 11-12, 2004, Saarbrücken, Germany.

Křepelová, A.
Fortsetzung der Sorptionsexperimente am System U(VI)/Kaolinit/Huminsäure
Workshop on research project "Migration von Actiniden im System Ton, Huminstoff, Aquifer", October 12–13, 2004, Heidelberg, Germany.

Kretzschmar, R.; Pfister, S.; Voegelin, A.; Scheinost, A.C.
Zinc speciation in an artificially contaminated soil: Formation of a new mineral phase within 3 years
13th Annual V.M. Goldschmidt Conference, June 5-11, 2004, Copenhagen, Denmark.

Merroun, M.
Gold and palladium nanoclusters formed by cells and s-layer of *Bacillus sphaericus* JG-A12 spectroscopic studies
SMWK Project Meeting Dresden University of Technology, October 21, 2004, Dresden, Germany.

Merroun, M.
Spectroscopic characterization of Pd nanoclusters formed by S-layer of *B. sphaericus* JG-A12 and biocers
BIO-CAT Project Meeting, November 5, 2004, Paris, France.

Merroun, M. L.
Interaction of uranium with bacterial strains isolated from uranium contaminated environments: Microscopic and spectroscopic studies
Institute for Nuclear Chemistry, University Mainz, June 16, 2004, Mainz, Germany (Invited lecture).

Merroun, M.; Raff, J.; Pollmann, K.; Hennig, C.; Rossberg, A.; Foerstendorf, H.; Scheinost, A.C.; Selenska-Pobell, S.
Perspectives for biotechnological applications of the uranium mining waste pile isolate *Bacillus sphaericus* JG-A12
VAAM 2004, March 28-31, 2004, Braunschweig, Germany.

Merroun, M.; Raff, J.; Rossberg, A.; Hennig, C.; Reich, T.; Selenska-Pobell, S.
Interaction of U(VI) with bacterial strains isolated from uranium mining piles: spectroscopic and microscopic studies
13th Annual V.M. Goldschmidt Conference, June 5-11, 2004, Copenhagen, Denmark.

Mibus, J.; Sachs, S.; Nebelung, C.; Bernhard, G.
Influence of humic acids on the migration of uranium (IV)/(VI) in quartz sand
WRI-11, *11th International Symposium on Water-Rock Interaction, June 27 – July 2, 2004, Saratoga Springs, New York, USA.*

Pollmann, K.; Raff, J.; Merroun, M. L.; Fahmy, K.; Mikeehenko, I.; Creamer, N.; Macaskie, L.; Selenska-Pobell, S.
Bacterial mediated formation of Pd-nanoclusters for the development of biocatalysts
Biometals 2004, September 3-5, 2004, Garmisch-Partenkirchen, Germany.

Pollmann, K.; Raff, J.; Merroun, M.; Schnorpfeil, M.; Fahmy, K.; Selenska-Pobell, S.
Interactions of the native and engineered S-layer of *Bacillus sphaericus* JG-A12 with U, Pd, and other metals
Biotechnology 2004 - Conference, October 17-22, 2004, Santiago de Chile.

Pollmann, K.; Raff, J.; Schnorpfeil, M.; Fahmy, K.; Selenska-Pobell, S.
Molecular analysis of the S-layer protein of the uranium mining waste pile isolate *Bacillus sphaericus* JG-A12
VAAM 2004, March 28-31, 2004, Braunschweig, Germany.

Raff, J.

Biotechnological potential of bacteria from extreme environments

International Microfluidics Sales Meeting, June 17-18, 2004, Lampertheim, Germany.

Raff, J.; Merroun, M.; Rossberg, A.; Foerstendorf, H.; Selenska-Pobell, S.

Uranium binding by the natural isolate *Bacillus sphaericus* JGA-12 and its application for bioremediation

Biometals 2004, September 3-5, 2004, Garmisch-Partenkirchen, Germany.

Raff, J.; Merroun, M.; Rossberg, A.; Soltmann, U.; Böttcher, H.; Selenska-Pobell, S.

Interactions of the U mining waste pile isolate *Bacillus sphaericus* JG-A12 with U

WRI-11, *11th International Symposium on Water-Rock Interaction, June 27 – July 2, 2004, Saratoga Springs, New York, USA.*

Richter, A.; Brendler, V.

Capabiliy of SCM and RES^{3}T database for blind predictions

SOPRO 2004, International Workshop on Sorption Processes at Oxide and Carbonate Mineral Water Interfaces, March 25-26, 2004, Karlsruhe, Germany.

Richter, A.; Brendler, V.; Nebelung, C.

The effect of parameter uncertainty on blind prediction of Np(V) sorption onto haematite using surface complexation modelling

NRC-6, 6th International Conference on Nuclear and Radiochemistry, August 29 – September 3, 2004, Aachen, Germany.

Rossberg, A.; Scheinost, A.C.

Actinide speciation based on EXAFS spectroscopy: From shell fitting to MCTFA

Actinide-XAS-2004, 3rd Workshop on Speciation, Techniques, and Facilities for Radioactive Materials at Synchrotron Light Sources, September 14-16, 2004, Berkeley, CA, USA.

Sachs, S.

Spektroskopische Untersuchungen zur Wechselwirkung von Actiniden mit Huminsäuren unter Einsatz von spezifischen Huminsäure-Modellverbindungen

4. Mainzer Symposium über Spurenanalytik, November 26, 2004, Johannes Gutenberg-Universität Mainz, Mainz, Germany.

Sachs, S.

Studies on the redox behavior of humic acids and the redox stability of U(VI) humate complexes

Workshop on research project "Humic Substances in Performance Assessment of Nuclear Waste Disposal: Actinide and Iodine Migration in the Far-Field", April 26-27, 2004, Budapest, Hungary.

Sachs, S.

Untersuchungen zur Huminstoffbildung in Gegenwart von Kaolinit

Workshop on research project „Migration von Actiniden im System Ton, Huminstoff, Aquifer“, May 11-12, 2004, Saarbrücken, Germany.

Scheinost, A.C.

Lead corrosion in soils: A literature review

International Symposium: Sport Shooting and the Environment -Sustainable Use of Lead Ammunition, September 9-10, 2004, Rome, Italy.

Scheinost, A.C.

The Rossendorf Beamline at the ESRF: An XAS experimental station for actinide research

Actinide-XAS-2004, 3rd Workshop on Speciation, Techniques, and Facilities for Radioactive Materials at Synchrotron Light Sources, September 14-16, 2004, Berkeley, CA, USA.

Scheinost, A.C.; Bernhard, G.; Selenska-Pobell, S.

Fate of uranium in the environment

13th Annual V.M. Goldschmidt Conference, June 5-11, 2004, Copenhagen, Denmark.

Scheinost, A.C.; Rossberg, A.; Hennig, C.; Vantelon, D.; Kretzschmar, R.; Johnson, C.

Quantitative antimony speciation in Swiss shooting range soils

13th Annual V.M. Goldschmidt Conference, June 5-11, 2004, Copenhagen, Denmark.

Schmeide, K.

Neptunium(V) reduction by various natural and synthetic humic substances

Workshop on research project "Humic Substances in Performance Assessment of Nuclear Waste Disposal: Actinide and Iodine Migration in the Far-Field", October 18-19, 2004, Karlsruhe, Germany.

Schmeide, K.

Untersuchung der Redoxstabilität von Neptunium(V) in Gegenwart natürlicher und synthetischer Huminstoffe

Workshop on research project "Migration von Actiniden im System Ton, Huminstoff, Aquifer", October 12-13, 2004, Heidelberg, Germany.

Schmeide, K.; Bernhard, G.; Keil, D.; Buschmann, H.-J.; Praschak, D.

Separation of uranium(VI) from aqueous solution by textile bound calix[6]arenes

55. Berg- und Hüttenmännischer Tag, Treatment Technologies for Mining Impacted Water, June 18, 2004, Freiberg, Germany.

Schmeide, K.; Brendler, V.

Auswertung der Komplexierungsdatenbasis bezüglich weiterführender Experimente und der Weiterentwicklung des Ladungsneutralisationsmodells

Workshop on research project "Migration von Actiniden im System Ton, Huminstoff, Aquifer", May 11-12, 2004, Saarbrücken, Germany.

Schmeide, K.; Zänker, H.; Weiß, S.; Ulrich, K.-U.

Colloid-chemical investigation of the Kaitzbach stream

Workshop on research project "Humic Substances in Performance Assessment of Nuclear Waste Disposal: Actinide and Iodine Migration in the Far-Field", April 26-27, 2004, Budapest, Hungary.

Selenska-Pobell, S.; Geißler, A.; Radeva, G.; Merroun, M.; Flemming, K.; Satchanska, G.; Tzvetkova, T.

Comparative microbial diversity in uranium wastes in Germany and in the USA

ISME 10, August 22-27, 2004, Cancum, Mexico.

Selenska-Pobell, S.; Nedelkova, M.

Bacterial and archaeal diversity in ground waters of the Siberian deep-well radioactive disposal site Tomsk-7

ISME 10, August 22-27, 2004, Cancum, Mexico.

Somogyi, A.; Martinez-Criado, G.; Scheinost, A.C.; Tucoulou, R.

Application of synchrotron radiation excited X-ray microprobe techniques in material and environmental science

European Conference on Energy, Dispersive X-Ray Spectrometry, June 6-11, 2004, Alghero, Italy.

Stumpf, S.; Stumpf, T.; Fanghänel, T.; Dardenne, K.; Hennig, C.; Klenze, R.

Sorption of Am(III) onto 6-line-ferrihydrite and its alteration products: Investigation by EXAFS

Actinide-XAS-2004, 3rd Workshop on Speciation, Techniques, and Facilities for Radioactive Materials at Synchrotron Light Sources, September 14-16, 2004, Berkeley, CA, USA.

Ulrich, K.-U., Foerstendorf, H., Zänker, H., Jenk, U.

Colloid-borne uranium in an abandoned uranium mine in the stage of flooding

NRC-6, *6th International Conference on Nuclear and Radiochemistry, August 29 – September 3, 2004, Aachen, Germany.*

Zänker, H.; Wichter, W.; Ulrich, K.-U.; Moll, H.; Hüttig, G.

Kolloide in Bergwerkswässern

6th Workshop of research group "Kolloide" (Wasserchemische Gesellschaft in GDCh), Institut für Medizinische Balneologie und Klimatologie der LMU, March 9, 2004, München, Germany.

▶ *Posters*

Baumann, N.; Brendler, V.; Arnold, T.; Geipel, G.
Investigations of uranyl sorption onto gibbsite
SOPRO 2004, International Workshop on Sorption Processes at Oxide and Carbonate Mineral Water Interfaces, March 25-26, 2004, Karlsruhe, Germany.

Funke, H.; Chukalina, M.; Hennig, C.; Rossberg, A.; Scheinost, A.C.
Wavelet analysis of EXAFS data
Actinide-XAS-2004, 3rd Workshop on Speciation, Techniques, and Facilities for Radioactive Materials at Synchrotron Light Sources, September 14-16, 2004, Berkeley, CA, USA.

Geißler, A.; Tzvetkova, T.; Selenska-Pobell, S.
Microbial diversity in uranium contaminated soils
VAAM-2004, March 28-31, 2004, Braunschweig, Germany.

Hennig, C.; Scheinost, A.C.
Polarized EXAFS of uranium L1 and L3 edges - A comparison
14th ESRF Users Meeting, February 10-11, 2004, Grenoble, France.

Hübener, S.; Bernhard, G.; Fanghänel, T.
Thermochromatographic volatility studies of actinide oxides
NRC-6, *6th International Conference on Nuclear and Radiochemistry, August 29 – September 3, 2004, Aachen, Germany*.

Křepelová, A.; Mibus, J.; Sachs, S.; Nebelung, C.; Bernhard, G.
Interaction processes of tetravalent actinides in the system humic acid / quartz sand / solution
SOPRO 2004, International Workshop on Sorption Processes at Oxide and Carbonate Mineral Water Interfaces, March 25-26, 2004, Karlsruhe, Germany.

Merroun, M. L.; Rossberg, A.; Hennig, C.; Selenska-Pobell, S.
Isolation, characterization and U(VI)-immobilizing potential of bacterial Strains from uranium contaminated environments
Biometals 2004, September 3-5, 2004, Garmisch-Partenkirchen, Germany.

Merroun, M.; Raff, J.; Pollmann, K.; Rossberg, K.; Hennig, C.; Scheinost, A.C.; Selenska-Pobell, S.
Interaction of bacteria with metals: EXAFS studies
14th ESRF Users Meeting, February 10-11, 2004, Grenoble, France.

Mibus, J.; Lambarki, M.; Küchler, R.
Determination of effective diffusion parameters in compacted kaolinite
13th Annual V.M. Goldschmidt Conference, June 5-11, 2004, Copenhagen, Denmark.

Moll, H.; Geipel, G.; Bernhard, G.
Complex formation of curium with adenosine 5'-triphosphate (ATP) studied by TRLFS
NRC-6, *6th International Conference on Nuclear and Radiochemistry, August 29 – September 3, 2004, Aachen, Germany*.

Nedelkova, M.; Selenska-Pobell, S.
Bacterial diversity in waters at the Siberian deep-well monitoring site Tomsk-7
VAAM-2004, March 28-31, 2004, Braunschweig, Germany.

Opel, K.; Hübener, S.; Zänker, H.
Determination of low concentrated small-sized colloids by Laser Induced Breakdown Detection
12th Wolfgang-Ostwald-Kolloquium, Inorganic Colloid Science - Importance of Layered Materials, March 25-26, 2004, Kiel, Germany.

Poineau, F.; Fattahi, M.; Grambow, B.; Den Auwer, C.; Hennig, C.
Spéciation des complexes du technétium par couplage SAX - Electrochimie
Journée de Radiochimie, February 5-6, 2004, Avignon, France.

Pollmann, K.; Raff, J.; Merroun, M.; Fahmy, K.; Mikeehenko, I.; Creamer, N.; Macaskie, L.; Selenska-Pobell, S.
Analysis and engineering of the S-layer protein of *Bacillus sphaericus* JG-A12 and potential technological applications
Biotechnology 2004, October 17-22, 2004, Santiago de Chile, Chile.

Rossberg, A.; Scheinost, A.C.
Linking Monte Carlo simulation and target transformation factor analysis: A novel tool for EXAFS analysis
14th ESRF Users Meeting, February 10-11, 2004, Grenoble, France.

Sachs, S.; Geipel, G.; Bernhard, G.
Redox stability of uranium(VI) in presence of synthetic and natural humic acids
12th International Meeting of the International Humic Substances Society, July 25-30, 2004, Sao Pedro, Sao Paulo, Brazil.

Scheinost, A.C.; Rossberg, A.; Hennig, C.; Vantelon, D.; Kretzschmar, R.; Johnson, C.
Quantitative antimony speciation in shooting-range soils by EXAFS spectroscopy and iterative transformation factor analysis
14th ESRF Users Meeting, February 10—11, 2004, Grenoble, France.

Schmeide, K.; Bernhard, G.
Influence of humic acid on the neptunium(V) sorption onto granite and its mineral constituents
SOPRO 2004, International Workshop on Sorption Processes at Oxide and Carbonate Mineral Water Interfaces, March 25-26, 2004, Karlsruhe, Germany.

Schumacher, M.; Scheinost, A.C.; Christl, I.; Jacobsen, C.; Kretzschmar, R.
Chemical heterogeneity of humic substances and mobile soil colloids studied by X-ray microscopy and microspectroscopy
13th Annual V.M. Goldschmidt Conference, June 5-11, 2004, Copenhagen, Denmark.

Seidel, W.; Foerstendorf, H.; Glotin, F.; Ortega, J.-M.; Prazeres, R.
Exploring the spatial resolution of the photothermal beam deflection technique in the infrared region
26th International Free Electron Laser Conference & 11th FEL User Workshop, ELETTRA, August 29 – September 3, Trieste, Italy.

Stumpf, S.; Stumpf, T.; Fanghänel, T.; Dardenne, K.; Hennig, C.; Klenze, R.
Sorption of Am(III) onto 6-line-ferrihydrite and its alteration products: Investigation by EXAFS
Actinide-XAS-2004, 3rd Workshop on Speciation, Techniques, and Facilities for Radioactive Materials at Synchrotron Light Sources September 14-16, 2004, Berkeley, CA, USA.

Theses

Walter, M.
Spektroskopische Charakterisierung von Uran(VI) sorbiert an Oberflächen ausgewählter Minerale (Schwertmannit, Goethit, Chlorit, Pyrophyllit, Albit)
(Spectroscopic characterization of Uranium(VI) sorbed onto surfaces of selected minerals (Schwertmannite, Goethite, Chlorite, Pyrophyllite, Albite))
Dresden University of Technology, 2004.

Patents

Walter, M.; Arnold, T.
Verfahren zur Reinigung von Wasser mit hohen Uran-Konzentrationen
Patentanmeldung: 102 38 957.8
Patent: DE 102 38 957 A!

Awards

Walter, M.
FZR Ph. D. student award (third prize)
Doctoral Thesis (see above).

- *Seminars (Talks of visitors)*
- *Workshops (organized by the IRC)*
- *Teaching activities*

▸ *Seminars (Talks of visitors)*

Dr. Thomas Monecke
Institute of Mineralogy, TU Bergakademie Freiberg, Germany
"Geochemie der Lanthanide: Der Tetradeneffekt in natürlichen Proben aus granitgebundenen Lagerstätten"
January 13, 2004

Dr. Claus Herold
Engineering Services GmbH (ESG), Rheinsberg / Mark, Germany
"Tschernobyl nach der Katastrophe – Ergebnisse bisheriger und Möglichkeiten zukünftiger Forschungsarbeiten"
January 20, 2004

Dr. Maria Romero González
Lecturer in Aquatic Surface Chemistry, Groundwater Protection & Restoration Group, Dept. of Civil and Structural Engineering, University of Sheffield, U.K.
"Combining traditional wet chemistry with spectroscopic methods for the chemical characterisation of environmental surfaces"
February 26, 2004

Dr. Karim Fahmy
Institute of Nuclear and Hadron Physics, Forschungszentrum Rossendorf e. V., Dresden, Germany
"Protein-Konfirmation und biomolekulare Erkennung: Spektroskopische Untersuchungen zur Signaltransduktion beim Sehvorgang"
April 20, 2004

Prof. Dr. Petra Schwille
Institute of Biophysics / Bio Tec, Dresden University of Technology, Germany
"Einzelmolekülmethoden in der zellulären Biophysik"
June 14, 2004

Dr. Sebastien Dementin
Centre National de la Recherche Scientifique (CNRS), Marseille, France
"Biochemical studies of hydrogenases from *Desulfovibrio fructosovorans*"
June 22, 2004

Dr. Frank Cichos
Photonics and Optical Materials, Center for Nanostructured Materials and Analytics, Institute of Physics, Chemnitz University of Technology, Germany
"Exploring nanoscale dynamics with single molecules and quantum dots"
June 29, 2004

Prof. Peter Belser
Department of Chemistry, University of Fribourg, Switzerland
"Molecular switches: On the way to molecular electronics"
September 16, 2004

Dr. Andrew Leis
Max-Planck-Institute for Biochemistry, Department of Molecular Structural Biology, Martinsried, Germany
"Non-destructive visualisation and monitoring of biocolloids"
September 21, 2004

Prof. Dr. Kazuharu Yoshizuka
University of Kitakyushu, Japan
"Selective recovery of lithium ion in seawater using a λ-MnO_2 adsorbent"
September 23, 2004

Prof. Dr. Takuya Suzuki
University of Kitakyushu, Japan
"Speckle image observations using high coherent X-ray beams focused by Fresnel zone plate"
September 23, 2004

Prof. Dr. Katsutoshi Inoue
Saga University, Japan
"Remediation of polluted environment by using biomass wastes"
October 12, 2004

Prof. Dr. Fritz Vögtle
University of Bonn, Germany
"Functional dendrimers – Synthesis, properties, and application in material sciences and life sciences"
October 28, 2004

Prof. Dr. Andreas Türler
Institute of Radiochemistry, University of Munich, Germany
"Forschungsschwerpunkte am Institut für Radiochemie der Technischen Universität München"
November 23, 2004

Dr. Irina Perminova
Department of Chemistry, Lomonosov Moscow State University, Russia
"Design of humic materials of a desired remedial action"
December 21, 2004

▸ *Workshops (organized by the IRC)*

The Äspö – FZR Workshop: "Wechselwirkung von Actiniden mit dominanten Bakterien des Äspö-Grundwasserleiters" (project supported by the Bundesministerium für Wirtschaft und Arbeit, BMWA). FZR, Dresden, Germany, May 17–18, 2004.

Pedersen, K. (Department of Cell and Molecular Biology, Göteborg University, Sweden)
"Presentation of the MICROBE sites at Äspö hard rock laboratory"

Albinsson, Y. (Department of Materials and Surface Chemistry (Nuclear Chemistry), Chalmers University of Technology, Göteborg, Sweden)
"Leaching of spent UO_2-fuel with and without siderophores under inert/reducing conditions"

Jacobsson, A.-M. (Department of Materials and Surface Chemistry (Nuclear Chemistry), Chalmers University of Technology, Göteborg, Sweden)
"Planned studies of anaerobic biofilm sorption capacity and redox impact on different plutonium oxidation states"

Arlinger, J. (Department of Cell and Molecular Biology, Göteborg University, Sweden)
"Biomobilisation of metals in solution"

Johnson, A. (Department of Cell and Molecular Biology, Göteborg University, Sweden)
"Anaerobic bacteria: Their effect on the mobility of metals and actinides"

Anderson, C. (Department of Cell and Molecular Biology, Göteborg University, Sweden)
"Radionuclide sorption to anaerobic subsurface biofilms"

Geipel, G. (IRC)
"Laser spectroscopic techniques - tools to study the speciation of actinides in environmental systems"

Merroun, M.; Raff, J.; Roßberg, A.; Hennig, C.; Reich, T.; Selenska-Pobell, S. (IRC)
"Characterization and localization of uranium complexes formed by bacterial cells and S-layers"

Moll, H.; Merroun, M.; Geipel, G.; Stumpf, Th.; Roßberg, A.; Selenska-Pobell, S.; Bernhard, G. (IRC)
"Interaction of actinides with Desulfovibrio äspöensis. What have we achieved after 3 years of research on this topic?"

Nedelkova, M.; Radeva, G.; Selenska-Pobell, S. (IRC)
"Microbial diversity in ground water from a deep-well monitoring site at a Siberian radioactive subsurface repository"

Geißler, A.; Tzvetkova, T.; Flemming, K.; Satchanska, G.; Radeva, G.; Selenska-Pobell, S. (IRC)
"Comparative analysis of microbial communities in soils of several uranium mining waste piles and mill-tailings"

Raff, J.; Soltmann, U.; Matys, S.; Selenska-Pobell, S. (IRC)
"Bacteria-based nano-ceramics for remediation of uranium mining waste waters"

Moll, H.; Bernhard, G. (IRC)
"The mobilization of actinides by microbial ligands taking into consideration the final storage of nuclear waste - A proposal for a new BMBF/BMWA proposal"

Workshop of the Institute of Radiochemistry (IRC) and the Paul Scherrer Institute (PSI), Villigen , Switzerland
FZR, Dresden, Germany, October 25–26, 2004.

Scheinost, A.C. (IRC)
"Strukturanalytik von Actinidkomplexen mittels EXAFS-Spektroskopie"

Pfingsten, W. (PSI)
"Modellierung von reaktiven Transport-Experimenten (Gipsauflösung) – Einfluss von Kinetik, beteiligter Mineraloberfläche und Heterogenität"

Brendler, V. (IRC)
"Application of surface-sensitive TRLFS to uranyl sorption onto clay model substances"

Křepelová, A. (IRC)
"Study of the influence of humic acid on the U(VI) sorption onto kaolinite"

Curti, E. (PSI)
"Solid solutions of trace Eu(III) in Calcite"

Raff, J. (IRC)
"Selektive Bindung von Uran an *Bacillus sphaericus*–Bioceren"

Glaus, M. (PSI)
"Cellulosehaltige Abfälle: Ein stör(rischer)-Faktor in der Sicherheitsanalyse?"

Workshop of the Rossendorf-Beamline (ROBL) at the ESRF, Grenoble FZR, Dresden, Germany, December 13, 2004.

Rossberg, A.; Scheinost, A.C.
"Actinide speciation based on EXAFS spectroscopy: From shell fitting to MCTFA"

Hennig, C.; Tutschku, J.; Rossberg, A.; Scheinost, A.C.; Bernhard, G.
"Strukturuntersuchung von U(VI) und U(IV)-Komplexen in konzentrierten Chloridlösungen"

Reich, T.
"Ergebnisse einer EXAFS-Machbarkeitsstudie zur Sorption von Neptunium(V) an Kaolinit KGa-1b"

Ulrich, K.-U.; Rossberg, A.; Foerstendorf, H.; Scheinost, A.C.; Zänker, H.
"Untersuchungen zur Bindungsstruktur von kolloidgetragenem Uran(VI)"

Funke, H.; Hennig, C.; Rossberg, A.
"Application of wavelet transformation to EXAFS spectra of uranyl carbonates"

Günther, A.; Rossberg, A.; Merroung, M.; Raff, J.
"EXAFS-Untersuchungen von U(VI)-Komplexlösungen mit ausgewählten Aminosäuren und Peptiden"

Rossberg, A.; Geipel, G.; Suzuki, T.; Stephan, H.
"EXAFS-Untersuchung der Wechselwirkung von Bisbidon-Derivaten mit Np(V) in wässriger Lösung"

Scheinost, A.C.; Geipel, G.; Foerstendorf, H.; Leckelt, M.; Eichhorn, F.; Vochten, R.
"The Vochten uranium minerals collection: First EXAFS, TRLFS and FT-IR spectroscopy results"

Hennig, C.; Strauch, U.
"Die ROBL-Probenhalter – Neue Darstellung durch Zeichnungen und Veranschaulichung der Handhabung durch Fotos"

Merroun, M.; Pollmann, K.; Raff, J.; Hennig, C.; Rossberg, A.; Funke, H.; Scheinost, A.C.; Selenska-Pobell, S.
"Spectroscopic characterization of metallic nanoclusters (gold and palladium) formed by cells, S-layer sheets and biocers"

Merroun, M.; Nedelkova, M.; Heilig, M.; Rossberg, A.; Hennig, C.; Funke, H.; Scheinost, A.C.; Selenska-Pobell, S.
"EXAFS spectroscopic study of uranium coordinated to bacterial strains isolated from extreme habitats: pH effects"

Scheinost, A.C.; Hennig, C.; Leckelt, M.; Krogner, K.; Gerdes, A.; Knappik, R.
"Uranium speciation in soils and sediments contaminated by uranium mining and DU ammunition"

Schöner, A.; Sauter, M.; Büchel, G.
"Hydrogeochemische Untersuchungen von Uran-Akkumulationen in natürlichen Wetlands"

▶ *Teaching Activities*

Lectures

Bernhard, G.
"Radiochemistry – Radiochemical methods"
Dresden University of Technology
Summer term 2004

Bernhard, G.
"Environmental analysis (Trace analysis) "
Dresden University of Technology
Summer term 2004

Bernhard, G.
"Environmental chemistry (Environment – Substance – Energy) "
Dresden University of Technology
Winter term 2004 / 2005

Courses

The IRC provided two experiments of the laboratory course "Instrumental Analysis" held by the Institute for Analytical Chemistry, Dresden University of Technology, during both summer and winter terms:

- Technetium analysis in environmental samples
- Alpha spectrometric isotope dilution analysis of uranium

Advisers:
Hübener, S.
Krogner, K.

Teaching Assistants:
Geißler, A.
Großmann, K.
Opel, K.
Weiß, S.

Prof. Dr. G. Bernhard (Director)

Administrative Staff
C. Kirmes, G. Kreusel

Radiation Protection Technics
H. Friedrich, D. Falkenberg, S. Henke, B. Hiller, A. Rumpel

AQUATIC CHEMISTRY

Dr. G. Geipel

Dr. H.-J. Engelmann
Dr. K.-H. Heise
Dr. S. Hübener
Dr. K. Krogner
Dr. W. Richter
Dr. S. Sachs
Dr. K. Schmeide
Dr. J. Tutschku
Dr. K.-U. Ulrich
Dr. H. Zänker

Technical Staff

M. Eilzer
C. Fröhlich
G. Grambole
S. Heller
W. Knebel
M. Meyer
I. Muschter
R. Ruske
S. Weiß

BIOGEOCHEMISTRY

Dr. A.C. Scheinost

Dr. H. Funke
Dr. A. Günther
Dr. C. Hennig
Dr. M. Merroun
Dr. H. Moll
Dr. K. Pollmann
Dr. J. Raff
Dr. D. Regenhardt
Dr. A. Roßberg
Dr. S. Selenska-Pobell

Technical Staff

M. Dudek
K. Flemming
M. Leckelt
U. Schaefer

MIGRATION

Dr. V. Brendler

Dr. T. Arnold
Dr. N. Baumann
D. Birnstein
Dr. H. Foerstendorf
Dr. J. Mibus
C. Nebelung
Dr. A. Richter

Technical Staff

C. Eckhardt
R. Jander
C. Müller
K. Muschter
H. Neubert
R. Nicolai

Ph. D. Students

A. Geißler
K. Großmann
A. Křepelová
M. Nedelkova
K. Opel
M. Walter

Guest Scientists

N. Chantaraprachoom	*Radioactive Waste Management Program, Office of Homes for Peace, Bangkok, Thailand*
M. Chukalina	*Institute of Microelectronics Technology, Chernogolovka, Russia*
R. Han	*Centre of Environmental Measurements, Province Liaoning, China*
G. Radeva	*Institute of Molecular Biology of the Academy of Science of Bulgaria, Sofia, Bulgaria*
Prof. S. Nagasaki	*Department of Quantum Engineering, Graduate School of Engineering, The University of Tokyo, Japan*
G. Satchanska	*Institute of Molecular Biology of the Academy of Science of Bulgaria, Sofia, Bulgaria*

Graduate Assistants, Student Assistants, Trainees

T. Birk
N. Betzl
S. Brockmann
M. Heilig
A. Heller
M. Kaufmann
C. Schaefer
I. Schubert
U. Siewert
D. Sompolski
R. Steudtner
C. Trautmann
P. Trepte
D. Vulpius
M. Wenzel
T. Witschel

Acknowledgements

The Institute of Radiochemistry is part of the Forschungszentrum Rossendorf e. V. which is financed in equal parts by the Federal Republic of Germany and the Free State of Saxony.

The Commission of the European Communities supported the following projects:

- ACTINET Network for Actinide Sciences
  Contract No.: FIR1-CT-2002-20211
  Contract No.: FI6W-CT-2004-508836.
- Novel Precious Metal-Based Bionanocatalysts from Scarp
  Contract No.: G5RD-CT-2002-00750.
- Humic Substances in Performance Assessment of Nuclear Waste Disposal Actinide and Iodine Migration in the Far-Field
  Contract No.: FIKW-CT-2001-00128.
- Understanding and Physical and Numerical Modelling of the Key Processes in the Near-Field and their Coupling for Different Host Rocks and Repository Strategies
  Contract No.: F16W-CT-2003-002389.

Six projects were supported by the Bundesministerium für Wirtschaft und Arbeit (BMWA) and by the Bundesministerium für Bildung und Forschung (BMBF):

- Biocere auf Basis bakterieller Membranproteine für schwermetallbindende Filter zur Behandlung von industriellen Abwässern und kontaminierten Grundwasser
  Contract No.: BMBF 03I4004B.
- Diversity of bacteria in Bulgarian and German uranium waste piles – a comparative analysis
  Contract No.: BMBF DLR-IB/BGR 99011
- Integriertes Sorptionsdatenbanksystem für Wechselwirkungen chemisch-toxischer und radioaktiver Kontaminanten mit mineralischen Systemen in geologischen Formationen (ISDA-FZR)
  Contract No.: BMBF 02C1144.
- Wechselwirkung von Actiniden mit dominanten Bakterien des Äspö-Grundwasserleiters
  Contract No.: BMWA 02E9491.
- Entwicklung einer mineralspezifischen Sorptions-Datenbank für Oberflächenkomplexierungsmodelle
  Contract No.: BMWA 02E9471.
- Untersuchungen über die Komplexierung und die Migration von Actiniden und nichtradioaktiven Stoffen mit Huminsäuren unter geogenen Bedingungen
  Contract No.: BMWA 02E9673.

The Sächsisches Staatsministerium für Wissenschaft und Kunst provided support for the following project:

- Biologische Synthese von Metallclustern an Proteinen und deren technische Nutzung
  Contract No.: 4-7531.50-03-0370-01/5.

Two projects were supported by the Deutsche Forschungsgemeinschaft (DFG):

- Biocere mit spezifischer Metallbindungsaktivität
  Contract No.: SE 671/7-2.
- Kolloidgetragener Transport von Uran und anderen radiotoxischen Schwermetallen in toxischen Bergwerkswässern
  Contract No.: ZA 238/2-1.

One project was supported by AMD Saxony Manufacturing GmbH:

- Alphaspektrometrie an Si-Wafern
  Contract No.: AMD 5200030223.

Forschungszentrum Rossendorf
Institute of Radiochemistry
P.O. Box 51 01 19 - 01324 Dresden/Germany
Tel.: +49 351 260-3210
Fax: +49 351 260-3553
e-mail: contact.radiochemistry@fz-rossendorf.de
www.fz-rossendorf.de

Member of the Leibniz Association